BIOACTIVE CERAMIC COATING ON ORTHOPEDIC IMPLANTS FOR ENHANCED BONE TISSUE INTEGRATION

by

Aniket

A dissertation submitted to the faculty of
The University of North Carolina at Charlotte
in partial fulfillment of the requirements
for the degree of Doctor of Philosophy in
Mechanical Engineering

Charlotte

2012

Approved by:

_____
Dr. Ahmed El-Ghannam

_____
Dr. Qiuming Wei

_____
Dr. Didier Dreau

_____
Dr. Stuart Smith

_____
Dr. Patrick Moyer

ABSTRACT

ANIKET. Bioactive ceramic coating on orthopedic implants for enhanced bone tissue integration (Under the direction of DR. AHMED EL-GHANNAM)

Tissue integration between bone and orthopedic implant is essential for implant fixation and longevity. An immunological response leads to fibrous encapsulation of metallic implants leading to implant instability and failure. Bioactive ceramics have the ability to directly bond to bone; however, they have limited mechanical strength for load bearing applications. Coating bioactive ceramics on metallic implant offers the exciting opportunity to enhance bone formation without compromising the mechanical strength of the implant. In the present study, we have developed a novel bioactive silica-calcium phosphate nanocomposite (SCPC) coating on medical grade Ti-6Al-4V orthopedic implant using Electrophoretic Deposition (EPD) and evaluated bone tissue response to the coated implant at a cellular level.

The effect of SCPC composition and suspending medium pH on the zeta potential of three different SCPC formulations; SCPC25, SCPC50 and SCPC75 were analyzed. The average zeta potential of SCPC50 in pure ethanol was more negative than that of SCPC25 or SCPC75; however the difference was not statistically significant. Ti-6Al-4V discs were passivated, coated with SCPC50 (200 nm - 10 μm) and thermally treated at 600 - 800 ºC to produce a coating thickness in the range of 43.1 ± 5.7 to 30.1 ± 4.6 μm. After treatment at 600, 700 and 800 ºC, the adhesion strength at the SCPC50/Ti-6Al-4V interface was 42.6 ± 3.6, 44.7 ± 8.7 and 47.2 ± 4.3 MPa, respectively. XRD analyses of SCPC50 before and after EPD coating indicated no change in the crystallinity of the material. Fracture surface analyses showed that failure occurred within the ceramic layer

or at the ceramic/polymer interface; however, the ceramic/metal interface was intact in all samples. The adhesion strength of SCPC50-coated substrates after immersion in PBS for 2 days (11.7 ± 3.9 MPa) was higher than that measured on commercially available hydroxyapatite (HA) coated substrates (5.5 ± 2.7 MPa), although the difference was not statistically significant. SEM - EDX analyses of SCPC50-coated Ti-6Al-4V pre-immersed in PBS for 7 days showed the formation of a Ca-deficient HA surface layer. Bone cells attached to the SCPC50-coated implants expressed significantly higher ($p <$ 0.05) alkaline phosphatase activity (82.4 ± 25.6 nmoles p-NP/mg protein/min) than that expressed by cells attached to HA-coated or uncoated implants. Protein adsorption analyses showed that SCPC50-coated substrates adsorbed significantly more ($p < 0.05$) serum protein (14.9 ± 1.2 μg) than control uncoated substrates (8.9 ± 0.7 μg). Moreover, Western blot analysis showed that the SCPC50 coating has a high affinity for serum fibronectin. Protein conformation analyses by FTIR showed that the ratio of the area under the peak for amide I/amide II bands was significantly higher ($p < 0.05$) on the surface of SCPC50-coated substrate (5.0 ± 0.6) than that on the surface of the control uncoated substrates (2.2 ± 0.3). Moreover, ICP-OES analyses indicated that SCPC50-coated substrates withdrew Ca ions from, and released P and Si ions into, the tissue culture medium, respectively. In conjunction with the favorable protein adsorption and modifications in medium composition, MC3T3-E1 osteoblast-like cells attached to SCPC50-coated substrates expressed 10-fold higher level of mRNA encoding osteocalcin and had significantly higher production of osteopontin and osteocalcin proteins than cells attached to the uncoated Ti-6Al-4V substrate. In addition, osteoblast-like cells attached to the SCPC50-coated substrates produced significantly lower levels of the inflammatory

and osteoclastogenic cytokines, IL-6, IL-12p40 and RANKL than those attached to uncoated Ti-6A1-4V. Surface topography analyses using AFM suggested that the SCPC50 particles deposit onto the metal surface in a manner that preferentially fills the grooves on the substrate created during substrate preparation. An increase in the surface roughness of the SCPC50-coated substrate from 217.8 ± 54.6 nm to 284.3 ± 37.3 nm was accompanied by enhanced material dissolution, reduced cell proliferation and poor actin cytoskeleton organization, which are characteristics typical of differentiating bone cells on bioactive ceramic surfaces. Results of the study demonstrate that bioactive SCPC50 can efficiently be coated on Ti-6Al-4V using EPD. Moreover, the *in vitro* bone cell response suggests that SCPC50-coating has the potential to enhance bone integration with orthopedic and maxillofacial implants while minimizing the induction of inflammatory bone cell responses.

DEDICATION

This dissertation is dedicated to my parents, Dr. Mithilesh Kumar and Mrs. Sarita Kumari, for their guidance and endless support in all my endeavors.

ACKNOWLEDGEMENTS

I would like to express my deepest gratitude and sincere thanks to my advisor, Dr. Ahmed El-Ghannam, for his excellent mentorship, patience, and guidance that has allowed me to transform into an independent researcher. Dr. El-Ghannam's knowledge, wisdom, and unsurpassed commitment to highest quality scientific work have immensely inspired and motivated me. I would also like to thank Dr. Qiuming Wei, Dr. Didier Dreau, Dr. Stuart Smith and Dr. Patrick Moyer for being a part of my advisory committee and for their valuable inputs in the preparation of this dissertation.

I would like to thank Dr. Ian Marriott for allowing me to us his lab facilities to undertake molecular biology assays and assistance with manuscript preparation. I would also like to thank Dr. Jimmie Miller for training me on the atomic force microscope. I would like to thank Mr. Hernando Pacheco for his assistance in machining Ti-6Al-4V discs. Special thanks to the staff of the Mechanical Engineering department, whose help and support have been indispensable.

I would like to thank UNC Charlotte for the financial support offered by the Graduate Assistant Support Plan (GASP) award. I would also like to thank DePuy Orthopaedics, Inc., a Johnson & Johnson company, for funding the research project (Grant # 540661).

Finally, I would like to thank my family and friends for their unending support and encouragement throughout my career.

TABLE OF CONTENTS

LIST OF TABLES

LIST OF FIGURES

1.8 ppm was measured up to 12 days of incubation, followed by a decrease in Si release thereafter.

LIST OF ABBREVIATIONS

AFM	Atomic Force Microscopy
AP	Alkaline Phosphatase
ASTM	American Society for Testing and Materials
BG	Bioactive Glass
CaP	Calcium Phosphate
CDHA	Calcium Deficient Hydroxyapatite
CNT	Carbon Nano-Tube
Col-I	Collagen-I
CP	Commercially Pure
DMEM	Dulbecco's Modified Eagle Medium
EDX	Energy Dispersive X-ray spectroscopy
ELISA	Enzyme-linked immunosorbent assay
EPD	Electrophoretic Deposition
FBS	Fetal Bovine Serum
FC	Focal Contact
FTIR	Fourier Transform Intra-red Spectroscopy
HA	Hydroxyapatite
ICP - OES	Inductively Coupled Plasma - Optical Emission Spectroscopy
IL	Interleukin
OCN	Osteocalcin
OCP	Octacalcium Phosphate
OPN	Osteopontin

OSN	Osteonectin
PBS	Phosphate Buffer Saline
PCR	Polymerase Chain Reaction
p-NP	p-nitrophenol
p-NPP	p-nitrophenylphosphate
SBF	Simulated Body Fluid
RANKL	Receptor Activator for Nuclear Factor κ B Ligand
RT-PCR	Real Time Polymerase Chain Reaction
SCPC	Silica-Calcium Phosphate Nanocomposite
SEM	Scanning Electron Microscopy
TCM	Tissue Culture Medium
TCP	Tricalcium Phosphate
TEM	Transmission Electron Microscopy
THA	Total Hip Arthroplasty
XRD	X-Ray Diffraction

CHAPTER 1: INTRODUCTION

1.1. Background

Osteoarthritis is a chronic condition of the synovial joint which manifests as joint pain and is characterized by tenderness, limitation of movement and inflammation of the joint.[1] Such a condition develops over many years due to the thinning and loss of the cartilage covering of the bone resulting in reduced joint spaces and direct bone-to-bone contact. Although osteoarthritis of the knee continues to be the leading cause of joint pain, osteoarthritis of the hip joint is an equally serious concern. The continuous use of the hip throughout our life causes wear-and-tear of the joint. The body reacts to the changes in the joint structure by forming large bone spurs, effusing tissue fluids and forming hard underlying bony surfaces and cysts around the joint.[2] All of these responses gradually compromise the functionality of the hip and causes acute pain that restricts daily movements. The common line of treatment is the surgical intervention for total joint replacement via total hip arthroplasty (THA) wherein the articulating surfaces of the femoral head and the acetabulum of the hip are replaced by a prosthetic implant. The technique involves the surgical excision of the head and proximal neck of the femur along with removal of the acetabular cartilage and subchondral bone.[3] An artificial cavity is created in the proximal medullary region of the femur in which the hip prosthesis consisting of a metallic femoral shaft and a hemispherical femoral head is partially inserted. The most widely used metals are Ti-6Al-4V and Co-Cr alloys. The acetabulum

(socket) is debrided and reamed to remove the arthritic tissue and accommodate the femoral ball.[3] The bearing surface between the femoral ball and the acetabulum can be lined with either metal (metal-on-metal), ceramic (metal-on-ceramic) or ultra-high molecular weight polyethylene (metal-on-plastic). Recent data from the National Hospital Discharge Survey shows that there were 230,000 cases of primary THA surgeries in the US in 2007. It was found that 39.5% of all patients were in the age group of 45-64 and 54.3% were older than 65.[4] The average cost of THA was estimated to be in excess of $ 35,000, depending upon the procedure, hospital and location.[5] Moreover, it was estimated that the total number of patients undergoing THA would increase to about 600,000 by 2015, and the annual hospital charges would increase to about $ 17.7 billion by 2015.[6]

1.1.1   Failure of THA

Despite advances in surgical techniques and implant design, failure of the primary THA remains a concern. It is estimated that almost 20% of the patients require a revision surgery due to the failure of the primary implant.[7] The demand for revision hip arthroplasty is expected to grow by 137% between 2005 and 2030. The failure of total joint replacement is mainly caused due to the mismatch of the physico-chemical properties between bone and the synthetic implant material. Loosening of the implant may arise due to micro-motion resulting from either insufficient press-fit at the time of surgery, excessive cyclic loading during daily activities or bone resorption around the implant.[8] The micro-motion at the bone-implant interface impedes tissue integration with the device and ultimately leads to poor fixation and implant failure.[9] Another factor that contributes to the poor implant fixation is the fibrous capsule that forms at the implant/bone interface. The formation of the fibrous capsule constitutes a chronic

immunological response against the synthetic material manifesting as non-mineralized encapsulation of the implant. Micro-motion at the bone/implant interface irritates the immune system and results in sustained presence or over-development of the fibrous capsule.[10] If such a condition persists, surgical removal of the implant needs to be carried out. Recent data indicates that 71% of the revision surgery cases have been attributed to poor bone-implant integration.[5] Of these, 22.5% cases were due to implant dislocation and 19.7% cases were due to the mechanical loosening of the implant. The other 29% of the cases were attributed to infection/inflammation at the site of implant (14.8%), peri-prosthetic fracture (6.2%) or peri-prosthetic osteolysis (6.6%). The average total cost of revision surgery was estimated between $ 45,000 to $ 69,000 depending upon the procedure, hospital and location.[5,11] These figures impress upon the need to design hip implant materials and surgical techniques in a way that is more cost-effective, patient-friendly and provides a permanent and strong fixation of the implant within the bone. Recent attempts have focused on surface engineering of the implant that can promote osteo-integration with the device and improve the performance and biocompatibility of the synthetic material.

1.1.2   Stress shielding problem

Even in the absence of implant micro-motion or fibrous encapsulation, the mismatch in the mechanical properties between bone and implant can weaken the peri-prosthetic bone and lead to implant failure. Although the high mechanical strength of metals is beneficial for load-bearing applications, the high stiffness of the metal is counter-productive. Due to its greater modulus of elasticity, the metal component bears a greater proportion of the body weight as compared to the surrounding bone.[12]

Consequently, the metal shields the bone from loading, a phenomenon known as stress shielding. The stress shielding hinders proper transfer of mechanical stimulus from the implant to the bone and interferes with normal bone development and remodeling. Cells in the bone matrix called osteocytes sense the mechanical strain and modulate the formation or resorption of the bone tissue depending upon the intensity and distribution of the mechanical signal.[13] However, in stress shielded bone, osteocytes tend to promote bone resorption which depreciates the mechanical strength of the bone and makes it prone to fracture.

1.2 Metals for total joint replacement

Implants that are designed for fixation and stabilization of load-bearing conditions are generally made of metals such as Ti-6Al-4V and Co-Cr alloys that offer high mechanical strength and are generally bio-inert. Table 1.1 shows the mechanical properties of Ti-6Al-4V and Co-Cr alloys as compared to the adult human cortical bone. Ti-6Al-4V is an α+β alloy, which has 6 wt% Al stabilizing the α-phase and 4 wt% V stabilizing the β-phase. At room temperature, the alloy is composed predominantly of the α-phase as hexagonal closed packed (HCP) lattice with minor amount of β-phase as body centered cubic (BCP) lattice. The high fracture toughness, low strength-to-weight ratio, superior corrosion resistance and excellent biocompatibility of Ti-6Al-4V makes it one of the best alloys for artificial joint replacement.[14] Ti is highly reactive and combines rapidly with oxygen to form a protective passive layer of TiO_2 which resists corrosion.[14,15] Co-Cr alloys have higher hardness and abrasion resistance than Ti-6Al-4V and are widely used in plastic-on-metal type of articulating surface. However, since Co is not as reactive as Ti, the formation of passive oxide layer is limited, thus allowing for the

release of Co and Cr ions.[16] Data in the literature suggests that the toxicity of Co and Cr

ions is 5 times higher than that of Ti or Al ions.[17] Allen *et al* studied osteoblast response

to Co, Cr and Co-Cr alloy particles and reported that Co concentration as low as 0.1

mg/mL inhibited the synthesis of collagen I, osteocalcin and alkaline phosphatase (AP),

and showed cytotoxic effects on osteoblast-like cells.[18] An important difference between

Ti-6Al-4V and Co-Cr alloy is the lower modulus of elasticity of the former material

which alleviates the stress shielding effect on peri-prosthetic bone and impedes bone

resorption.[19] In fact, of all the metals used in orthopedics, Ti-6Al-4V possesses

mechanical properties closest to bone. Moreover, Ti-6Al-4V allows direct bone

apposition on the surface of the metal unlike Co-Cr alloys.[16] Implant retrieval studies

have shown that bone ingrowth on Ti-6Al-4V implants occurred over the entire surface

of the implant with direct contact between the metal and the bone.[20] On the other hand,

bone ingrowth was observed on Co-Cr implant with no evidence of direct contact

between the metal and bone.[16]

	Young's modulus (GPa)	Yield Strength (MPa)	Fracture Toughness (MPa m$^{1/2}$)
Ti-6Al-4V	115	795 - 875	60 - 80
Co-Cr	209	450 - 1000	58 - 62
Cortical Bone	7 - 30	140	3.5 - 6.4

Table 1.1: Comparison of mechanical properties of Ti-6Al-4V and Co-Cr alloy with adult human cortical bone

1.2.1   Limitations of metallic implants in joint fixation

Despite the high mechanical strength, the corrosion of metallic implants over their

lifetime remains a serious challenge to their long-term biocompatibility. In the bulk form,

metallic implants are biocompatible and demonstrate minimal immune response; however, the particulate form of the material triggers macrophage activity and incites immunological responses. The continuous interaction between metallic implants and tissue fluids together with material fatigue and friction between the articulating surfaces generates wear debris and releases metal ions.[21] The release of such particulate matter and the ensuing inflammatory responses affects normal bone metabolism by increasing the release of osteolytic factors. A consequence of such a reaction is a foreign body response and soft-tissue reaction that leads to the fibrous encapsulation of the device.[22,23] Lalor *et al* examined Ti screws explants and found extensive presence of macrophages around the material that contained Ti particles.[24] In another study on Ti-6Al-4V and Co-Cr alloy hip explants, abundant presence of metal particles and T-lymphocytes were noticed around the both the implants.[25] *In vitro* studies by Thomson *et al* showed that the ions released from Ti-6Al-4V inhibit the normal differentiation of bone marrow stromal cells into mature osteoblasts.[26] Recent reports by Cadosch *et al* suggest that Ti ions enhance osteoclast differentiation which encourages bone resorption.[27] In support of this idea, Saldana *et al* reported that Al ions, in conjunction with Ti ions, impede osteoblast differentiation.[28] It has also been reported that the metallic particles may be systemically distributed in body tissues other than the implanted regions.[21,29] In one study, Case *et al* reported that metal particles accumulated in lymph nodes and caused necrosis and fibrosis of the tissue.[29] Other reports have suggested that metal ions released from the implants bind to proteins, such as those on immunostimulatory dendritic cells and induce hypersensitivity reactions.[21] Indeed, metallic debris induced hypersensitivity reactions have been reported in some individuals.[30,31] In addition to the biocompatibility issues of

Ti-6Al-4V implants, the stress shielding problem of the periprosthetic bone due to improper mechanical stimulation remains unaddressed.

1.3   Strategies for implant fixation

1.3.1 Porous-coated metal implants

The fixation of implant with the bone can be enhanced by modifying the surface characteristics and/or geometrical design of the implant that allows bone growth into or onto the device.[32] Coating the surface of Ti-6Al-4V implant with porous metal beads has demonstrated some success in enhancing mechanical fixation. Figure 1.1 shows an SEM image of the surface of porous-coated Ti-6Al-4V implant. These implants are characterized by a three-dimensional interconnected porous structure having pores in the range of 100 - 400 µm, which is on the same order as the pore size for cancellous bone (400 – 500 µm). The porous geometry provides greater space for bone tissue ingrowth, improves mechanical interlocking and enhances the surface area available for implant-bone contact.[33] Moreover, the interconnected porosity encourages tissue ingrowth and integration with the device, which enhances the long-term stability of the implant. Thus, bone tissue ingrowth into the three-dimensional porous structure provides resistance to shear, compressive, and tensile forces at the tissue/implant interface.[34] Simmons *et al* evaluated the osteointegration potential of bone-interfacing implants and found that the modified geometry of the porous coating provided a large region of low distortional and volumetric strains that favor osteogenesis.[35,36] Recent clinical studies have shown that porous-coated implants show minimal aseptic loosening in ≥ 99% cases even after15 years of implantation in both, osteoporotic and non-osteoporotic bone.[37] However, a limitation of the porous coated implant is its low volumetric porosity, suboptimal frictional characteristics and reduced fatigue resistance.[34,38] Previous studies have shown
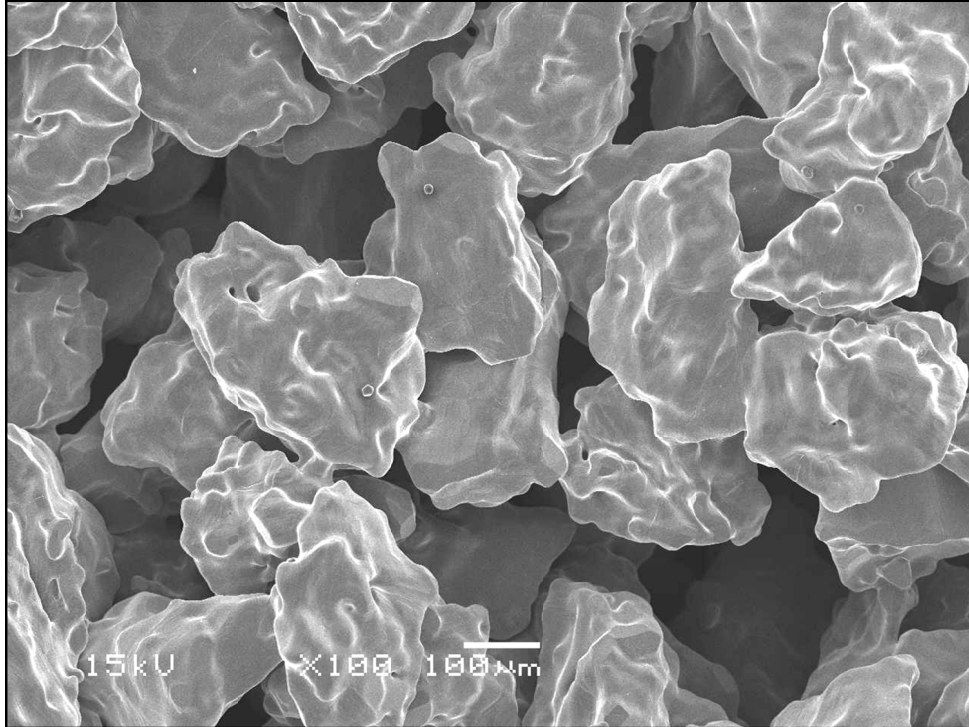
Figure 1.1: SEM image of porous-coated Ti-6Al-4V showing the metallic beads on the surface of the implant. The pores range in size from 100 – 400 µm.

that the fatigue strength of Ti-6Al-4V decreased from 600 MPa to 200 - 370 MPa due to the porous coating.[39] The decrease in the mechanical strength has been attributed to easier fatigue crack initiations at the interface of porous beads with the metallic substrate.[40] Moreover, insufficient adhesion strength between beads and the substrate or between individual beads as a result of improper processing significantly decreases the mechanical strength of the implant.[39] In addition, the increase in the surface of area of the implant due to the porous coating enhances the interaction between tissue fluids and the implants and hence increases the chances of corrosion and metal ion release.

1.3.2 Bioactive ceramic coating on metal implant

Bioactive ceramics, such as calcium phosphates (CaP), have the ability to directly bond with the bone and enhance bone formation;[41-43] therefore they have been applied as

a coating on orthopedic implant materials.[44,45] The bioactive ceramic surface stimulates bone growth onto the implant, while the inner metal core provides mechanical strength to the device.[45] Data in the literature indicates that CaP ceramics have the potential to affect bone cell behavior at the gene level and produce pro-osteogenic proteins that encourage bone apposition.[41,46-48] There are different types of CaP ceramics, such as hydroxyapatite (HA), tri-calcium phosphate (TCP), octa-calcium phosphate (OCP), etc. that vary in their chemical structure, mechanical properties and osteogenic potential. However, HA having the chemical formula $Ca_{10}(PO_4)_6(OH)_2$ is the most popular CaP ceramic that has found extensive applications in medicine and dentistry over the last three decades. An important characteristic of HA is that it has a structure similar to the mineral phase of the bone which makes it an attractive bone-substitute material.[42,49]

Plasma spraying is the most popular commercially used method for coating HA on Ti-6Al-4V implants. The coating process involves the deposition of a finely ground ceramic powder in a molten or semi-molten state on the Ti-6Al-4V substrate.[50] A direct current (DC) arc or a radiofrequency (RF) inductively coupled plasma discharge generates the plasma; providing temperatures in the range of 8,000 - 30,000 K. HA powder is introduced within the plasma (RF) or the plasma jet (DC-arc) where the particles undergo partial or complete melting before impinging and rapidly cooling on the metal substrate.[51] HA-coated Ti-6Al-4V implants have been approved by the US-FDA for THA procedures since the 1990's and have found remarkable commercial success. Clinical studies on HA-coated Ti-6Al-4V hip implants have shown reduced bone migration and superior osteointegration as compared to uncoated Ti-6Al-4V implants.[52,53] HA-coated implants have been successfully tested in gap-healing models, closing a gap

of 1 mm between the bone and the implant in both mechanically stable and unstable conditions.[51] Hermida *et al* evaluated intramedullary bone response in rabbits to HA-coated and uncoated Ti implants of similar surface topography and showed that that the presence of HA coating maximized the bone-to-implant contact area and resulted in superior osteointegration.[54] Landor *et al* compared the osteointegration potential of plasma sprayed HA coated Ti-6Al-4V and uncoated Ti-6Al-4V hip implants in 50 human subjects and found significantly more bone apposition on the HA-coated implant.[55] On the other hand, uncoated Ti-6Al-4V implants showed evidence of fibrous encapsulation due to micro-motion and/or stress shielding. Similar results were reported by D'Antonio *et al* who evaluated the performance of 380 hip implants in human subjects over 10-13 years and found that the HA coating enhanced bone ingrowth and improved the mechanical fixation of the device.[56]

1.3.2.1. Mechanism of bioactivity

The dissolution of CaP ceramics increases the local concentration of Ca and P ions in the vicinity of the implant material and provides stimulatory signals to osteoblasts. Continued dissolution of the material supersaturates the solution, causing a re-precipitation of the excess Ca and P ions back onto the material surface in the form of carbonated hydroxyapatite (HCA), the mineral phase of the bone. The formation of HCA is thought to be a critical step in establishing the mineralization front of the implant material with the host tissue.[41,42] In silica containing biomaterials, such as bioactive glasses (BG), the silanol groups (Si-OH) undergo polymerization to form a silica-rich surface.[42] Ion-exchange and structural rearrangements at the surface promote Ca and P to diffuse through the silica-rich layer and form an amorphous layer of CaP which gradually

crystallizes into HCA by recruiting CO_3^{2-} ions from the surroundings. In conjunction with the HCA formation, cell attachment proteins, such as fibronectin and vitronectin, attach to the material surface and modulate cell adhesion and function. The cells produce collagen fibrils that interdigitate with the HCA crystals and trigger a chemotactic response that stimulates cell proliferation, differentiation and bone-matrix synthesis.[42]

1.4   Drawbacks of plasma sprayed HA-coated Ti-6Al-4V implants

1.4.1   Low adhesion strength

The stability of the ceramic coating is determined by the adhesion strength between the coating and the metal substrate. Due to the high temperature of the plasma spraying process, the mismatch in the thermal expansion coefficient of HA (11.5 - 14.7 x 10^{-6} K^{-1}) and Ti-6Al-4V (8.60 x 10^{-6} K^{-1}) causes differential expansion and contraction at the interface between metal and ceramic.[57] Thus, the residual stresses at the metal/ceramic interface, whether tensile or compressive, lead to cracking and limits the adhesion strength of the coating.[58] Poor adhesion between the metal and ceramic compromises the structural integrity of the HA layer and renders the implant prone to micro-motion.

1.4.2   Thermal decomposition of HA

The high temperature of the plasma spraying process can decompose HA into various by-product phases, such as tri-calcium phosphate, tetra-calcium phosphate, oxy-hydroxyapatite, calcium oxide, and other amorphous phases.[51] These phases are characterized by altered crystallinity, varied solubility and limited or no biocompatibility, all of which is detrimental to the stability and bioactivity of the coating. Moreover, the high temperature of the plasma spraying process promotes extensive inter-atomic

diffusion between the atoms of HA and Ti-6Al-4V. Although such diffusion at the ceramic/metal interface promotes physico-chemical linkages between the two materials, at the same time Ti ions have the potential to catalyze the decomposition of HA at temperatures in excess of 1050 ˚C.[59,60]

1.4.3 Structural changes in Ti-6Al-4V

At temperatures $\geq$ 882 ˚C, Ti-6Al-4V undergoes α→β transformation with a change in its crystal structure from the HCP to the BCC type.[59,61] Cooling the metal induces a recrystallization of the β–phase (β→α transformation) in the alloy. However, during the cooling process, some of the β-phase may be retained within the α-phase that affects the mechanical strength of the material. Moreover, Ti-6Al-4V is highly reactive at high temperatures and can oxidize easily, leading to oxygen diffusion and metal embrittlement.[61]

1.5 Low temperature coating techniques

A major disadvantage of plasma spray coating is the high temperature of plasma that is not well tolerated by both, the bioceramic and Ti-6Al-4V. Therefore, other coating techniques that use relatively low temperature have been employed for bioactive ceramic coating. Some of these methods include sol-gel coating, magnetron sputtering, electrophoretic deposition, etc. All of these techniques deposit ceramic coating at room temperature which can then be sintered at moderate temperatures, typically less than 1200 ˚C.[44] Moreover, they permit the deposition of a highly pure material with minimal changes in the crystalline structure before or after coating.

1.5.1 Sol-gel deposition

Sol-gel is a process capable of producing bioactive ceramic coating from solutions. The process is based on the controlled hydrolysis of metal alkoxides to form a suspension of colloidal particles, called sol, which upon polycondensation forms an interconnected network structure, the gel. Typically, HA sol is prepared using a Ca salt such as calcium nitrate tetrahydrate or calcium diethoxide and a P salt such as triammonium phosphate trihydrate or triethyl phosphite.[62,63] The ratio of Ca/P components is maintained between 1.67 - 2.2 at a pH of 6.0 - 7.8 and the mixture is aged for 24 hr under continuous stirring. Ti-6Al-4V substrates are dip-coated or spin-coated by the sol and fired at a temperature of 400 – 1000 ˚C. The thickness of the coating layer can be controlled by the repetition of the dipping process. Sol-gel processing has been very successful in producing fine-grained, homogeneous HA coatings at a relatively low sintering temperature that minimized HA decomposition.[64] Moreover, sol-gel is not a line-of-sight process and can be used to coat complex geometrical shapes, such as porous-coated Ti-6Al-4V implants. However, sol-gel derived HA has been reported to contain small amounts of CaO that has limited biocompatibility.[64]

1.5.2 Magnetron sputtering

The use of magnetron sputtering to deposit thin films for Si-integrated circuits has been used in the electronic devices industry for a long time; however its application in the field of bioactive ceramic coating has only been recently recognized.[65] Magnetrons make use of the fact that a magnetic field parallel to the target surface can constrain secondary electrons in the vicinity of the target.[66] The chamber in which the coating is carried out is evacuated, typically to pressures of 2.5 x 10^{-3} Pa and filled with high purity argon in

combination with oxygen.[67] The high ionization efficiency of the magnetron densifies the plasma in the proximity of the target material, such as bio-ceramics. As a result, the ion bombardment increases leading to enhanced deposition rates on the metal substrate. The advantages of magnetron sputter-coating over other sputtering processes include the high deposition rate, excellent adhesion with the substrate and the ability to coat implants with difficult surface geometries.[44] Moreover, the Ca/P ratio and the crystallinity of the deposit can be tightly controlled.[68] A major advantage of magnetron sputtering is that the process involves low temperature, typically < 600 ˚C, which conserves the crystalline structure of the ceramic and the metal.[66] However, being a line-of-sight process, magnetron sputtering has limited applications in coating porous-coated or foam mesh orthopedic implants.

1.5.3   Electrophoretic deposition

Electrophoretic deposition (EPD) is a wet coating process wherein ceramic particles contained in a suspending medium are directly deposited onto a conductive metallic substrate using an electrical voltage.[69] The simple, inexpensive setup and the possibility of coating stochiometric, high purity material without compromising crystallinity even on complex geometries and porous substrates in a short time makes EPD an attractive method for coating. Figure 1.2 shows a schematic representation of the EPD coating process. The implant to be coated is used as one of the electrode, the polarity of which depends upon the zeta potential of the ceramic particles suspended in a suitable medium. The counter-electrode may be of the same material, or some other inert material such as platinum. The direction of particle migration is determined by the zeta potential of the particles; negatively charged particles move towards the anode, while the positively charged particles move towards the cathode.[70] The two electrodes are attached

to a source of power supply and immersed in the electrophoretic cell. Upon application of electric voltage, the ceramic particles migrate towards the surface of the implant and form the deposit which can then be densified by thermal treatment. The various processing parameters involved in EPD are:

(a) Suspension related: ceramic composition, particle size, chemical nature and pH of the suspending medium, zeta potential of ceramic particles, and the conductivity of the suspension

(b) Process related: deposition time, voltage, concentration of particles, and electrical conductivity of the substrate
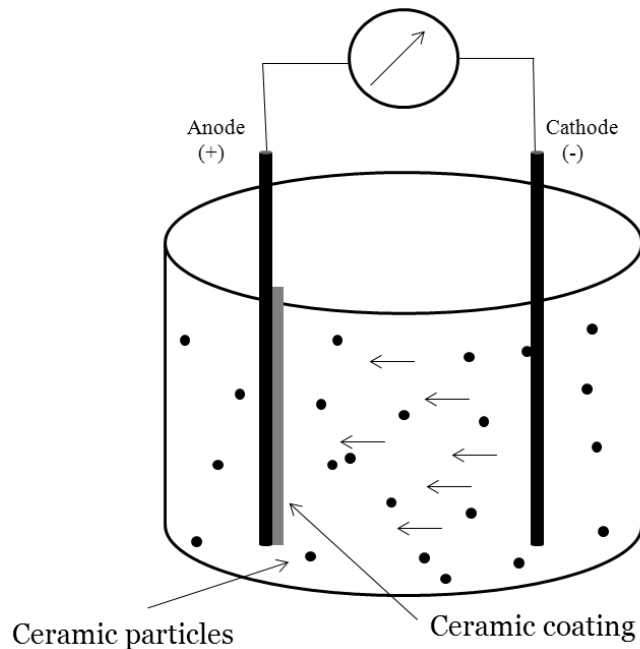
Figure 1.2: Schematic representation of the EPD coating process

1.5.3.1. Origin of zeta potential

Ionic interactions between the ceramic particles and suspending medium such as ionization of functional groups, differential loss of ions from crystal lattice, adsorption or desorption of charged species, etc., increase the concentration of oppositely charged counter-ions in the proximity of the particle.[69,71] The counter-ions initially approach the particle to neutralize their surface charge; however their thermal motion restricts any accumulation on the particle surface.[71] Thus, the particle gets surrounded by an ionic cloud of counter-ions distributed in the form of an electrical double layer around the particle. The electric potential across the double layer is the zeta potential of the particle. Colloidal suspensions exhibiting high zeta potential demonstrate enhanced inter-particle repulsion and are more stable which facilitates their uniform deposition.

1.6   Literature review on bioactive ceramic coating

The concerns highlighted above impress upon the need to address the limitations of bioactive ceramic coating on orthopedic Ti-6Al-4V implants from a processing perspective as well as material considerations. The following section contains a literature review highlighting various strategies employed in the last decade to enhance the adhesion strength of the coating and improve its long-term stability on the metal.

1.6.1   Strategies to improve adhesion strength

Perhaps the most important deterrent to the long-term stability of the bioactive ceramic coating is the poor adhesion between the metal and the ceramic. Various strategies have been evaluated to improve the adhesion strength of the ceramic coating.[62,72-80] One of the methods has been the use of HA/Ti composite coatings.[72,73] Zheng *et al* plasma-sprayed a mixture of HA and Ti powders in a ratio of $0 - 60$ wt% on

Ti-6Al-4V substrate and evaluated the adhesion strength at the interface between the HA/Ti coating layer and the underlying metal substrate according to ASTM C-633 protocol (Standard Test Method for Adhesion or Cohesion Strength of Thermal Spray Coatings) using a polymeric glue.[72] It was found that the average adhesion strength of the coating increased from 13 MPa to 17 MPa as the Ti concentration in the composite increased. However, the bond strength after immersion in physiologic solution was not measured. Examination of the fractured surface of the samples showed adhesive failure mechanism, most probably due to the decomposition of HA. In a related work, Gu *et al* deposited a mixture of HA and Ti-6Al-4V particles (in a 1:1 ratio) on Ti-6Al-4V substrate and evaluated the adhesion strength of the coating according to the ASTM C-633 protocol.[73] They reported that the average adhesion strength at the metal/ceramic interface increased from 18.36 MPa for unmodified HA coating to 27.38 MPa for HA/Ti-6Al-4V composite coating. X-ray diffraction (XRD) analyses of the coating layer showed peaks for CaO while those characteristic for HA were largely absent due to HA decomposition after plasma spraying, as explained by the authors. Facture surface analyses showed a mixed mode of failure; a cohesive fracture within the lamellae of the HA/Ti-6Al-4V coating layer and an adhesive fracture at the metal/ceramic interface. The cohesive fracture observed was most probably due to the failure within the lamellae of the coating layer that forms during plasma spraying.[50,51] The adhesion strength of the coating layer reduced by 31% after 2 weeks immersion in physiologic solution due to the synergistic effects of surface cracking and material dissolution. Chen *et al* used magnetron sputtering to deposit multiple layers of HA/Ti mixtures in ratios of 0, 20, 50, 90 or 100% to generate a graded Ti concentration in the coating layer, with the 100% Ti

being at the interface with the metal substrate.[74] The effect of annealing treatment of the coated substrate on the adhesion strength was evaluated. In order to obtain a crystalline HA coating, the samples coated with HA or HA/Ti mixtures were again thermally treated at 600 ˚C for 1 hr under water vapor flow. Adhesion strength tests carried out in accordance with ASTM C-633 protocol showed that the second annealing treatment resulted in a reduction of the average adhesion strength, most probably due to dissolution at the interface between the coating layer and the metal substrate. The addition of Ti to HA powder increased the adhesion strength of the coating layer from 25 MPa (HA coating) to 40 MPa (HA/Ti coating). It should be noted that the authors did not analyze the structure of the ceramic layer after coating; therefore, the data from this study cannot be compared to other reports.

Other efforts to improve adhesion strength include the incorporation of TiO_2, either within the coating or as an intermediate layer between HA and metal substrate.[62,75,76] Kim *et al* used sol-gel processing to prepare HA and TiO_2 sols separately and mixed them in ratios of 10 - 40% to obtain HA-TiO_2 composite sols.[62] They coated pure HA as well as composite HA/TiO_2 sols on commercially pure (cp) Ti substrate and heat-treated the samples at 450 - 550 ˚C for 2 hr at a fixed heating and cooling rate of 1 ˚C min^{-1}. Mechanical tests using proprietary epoxy glue showed that the adhesion strength of the coating increased due to the addition of TiO_2 sols. The average adhesion strength increased from 36 MPa for pure HA coating to 56 MPa for HA mixed with 30% TiO_2 after heat treatment at 500 ˚C. However, XRD analysis showed that the HA formed was poorly crystalline even after heat treatment at 550 ˚C. Moreover, the heat treatment at 500 ˚C was accompanied by the formation of the anatase and rutile phases of Ti.

Previous studies using human dermal fibroblasts and human lung epithelial cells have shown that the anatase phase is 100 times more toxic than the rutile phase.[81] Fracture surface analysis showed a mixed failure mode, with failure taking place at the coating/metal interface, within the coating, at the coating/epoxy interface or within the epoxy for all samples. It was also found that the area on the fractured surface related to failure within the coating or at the coating/metal interface increased with decreasing TiO_2 concentration. However, the authors did not evaluate the effect of material dissolution on the adhesion strength of the coated layer. Albayrak *et al* studied the effect of intermediate TiO_2 layer between HA and Ti-6Al-4V substrate on enhancing the shear strength of the HA coating.[75] They passivated Ti-6Al-4V substrates in 25% HNO_3 and used EPD to deposit an intermediate layer of TiO_2 particles before finally coating with HA. The voltage used for coating TiO_2 was varied between 10 - 50 V and while HA was coated at a fixed voltage of 200 V. Mechanical tests using ASTM F1044-99 protocol (Standard Test Method for Shear Testing of Calcium Phosphate Coatings and Metallic Coatings) using a polymeric glue showed that the shear strength of the HA/TiO_2 coating layer increased from 11.9 ± 3.3 MPa to 21.0 ± 2.9 MPa as the voltage for TiO_2 deposition decreased from 50 V to 10 V. On the other hand, HA deposited on Ti-6Al-4V substrate in the absence of TiO_2 developed an adhesion strength of 13.8 ± 1.8 MPa. It was observed that surface cracks on the TiO_2 layer increased with increasing deposition voltage. The authors also reported that the thermal decomposition of HA was reduced by the incorporation of TiO_2 layer, most probably since the decomposition of HA induced by Ti begins at a lower temperature than that induced by TiO_2;[82] hence, it may be possible that the TiO_2 layer acted as a chemical barrier between Ti-6Al-4V and HA. The authors

explained that the enhancement of the shear strength was due to the thermal expansion coefficient of TiO_2 (9.36×10^{-6} K^{-1}) being intermediate to that of Ti-6Al-4V (8.60×10^{-6} K^{-1}) and HA (11.5-14.75×10^{-6} K^{-1}) which may have reduced the thermal stresses at the metal/ceramic interface. However, the authors ignored the effect of HNO_3 passivation on Ti-6Al-4V. Previous studies have shown that such passivation treatment produces a porous TiO_2 layer on the metal's surface.[83] Therefore, the explicit contribution of the deposited TiO_2 layer on the enhancement of shear strength may not be accurate. Moreover, they did not vary the voltage for HA deposition to analyze if this parameter could affect shear strength or coating characteristics. In addition, they did not analyze the stability of the coating in physiologic solution. The use of TiO_2 was also adopted by Cannillo *et al* who developed a multi-layered, functionally graded coating of TiO_2 and HA on Ti-6Al-4V substrate using plasma spraying.[76] The coating comprised 100% TiO_2 at the interface with the metal and progressively decreased in TiO_2 concentration towards the outer surface of the coating, which contained 100% HA. Moreover, they heat treated the coating again at 750 ˚C to further improve its mechanical properties. Vicker's micro-indentation tests of the HA rich areas on the sample showed that the hardness of HA layer increased from 208.3 ± 38.8 to 302.3 ± 101.2 $HV_{0.1}$ after heat treatment, thus confirming the strengthening effect of TiO_2. However, the authors did not measure the adhesion strength of the functionally graded coating at the metal/ceramic interface. Nor, did they evaluate the dissolution effects of the coating in physiologic solution.

The use of Ti or TiO_2 to enhance the adhesion strength of the coating should be treated with caution. Since the adhesion strength between the metal substrate and Ti particles is higher than that between the metal and HA particles, the final adhesion

strength between Ti/HA mixture and the Ti-6Al-4V substrate will be the average

contribution from Ti-Ti and HA-Ti adhesion, respectively. Although, improvement in the

adhesion strength between the metal substrate and a mixture of HA and Ti powder was

observed, this increase should be looked at as a result of a decrease in the contact area

between HA and substrate's surface, and not due to improved adhesion between HA and

Ti. Moreover, the dissolution of HA in aqueous environment would leave behind metallic

residual Ti/TiO$_2$ particulate matter that can irritate the immune system. Indeed, one of the

major reasons for the failure of hip implants is the release of high concentration of Ti

particles and wear-debris from the implant surface. Therefore, HA dissolution in the

HA/Ti coating layer would facilitate the release of Ti particles which could significantly

contribute to implant failure. In addition, none of the above studies reported the nature of

the interface between HA and Ti-6Al-4V substrate in the coating layer.

Other approaches to improve the mechanical strength of bio-ceramic coating on

metal implants include the use of modified CaP ceramics as described by Lin *et al*. They

coated OCP on metallic substrates with different surface topographies: grit-blasted, arc-

deposited, chemically textured and Co-Cr beaded surfaces using modulated

electrochemical deposition (MECD) technique.[77] OCP is a CaP ceramic that has

demonstrated greater resorbability and bone formation ability than pure HA or β-TCP

ceramics.[84,85] Analyses of the OCP-coated substrates using XRD and FTIR methods

showed characteristic peaks for OCP in both spectra. Adhesion strength measurements

carried out according to ASTM F1501 protocol (Specifications for calcium phosphate

coating for implantable materials) using polymeric glue showed that the average adhesion

strength on grit-blasted substrate (48 MPa) was significantly higher than on the other

substrates. The authors explained that the variations in adhesion strength might have been due to variability in the surface roughness of the substrate; however, they did not present the data on the substrate's roughness. Moreover, they did not analyze the fractured surface of the substrate to determine the mode of failure. It is not clear how the adhesion strength measurements were performed on the Co-Cr beaded substrates since the entire surface of the spherical bead structure cannot be uniaxially subjected to tensile loading. Immersion of the coated substrates in 0.1 M tris buffer solution at pH 7.3 and 3.0 for 4 hr showed that the samples released higher concentration of Ca^{2+} under acidic conditions than under neutral conditions. However, they did not analyze the change in the adhesion strength of the coating after immersion in physiologic solution.

Recent studies in the literature have reported on the use of carbon nanotubes (CNT) to enhance the mechanical properties of CaP coating.[78-80] Balani *et al* mixed HA particles (10 - 50 μm) with 4 wt% CNT (40 - 70 nm dia x 0.5 - 2.0 μm length) for 18 hr in a jar mill in an attempt to homogeneously disperse CNT over HA particles.[78] Powdered HA/CNT mixture was coated on Ti-6Al-4V substrate using plasma spraying. Microstructural observation of the coated substrates showed that the HA coating without CNT demonstrated sub-surface cracks and partially fused particles whereas HA coatings containing CNT showed melt-resolidified and nodular HA particles. XRD analyses showed an increase in the crystallinity of HA from 53.7% to 80.4% upon addition of CNT as per the differential peak degradation calculation. The authors hypothesized that the three orders of higher thermal conductivity of CNT (3×10^3 W m^{-1} K^{-1}) as compared to HA (0.7×10^3 W m^{-1} K^{-1}), may concentrate thermal energy around the CNT surfaces in contact with HA. As a result, the time available for HA nucleation at elevated

temperature would increase. Vicker's tests showed that the indentation toughness of the coating increased from 0.39 ± 0.09 MPa m$^{1/2}$ to 0.61 ± 0.09 MPa m$^{1/2}$ after CNT addition. The increase in toughness of the coating was attributed to the CNT distribution and anchoring of CNTs to form bridge structures that can withstand high bending deformation. However, the authors did not evaluate the stability of the HA/CNT coating or its interaction with physiologic solution, nor did they analyze the adhesion strength of the coating. Other studies by Kaya *et al* and Hahn *et al* have employed nano-size HA particles in conjunction with CNT to enhance the coating characteristics.[79,80] Kaya *et al* prepared a (0.5 – 2.0 wt%) mixture of acid-treated CNT (20 nm dia) with HA particles (20 nm dia) in an aqueous solution and coated the mixture on Ti-6Al-4V substrate using EPD at 20 V in a 5 wt% CNT containing HA suspension.[80] Acid treatment is thought to confer negative charge to the CNT particles which can then electrostatically associate with positively charged HA to form a single composite particle. SEM analyses of the coated samples after sintering at 600 ˚C for 2 hr under nitrogen showed that an increase in the coating duration from 4 min to 10 min increased the coating thickness from 25 to 40 μm. However, the increase in the coating thickness was accompanied by the appearance of surface micro-cracks after sintering. Mechanical tests showed that the shear strength of the coating increased from 0.7 ± 0.04 MPa to 1.84 ± 0.1 and 2.76 ± 0.14 MPa upon the addition of 1 and 2% CNT, respectively. The elastic modulus of the coating increased from 15 ± 0.4 GPa to 139 ± 7 and 178 ± 8.5 GPa and the hardness increased from 4.88 ± 0.2 GPa to 18.9 ± 1.2 and 36.44 ± 2.3 GPa, respectively. However, the authors did not investigate the influence of voltage, sintering temperature or the heating/cooling rate on the mechanical properties of the HA/CNT coating. Neither did

they evaluate the stability of the coating in physiologic solution. Hahn *et al* prepared a (1 - 3 wt%) mixture of acid-treated CNT (10 - 15 nm dia x 10 - 20 nm length) in an aqueous solution containing HA particles (15 nm) and coated the mixture on cp-Ti substrates using aerosol deposition at 900 ˚C.[79,86] Analysis of adhesion strength according to ISO 13779-4 protocol showed that the adhesion strength was in the range of 27.3 – 29.0 MPa with or without CNT. It was interesting to note that the addition of CNT had minimal effect on adhesion strength, most probably because CNT acted as a reinforcement phase for HA coating but did not physically or chemically bond to the metal substrate. Nano-indentation tests showed that the hardness and elastic modulus of the coating increased from 6.19 - 6.76 GPa and 122 - 125 GPa for unmodified HA to 9.02 GPa and 137.05 GPa for HA containing 3 wt% CNT, respectively. Thus, the increase in hardness and elastic modulus of coating serve to reduce the brittle nature of HA. XRD analysis of the HA/CNT coated substrate showed weak and broad peaks of HA. The authors hypothesized that such peaks may have been due to a reduction in the grain size during the coating process. However, the authors prepared HA/CNT mixtures in an aqueous solution which may have resulted in partial dissolution of HA even before coating fabrication. Moreover, the authors did not evaluate the effect of physiologic solution treatment on the adhesion strength and mechanical properties of the coating.

1.6.2   Evaluation of coating stability

Although stochiometric HA is quite stable in physiologic solution, the decomposition of HA during the plasma spraying process produces byproduct phases within the coating that have variable crystallinity and solubility, and can therefore affect the stability of the HA coating. Fazan *et al* studied the stability of plasma sprayed HA

coating on cp-Ti substrate for 2 weeks in aqueous (double distilled DI water) and tris-buffer solution and found that the surface cracks on the HA increased after 2 weeks of immersion.[87] Moreover, the dissolution of the HA coating was more severe and rapid in the physiologic solution than in aqueous solution, most probably due to the high ionic content of the latter solution. XRD and ion concentration analyses suggested that the TCP phase produced during plasma spraying dissolved faster than the bulk of the HA coating. The authors suggested that TCP may react with water and initiate dissolution-precipitation reactions which can increase the crystallinity of the coating. To ascertain the effect of HA crystallinity on coating dissolution behavior, the HA-coated samples were heat-treated 600 ˚C for 1 hr. It was found that the increase in the crystallinity of the coating decreased the rate of HA dissolution and enhanced its stability. However, the authors conducted the study under static fluid conditions which may have increased in the concentrations of solutes beyond the physiological limits. Moreover, they did not analyze the adhesion strength at the metal/ceramic interface before or after the immersion period. Zheng *et al* coated HA or a mixture of HA/Ti on Ti-6Al-4V substrate by plasma spraying and analyzed the stability of the coating in simulated body fluid (SBF) for 2 weeks.[72] XRD analyses of the coating showed that that peaks corresponding to the TCP and CaO byproduct phases disappeared after the immersion period. Moreover, they found the appearance of TiO and TiO_2 peaks in the XRD spectra and concluded that the metal in the outer as well as inner coating layers became oxidized during immersion. However, the exposure of inner coating layers to SBF may enhance its dissolution and affect the overall stability of the ceramic coating. In addition, the authors did not analyze the

changes in the mass or the thickness of the coating during immersion, nor did they measure the ionic concentrations of the dissolution products.

Gu *et al* investigated the stability of HA/Ti-6Al-4V coated Ti-6Al-4V substrate in SBF for 8 weeks and found that the average Ca^{2+} concentration in the immersing solution increased by 54% after 1 week of immersion.[73] The increase in Ca^{2+} concentration was followed by an exponential decrease resulting from CaP precipitation due to the super-saturation of the solution. Moreover, XRD analyses of the samples showed that CaO phase of the coating started to dissolve as early as 1 day of immersion and was completely dissolved within 2 weeks. They found an increase in the crystallinity of the coating with increasing periods of immersion, similar to that reported by Fazan *et al* and Zheng *et al*.[72,87] The authors compared the dissolution rate of HA/Ti-6Al-4V composite coating to previous studies in the literature that measured dissolution rate of pure HA coating and reported that the former substrate exhibited slower dissolution rate. According to their explanation, the presence of Ti-6Al-4V in the coating might have reduced the porosity of the coating, thereby limiting the access of physiologic solution to the interior of the coating. However, it could also be argued that the lower rate of dissolution observed in this study was simply due to the lower amount of HA ceramic present in the coating. In another study, Dinda *et al* studied the stability of amorphous and crystalline HA coating on Ti-6Al-4V substrate in SBF with and without Ca.[88] They measured the mass of the sample immersed in both kinds of solution for 5 days and found that crystalline HA coating showed negligible mass loss in Ca-containing SBF solution and a partial mass loss in Ca-free SBF solution. On the other hand, amorphous HA coating showed partial mass loss in Ca-containing SBF solution, while immersion in Ca-

free SBF solution resulted in complete mass loss as early as 3 days. The authors considered the change the mass of the sample as a measure of coating dissolution and concluded that amorphous HA is more unstable than crystalline HA and that the dissolution of the material was enhanced in Ca-free SBF solution. However, they ignored that the synergistic effects of ceramic dissolution and back-precipitation onto the coating surface might contaminate the mass loss results. Moreover, they did not evaluate the ionic concentrations of Ca and P released from the HA coating which could be correlated to the mass-loss from the coating.

One of the well-known factors associated with implant failure is the release of ions from the implant that can irritate the immune system.[89,90] Increased presence of metal ions has the potential to attract macrophages and phagocytes to the site of the implant. The activity of these cells creates an acidic environment around the implant which may enhance coating dissolution.[91] However, none of the studies on coating stability described above measured the concentration of Ti ions released into the immersing solution. At the same time, these studies do not discuss the relationship among coating stability, material resorption and new bone formation. High rate of ceramic dissolution may lead to the depletion of coating layer before new bone formation or tissue integration can take place. On the other hand, slow degradation rate may fail to have a desired osteogeneic effect on the cells. Moreover, these studies did not evaluate the long-term stability of the coating and the nature of the metal/ceramic interface after immersion in physiological solution. A common observation in these studies was the initial increase in the Ca^{2+} of the medium due to HA dissolution, followed by the precipitation of a CaP layer onto the coating. However, it would be interesting if the material could rapidly

uptake Ca^{2+} from the medium and concentrate it onto the coating surface. This would serve two purposes; first, it would promote faster nucleation of the biological HA layer on the coating surface and second, it would enhance osteoblast activity by providing an abundance of Ca^{2+}.

1.7 Evaluation of bone cell response to bioactive ceramic coated implants

The ultimate purpose of coating bioactive ceramic on orthopedic implants is to provide an osteoconductive and/or osteoinductive surface that stimulates bone cell activity, in particular differentiation and bone matrix mineralization. Various research groups have adopted different techniques to assess bone cell response to bioactive ceramic coated implant including analyses of osteogenic protein markers, phenotypic expression or *in vivo* studies.

Kim *et al* evaluated cell activity of human osteosarcoma HOS (T-85) cells on HA/TiO_2 composite coatings containing 10 - 30% TiO_2 and found comparable cell proliferation on HA-coated substrates with or without TiO_2 or on uncoated substrates throughout 5 days of incubation.[62] Analyses of AP activity showed that cells attached to substrates containing 20% TiO_2/HA coating expressed slightly higher AP activity (0.150 μmol p-NP/hr/mg protein) than cells attached to unmodified HA-coated substrates (0.225 μmol p-NP/hr/mg protein), although the difference was not statistically significant. The increase in cell response to 20% TiO_2/HA substrate were attributed to the physical and chemical alterations in substrate's surface, such as homogeneity, grain size and surface chemistry as per the author's explanation. Thian *et al* studied the response of human osteoblast-like (HOB) cells to Ti substrates coated with nanocrystalline Si-substituted HA of different Si concentrations (0.8, 2.2 or 4.9 wt%)[92]. Their results showed that cell

proliferation increased on all substrates up to 14 days except for the substrate coated with 4.9% Si-HA, which showed decreased cell proliferation after 7 days. Visualization of actin cytoskeleton after 1 day in culture showed well-developed actin filaments on cells attached to substrates containing 2.2 or 4.9% Si-HA but less distinct on substrate with 0.8% Si-HA. In contrast, cells attached to the uncoated Ti substrates appeared devoid of microfilaments in the cell membrane. Cell morphology analyses showed well-spread cells on all Si-containing substrates; however, cells attached to uncoated Ti substrates showed less pronounced spreading and under-developed lamellipodia. The authors attributed the enhanced cell activity on 4.9% Si-HA coated substrate to the formation of silicate network structure which enhanced protein adsorption. Moreover, the decreased cell proliferation observed on 4.9% Si-HA coated substrate was attributed to enhanced CaP precipitation on the material surface which may stimulate cell differentiation. The authors argued that early cell differentiation resulted in a decrease in cell proliferation on this substrate, an idea shared by other researchers as well.[93,94] However, both these studies by Kim *et al* and Thian *et al* did not evaluate the effect of coating dissolution and ion release on bone cell activity; nor did they analyze the role of protein adsorption on cell attachment and differentiation.

The role of protein adsorption on bone cell activity was addressed by Zhu *et al* who studied the effect of HA coating on protein adsorption and bone cell response and compared it to that on uncoated or porous TiO_2-coated Ti substrates.[95] Their results showed that the HA-coated substrates adsorbed the highest quantity of proteins, fibronectin and laminin, followed by the porous TiO_2-coated substrates and uncoated Ti substrates, respectively. The authors explained that the differences in the protein

adsorption behavior were due to the variability in the surface roughness and chemistry of the substrates. However, they analyzed protein adsorption on the substrates using single, pure protein solution. Under *in vivo* conditions, physiologic fluids will contain a variety of proteins which may compete for binding on the substrate's surface. Therefore, a more accurate representation of protein adsorption is that from the serum, which is a complex mixture of many different proteins. Moreover, they did not analyze the conformation of the adsorbed protein molecules which is an important factor that dictates cell attachment to the implant surface. Previous studies have shown that substrate induced changes in the conformation of fibronectin can control the switch between cell proliferation and differentiation.[96] Analyses of cell response to the substrates showed higher cell proliferation and differentiation on cells attached to HA-coated substrates than porous-coated TiO_2 or uncoated substrates. The authors relied on AP activity measurement as an indicator of cell differentiation; however late stage cell differentiation markers such, as osteocalcin or osteopontin, were not analyzed. Nonetheless, animal studies demonstrated the greater stimulatory effect of HA-coating on new bone formation. Hahn *et al* evaluated the stimulatory effect of CNT/HA coated cp-Ti on bone cell activity and found that cell spreading on the substrate coated with 3% CNT/HA was higher than that on uncoated or HA-coated substrates.[79] Moreover, the cytotoxicity of CNT/HA coated substrate was lower than that of HA-coated substrate, which was in-turn lower than that of the uncoated Ti substrates. They also analyzed the effect of CNT concentration on cell proliferation after 5 days and found that an increase in the CNT concentration from 0% to 3% enhanced cell proliferation. Similarly, the AP activity of cells increased with increasing CNT concentration after 10 days in culture. However, the authors measured the AP

activity at 10th day only although AP expression is known to be time dependent.[97] Moreover, they did not analyze the expression of late-stage osteoblast differentiation markers, such as osteocalcin. Moreover, the biocompatibility of CNT continues to be an ongoing debate. Some researchers have questioned the long-term systemic effects and found that if CNT reaches the lungs, they can elicit strong inflammatory and fibrotic reactions and increase chances of lung cancer. [98,99]

The earliest signals for stimulatory effect of the material are manifested at the mRNA level; therefore it is prudent to evaluate the expression of osteogenic gene markers for cell proliferation and differentiation. Wang *et al* studied the effect of material composition, crystal size, crystallinity, solubility and surface topography of three different types of CaP coating; carbonate apatite deposited via biomimetic (BCA) or electrolytic methods (ECA) and OCP, on the proliferation and differentiation of bone cells.[100] It was found that cell proliferation and differentiation on the coating increased in the order of increasing solubility and decreasing crystallinity, as shown by osteogenic proteins assays (AP and collagen) and gene expression analyses (bone sialoprotein and octeocalcin). Thus, BCA coating which was characterized by high solubility, small crystal size and poorly crystalline structure stimulated bone cell activity more than ECA coating which had higher crystal size, higher crystallinity and lower solubility than BCA. OCP-coating demonstrated intermediate stimulatory effect on cell activity as compared to BCA and ECA coating, although it had higher crystallinity and crystal size but lower solubility than ECA coating. However, no definite relationship between surface roughness and cell activity were found; BCA coating with the highest surface roughness demonstrated greater stimulatory effect on cell proliferation and differentiation while

ECA coating with intermediate surface roughness had lower stimulatory effect on cell activity than OCP coating which had the lowest surface roughness. The results of the study suggest that the composition, crystallinity and solubility of the CaP coating have strong effects on cell proliferation and differentiation. However, the stimulatory or inhibitory effects of coating's surface roughness may be masked by the dissolution products of the ceramic as well as other chemical factors in the medium. Knabe *et al* investigated the effect of HA-coated cp-Ti implants on the temporal phenotypic expression of human bone derived cells for 21 days.[101] They used three different Ti substrates; machined Ti (Ti-ma), Ti with deep profile structure (Ti-DPS) and porous Ti plasma-sprayed (Ti-TPS) coating having average roughness (R_a) of 0.15 ± 0.04, 2.91 ± 0.53 and 3.43 ± 0.63 μm, respectively. HA-coated Ti samples had an average surface roughness of 2.07 ± 0.36 μm. They found that the bone cells attached to all uncoated Ti substrates showed comparable proliferation up to 21 days, indicating that surface roughness alone had minimal effect on cell proliferation. On the other hand, bone cells attached to the HA-coated substrates showed higher cell proliferation at all time-points. Analyses of osteogenic mRNA's and proteins showed that HA-coated substrates demonstrated the highest stimulatory effect on bone cell differentiation. However, it was found that at early time point, (day 3) the concentration of proteins expression on uncoated Ti substrates was higher than that on HA-coated substrates, most probably due to a lag-phase encountered by the bone cells on the latter substrate, as per the author's explanation. Moreover, bone cells attached to the smooth Ti-DPS samples showed greater cell differentiation than the cells on rougher Ti-TPS substrates, which may have been due to the variability in surface roughness. The authors found no correlation

between different levels of osteogeneic mRNA and their translated protein, either due to incomplete translation or due to the shorter half-life of mRNA compared to protein that might have compromises the sensitivity of the measurement. However, both studies, by Wang *et al* and Knabe *et al* did not analyze the effect of proteins adsorbed on the implant material on cell activity.

1.8   Motivation

The discussion presented above highlights two potential shortcomings: first, there is a need for the development of a bioactive ceramic material that has superior mechanical properties, bioactivity and resorbability than traditional ceramics. Second, the use a deposition technique that is simple, economical and can produce a uniform coating of homogeneous microstructure without damaging the ceramic or the metal substrate. Crystalline HA is characterized by high chemical stability that resists material dissolution and therefore has low resorbability. Moreover, the slow release of HA dissolution ions, such as Ca and P, limit the osteoconductive and/or osteoinductive effect of the coating on bone cell function. On the other hand, biphasic ceramic coating of HA and β-TCP have demonstrated enhanced material dissolution; however, the effect of material dissolution was not translated to an increased bone cell activity. The high temperature used in plasma spraying process causes some decomposition of HA and produces undesired phases of variable solubility and biocompatibility. Si containing biomaterials, such as BG, have shown enhanced bioactivity and bone bonding ability; however, the material is thermally unstable at temperatures $\geq$ 600 ˚C. Previous studies have shown that moderately low coating temperature of 600 – 700 ˚C can cause an uncontrolled precipitation of crystalline phases within the glass matrix that can compromise the bioactivity of the material.[102]

Another important factor that has not been adequately addressed is the adhesion strength at the interface between the ceramic and metal. Many reports in the literature have indicated that adhesion strength between HA and Ti-6Al-4V is often below the ASTM (F1147-05) recommended standard of 30 MPa. Inadequate adhesion between the ceramic and metal destabilizes the ceramic coating and increases the chance of implant micro-motion.

Recently, El-Ghannam *et al* have proposed a novel silica-calcium phosphate nanocomposite (SCPC) as potential bioactive resorbable bone graft material. Previous studies have shown that SCPC has superior mechanical strength and bone regenerative capability than HA or BG.[103] The enhanced bioactivity of the SCPC is attributed to its unique phase composition and modified nano-crystalline structure composed of β-NaCaPO$_4$ (β-rhenanite) and α-SiO$_2$ (α-cristobalite) solid solutions. Transmission electron microscopy (TEM) analysis showed that the grain size of SCPC is in the range of 50 – 300 nm.[104] Moreover, SCPC is characterized by a highly porous matrix with pores ranging from 2 nm to 650 μm. Such heterogeneous pore distribution enhances the resorption of the material by increasing the surface area in contact with tissue fluid. In addition, the high surface area of SCPC facilitates enhanced protein adsorption and cell adhesion to the material. SCPC has demonstrated its ability as a potential drug-delivery vehicle for various synthetic and peptide drugs including bone morphogenic protein (BMP)-2, gentamicin, vancomycin and 5-fluorouracil.[105-107] Bone marrow mesenchymal stem cells attached to SCPC samples loaded with recombinant BMP-2 synthesized mineralized extracellular matrix (ECM) as compared to HA-rhBMP-2 samples that showed unmineralized ECM.[104] Moreover, SCPC up-regulated the expression of genes

associated with osteoblast proliferation and differentiation such as collagen-I, osteopontin, osteonectin and osteocalcin significantly more than HA or BG.[108] *In vivo* studies in rabbits have shown that critical size bone defects implanted with SCPC particles demonstrated near-complete bone formation accompanied by graft resorption within 3 weeks of implantation.[103] On the other hand, similar defects grafted with BG particles also showed bone formation, however the defects contained significant amount of unresorbed BG particles.

1.9 Objective

The objective of this study was to coat bioactive SCPC on medical grade Ti-6Al-4V implant using electrophoretic deposition (EPD) and maximize the adhesion strength at the metal/ceramic interface. In addition, the bioactivity and stimulatory effect of SCPC coated Ti-6Al-4V implant on bone cell function was evaluated at a molecular level and correlated to SCPC's surface chemistry, protein adsorption and material dissolution characteristics. The specific aims are:

- Systematically vary the chemical composition of SCPC, suspending medium and medium pH to create a stable suspension wherein the SCPC particles will exhibit maximum zeta potential.

- Optimize the EPD coating parameters to obtain a homogeneous coating of SCPC particles on Ti-6Al-4V substrate

- Maximize the adhesion strength at the interface between SCPC coating and Ti-6Al-4V substrate by optimizing the thermal treatment protocol.

- Evaluate bone cell response to SCPC-coated Ti-6Al-4V substrate at the molecular level by analyzing mRNA expression and protein synthesis. Moreover, the bone cell

response would be correlated to the quantity, nature and conformation of proteins adsorbed onto the SCPC-coated substrate.

- Investigate the mechanism of SCPC coating development on Ti-6Al-4V and evaluate the relationship between implant surface roughness and bone cell activity.

CHAPTER 2: ELECTROPHORETIC DEPOSITION OF BIOACTIVE SILICA-CALCIUM PHOSPHATE NANOCOMPOSITE ON TI-6AL-4V ORTHOPEDIC IMPLANT

2.1 IntroductionTissue integration between bone and orthopedic biomaterials is essential for implant fixation and long-term stability. An adverse response to metallic implants is the formation of a non-adherent fibrous capsule.[109-112] Fibrous encapsulation of the implant is a non-ideal interface for two reasons: first, the fibrous capsule does not properly transfer the mechanical signal from metal to bone. Second, it allows micro-motion, the range of which would increase by time causing implant loosening. To enhance tissue integration, metal implants are coated with bioactive ceramics such as calcium phosphates.[62,77,113] Hydroxyapatite (HA) coating provides an osteoconductive surface that promotes rapid and direct bone bonding with the Ti-6Al-4V implants. Despite the commercial success, there are many shortcomings associated with the HA coated metals due to plasma spraying technique. The high temperature involved in the coating process results in the decomposition of HA into various undesirable phases including tri-calcium phosphate, tetra-calcium phosphate, calcium oxide and oxy-hydroxyapatite.[51,114,115] Moreover, several studies have shown that Ti-6Al-4V catalyzes the decomposition of HA at high temperature.[59,60]

Silica-calcium phosphate nanocomposite (SCPC) is a novel bioactive resorbable ceramic that has the ability to bond to bone and expedite bone formation. Previous reports have demonstrated the superior bone regenerative capability, mechanical

properties and resorbability of SCPC as compared to hydroxyapatite or bioactive glass.[104,108] The enhanced bioactivity of the SCPC has been attributed to its unique phase composition, modified nano-crystalline structure, and high porosity.[103,104,108,116] SCPC demonstrated the formation of a surface apatite layer within 2 hr of immersion in simulated body fluid.[108] Moreover, SCPC developed the apatite surface layer in the presence of serum proteins.[103,104] Real-time polymerase chain reaction analyses demonstrated that SCPC up-regulated osteoblastic gene expression significantly higher than HA.[108] *In vivo* studies have shown rapid bone formation and graft material resorption in critical size bone defects implanted with SCPC. In contrast, similar defects implanted with bioactive glass granules showed bone formation but minimal graft resorption.[103] Moreover, SCPC has demonstrated its ability as a potential drug-delivery vehicle for rh-BMP2, gentamicin, vancomycin, and 5-fluorouracil.[104-107] The objective in this study is to investigate the possibility of coating bioactive SCPC on medical grade Ti-6Al-4V implant using electrophoretic deposition (EPD). The relationship among the chemical compositions of SCPC, zeta potential and conductivity has been reported. The adhesion strength at the interface between SCPC and Ti-6Al-4V implant before and after immersion in physiological solution has been measured. Moreover, the bioactivity of the SCPC-coated Ti-6Al-4V implant was analyzed in-vitro.

2.2 Materials and Methods

2.2.1 Ceramic preparation

Three different formulas of SCPC ceramic: SCPC25 (in mol %: 52.53% CaO, 26.27% P_2O_5, 10.6% Na_2O and 10.6% SiO_2), SCPC50 (in mol %: 40.68% CaO, 20.34% P_2O_5, 19.49% Na_2O and 19.49% SiO_2) and SCPC75 (in mol %: 22.8% CaO, 11.4% P_2O_5, 32.9% Na_2O and 32.9% SiO_2) were prepared by sintering at 850 ºC for 2 hr in air.[103,108]

Chemicals for SCPC preparation were purchased from Sigma Aldrich, St. Louis, MO. The samples were ground in a roller jar mill for 12 hr and separated mechanically on stainless steel set of sieves. SCPC particles less than 600 μm were further ground in a PM-100 planetary ball mill (Retsch Technology, Newtown, PA) at 500 rpm for 24 hr.

2.2.2   Particle size distribution analysis

A 0.5 wt% suspension of SCPC50 particles was prepared in pure ethanol and subjected to ultra-sonic agitation for 45 min. 100 μL of the ceramic suspension was pipetted onto a stainless steel stub, dried, coated with gold and analyzed by scanning electron microscope equipped with energy - dispersive X-ray spectroscope (SEM-EDX, JSM-6480, JEOL USA Inc, Waterford, VA) at 10 kV. Multiple images (n = 20) of the ceramic particles (4288 SCPC50 particles) were obtained at a magnification of 7,500X or 10,000X and the size of each individual particle was determined using an image analysis program (Scandium, Soft Imaging Solutions, Center Valley, PA). The data were presented in the form of a histogram showing particle size distribution.

2.2.3   Zeta potential and conductivity measurements

The zeta potential and conductance of SCPC particles suspended in various dilutions of ethanol (100%, 50% and DI water) were measured using ZetaPALS (Brookhaven Instruments Corporation, Holtsville, NY). Moreover, to study the effect of pH on the surface charge, the zeta potential and conductance of SCPC particles were measured in 50% ethanol at pH values of 2 to 9 at 24 ºC. The pH of the suspension was varied using 0.01N NH_4OH or 0.01N HNO_3. Zeta potential (ζ) was determined by the Smoluchowski equation:

$$\zeta = 4\pi\, \eta\, \mu/\, \varepsilon$$

where μ (V s cm^{-2}), η (cm^2 s^{-1}) and ε are the electrophoretic mobility, viscosity and the dielectric constant of the medium, respectively. The conductance values were used to calculate the conductivity of the SCPC particles using the relationship:

$$\text{Conductivity} = \text{Cell constant} \times \text{Conductance}$$

A cell constant of 0.36 cm^{-1} was used based on experimental measurement of the conductance of 1mM KCl standard of known conductivity (137 μS cm^{-1} at 24 ºC). Each individual sample was subjected to 10 measurements to ensure repeatability. The experiment was carried out in triplicate (n = 3).

2.2.4 Surface preparation of Ti-6Al-4V for coating

Ti-6Al-4V ELI discs (ASTM F136-08e1) of dimensions 1.3 cm dia x 0.5 cm thick (supplied by DePuy Inc., Warsaw, IN) were ground on a 400 grit silicon carbide abrasive pad (Leco Corporation, St. Joseph, MI), washed and cleaned according to the ASTM standard protocol F86-04 (Standard Practice for Surface Preparation and Marking of Metallic Surgical Implants) using DI water, phosphate-free detergent and acetone. Passivation of the Ti-6Al-4V discs was carried out in 34% HNO$_3$ at 65 ºC for 40 min followed by rinsing with DI water. Previous studies have shown that such surface modification would create a thin homogenous TiO$_2$ layer on the material surface.[83]

2.2.5 Coating Ti-6Al-4V discs using EPD

As SCPC50 particles exhibited maximum zeta potential and lowest conductivity in pure ethanol (see results for this chapter), the latter was selected as the suspending medium for EPD. To study the effect of SCPC50 concentration on the efficacy of substrate's surface coverage, suspensions with 2, 3 or 5 wt% SCPC50 particles were used for EPD. The SCPC50-ethanol suspension was stirred for 15 min on a magnetic stirrer

and subjected to ultra-sonic agitation for 45 minutes. Intermittent stirring of the ceramic suspension was carried out every 15 minutes during the course of sonication. EPD was carried out in a 250 mL glass container with the two electrodes placed 4.5 cm apart. The Ti-6Al-4V disc to be coated served as anode while the cathode consisted of a larger Ti-6Al-4V disc (3.8 cm dia x 0.5 cm thick). Both the electrodes were secured by means of stainless steel tweezers and connected to E3612A DC power supply (Agilent Technologies, Santa Clara, CA). A voltage of 30 - 120 V was applied allowing a current density in the range 1.5 - 3.0 mA/cm^2. The coating duration was varied from 1 – 10 min with intermediate air drying of the disc for 1 min after every 1 min of EPD coating. At the end of the coating process, the samples were removed and dried in a desiccator for 24 hr before thermal treatment. Samples coated in 5 wt% SCPC50-ethanol suspension were thermally treated and analyzed for adhesion strength and bioactivity.

2.2.6   Thermal treatment of SCPC50-coated Ti-6Al-4V discs

SCPC50-coated Ti-6Al-4V discs were thermally treated in a muffle furnace at 600 ºC for 3 hr. As the prolonged thermal treatment at 600 ºC did not adequately sinter the SCPC50 particles (see results for this chapter), higher temperatures of 700 and 800 ºC for 1 hr were tested. All thermal treatments were performed under continuous flow of 99.998% pure argon (14 L min^{-1}) to prevent metal oxidation. Controlled rate of heating and cooling (2 ºC min^{-1}) was employed in all cases.

2.2.7   Characterization of SCPC50-coated Ti-6Al-4V discs

2.2.7.1 SEM analyses

The surface morphology and elemental composition of the SCPC50-coated samples were characterized using SEM – EDX as described earlier. To measure the

coating thickness, SCPC50-coated Ti-6Al-4V samples were embedded in an epoxy solution (Buehler, Lake Bluff, IL) and cured as per the manufacturer's instructions. The samples were sectioned using a diamond wheel at 100 rpm, ground on 1200 grit silicon carbide pad and polished on a micro cloth using 0.05 μm alumina particles. Multiple measurements (n = 5) of the thickness of SCPC50 coating were made throughout seven (n = 7) different zones along the SCPC50/Ti-6Al-4V interface using SEM at 5 kV. For comparison, parallel experiments were performed using hydroxyapatite (HA) coated Ti-6Al-4V discs manufactured by plasma-spraying process. The samples were provided by DePuy Inc. and coated by Orchid Biocoat (Southfield, MI).

2.2.7.2 XRD analysis

The crystalline structure of the SCPC50 before and after coating on Ti-6Al-4V discs as well as HA-coating on Ti-6Al-4V discs were analyzed by X-ray diffraction (XRD) analysis using X'Pert PRO diffractometer (PANalytical, Westborough, MA). Data was collected between 10º and 60º 2θ with 0.02º step size using nickel-filtered Cu K$_\alpha$ radiation at 45 KeV and 40 mA.

2.2.8   Measurement of adhesion strength

To test the mechanical stability at the interface between SCPC50 and Ti-6Al-4V substrate, the SCPC50-coated Ti-6Al-4V discs (n = 5) were glued to a Ti-6Al-4V cylinder of similar diameter using FM 1000 adhesive polymer (generous gift from DePuy Inc.) as per ASTM standard F1147-05 (Standard Test Method for Tension Testing of Calcium Phosphate and Metallic Coatings). FM 1000 was cured for 1.5 hr at 175 ºC and 25 psi pressure applied by means of a calibrated temperature-resistant spring. Adhesion strength was measured using an Instron 5582 testing machine (Instron, Norwood, MA) at

a crosshead rate of 2.54 mm min^{-1} until complete separation occurred and the maximum load to fracture was determined. The fractured surface was analyzed using SEM - EDX as described earlier.

2.2.9   Dissolution analyses of SCPC50-coated Ti-6Al-4V discs

SCPC50-coated Ti-6Al-4V   discs (n = 6) were immersed in 75 mL phosphate buffer saline (PBS) solution (Cellgro, Manassas, VA) and placed on an orbital shaker at 30 rpm for 7 days. 5 mL of the immersing solution was exchanged with fresh PBS solution every 24 hr. The dissolution of the SCPC50 layer was analyzed by measuring the ionic concentration of Ca, Si, P and Ti in the immersing solution at every time point using Optima 2100 DV inductively coupled plasma-optical emission spectrometer (ICP-OES; Perkin Elmer, Waltham, MA) as described under conditions previously reported.[108] At the end of the immersion period, the samples were dried at 37 ºC for 12 hr and the surface was analyzed using SEM - EDX. The weight of the discs before and after immersion was measured. The adhesion strength between the ceramic coating and the Ti-6Al-4V disc was determined and the fractured surface was analyzed as described earlier. In addition, the adhesion strength of SCPC50-coated substrate was compared with that of HA-coated substrate after 2 days of immersion.

2.2.10 Cell culture and measurement of alkaline phosphatase (AP) activity

Bone marrow mesenchymal stem cells were extracted from 16 week old rat and sub-cultured following the same procedures previously published.[104] Upon 70 - 80% confluency, the cells were trypsinized, centrifuged, and re-suspended in 2 mL of tissue culture media (TCM). Aliquots of the cell suspension containing 6 x 10^4 cells were seeded on SCPC50-coated, HA-coated and uncoated Ti-6Al-4V samples (n = 5) in a 100

mm culture dish containing 25 mL TCM. After 2 days, the TCM was exchanged with fresh media supplemented with 3 mM β-glycerol phosphate, 10^{-8} M dexamethasone and 50 μg/mL ascorbic acid. The media was exchanged every 2 days until the end of 14 days. Thereafter, the media was removed, the substrates were washed in PBS and the attached cells were lysed in 1 mL of 1% TritonX-100. The cell extract was centrifuged at 2000 rpm for 5 min at 4 ℃ and the supernatant was used for total protein and alkaline phosphatase activity measurements. The AP activity was determined based on the hydrolysis of p-nitrophenylphosphate (p-NPP) to p-nitrophenol (p-NP) as previously published.[104] Briefly, 100 μL of the cell extract was added to 900 μL of 5 mM p-nitrophenyl phosphate in glycine buffer (pH 10.4) and incubated at room temperature for 5 min. The release of p-nitrophenol was monitored by measuring the absorbance of the solution at 402 nm using a UV - Vis spectrophotometer (Becknam Coulter Inc, Fullerton, CA). Total protein concentration in the supernatant was quantified using the Micro BCA protein assay kit (Thermo Scientific, Rockford, IL) as per the manufacturer's instructions. The AP activity was expressed as nmoles p-NP/mg protein/min.

2.2.11 Statistical analyses

The data was expressed as means ± standard deviation for all experiments and analyzed using student's t-test. A p-value < 0.05 was considered statistically significant.

2.3 Results

2.3.1 Particle size distribution

Figure 2.1 shows the size distribution of SCPC50 particles used for coating Ti-6Al-4V by EPD. It was found that 74% of the ceramic particles were <1 μm in size; out of which 36% were in the size range of 0 to 0.5 μm and 38% in the size range of 0.5 to 1

μm. Out of the remaining 26% of the ceramic particles, 80% were in the size range 1 to 2 μm and 20% in the size range 2 to 10 μm.
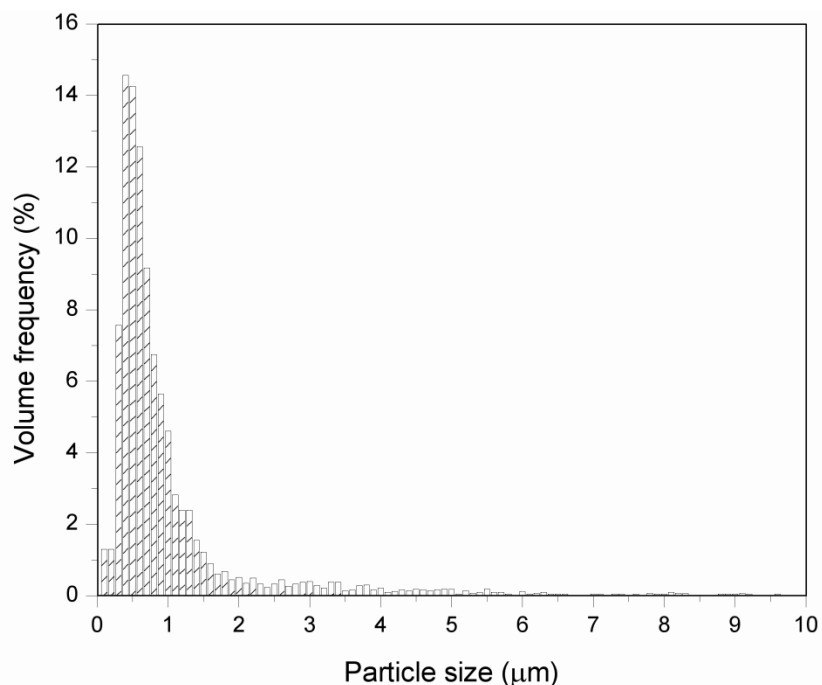
Figure 2.1: Size distribution of SCPC50 particles obtained after ball-milling for 24 hr. SCPC50 particles were in the size range of 200 nm – 10 μm with 74% of the particles being < 1 μm in size.

2.3.2   Evaluation of zeta potential and conductivity

2.3.2.1 Effect of medium pH and SCPC composition

Figure 2.2a illustrates the variation of zeta potential of SCPC particles of different compositions with the pH of the suspending medium (50% ethanol). At pH 2, all SCPC samples acquired comparable positive zeta potential in the range of 21.7 to 25.3 mV. However, at pH 3 the surface charge of all the samples was reversed from positive to negative values indicating that the suspension passed through the iso-electric point in the pH range 2 - 3. Moreover, SCPC25 samples exhibited zeta potentials that were

significantly more negative (p < 0.01) than SCPC50 or SCPC75 samples. The zeta

potential of SCPC50 significantly changed (p < 0.01) from -26.4 ± 1.7 mV at pH 4 to -

34.7 ± 1.4 mV at pH 5. For SCPC25 and SCPC75, the average change in the zeta

potential was not statistically significant at the same pH range. In the pH range of 6 - 8,

all the three SCPC compositions acquired the most negative zeta potential value of -43.6

± 0.5 mV. It is noteworthy that while SCPC25 acquired the most negative zeta potential

at pH 6, SCPC50 reached its most negative value at pH 7. SCPC75 acquired its most

negative zeta potential at pH 6 and continued to have similar potential until pH 8.

Beyond pH 8, the zeta potential of all the three SCPC compositions became less negative.
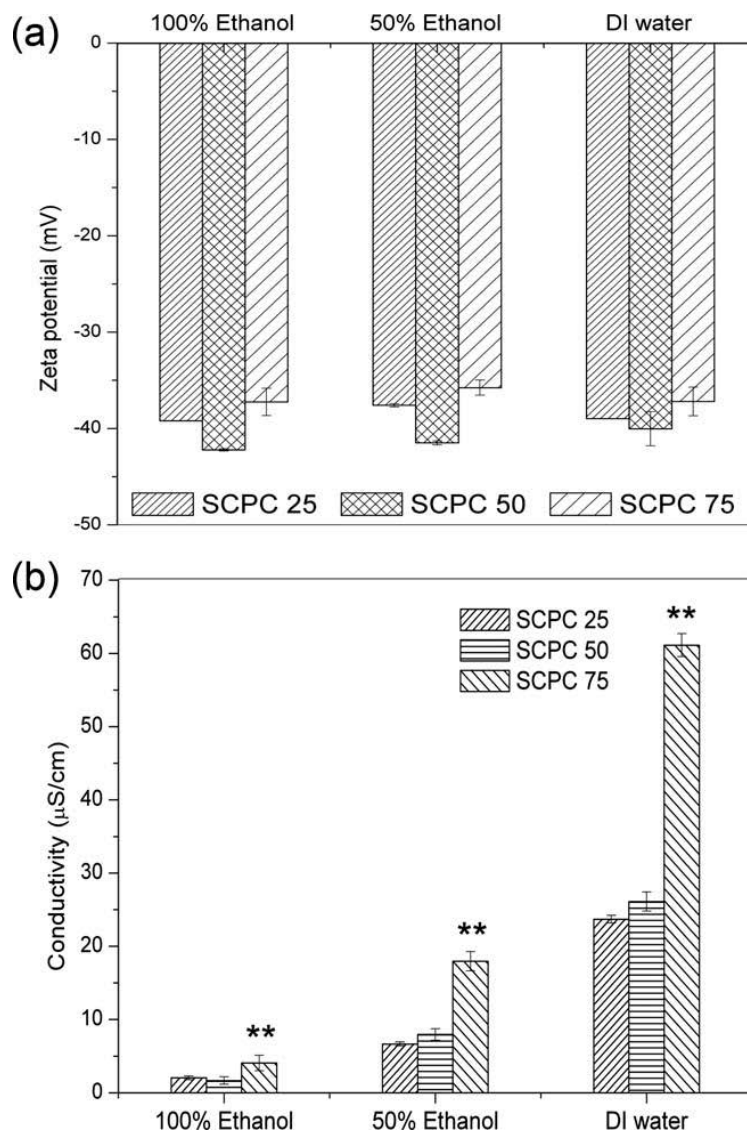
Figure 2.2: (a) Variation of zeta potential of SCPC25, SCPC50 and SCPC75 with pH measured in 50% ethanol. All the SCPC's showed maximum zeta potential between pH 6 − 8 (**p < 0.01); (b) Variation of conductivity of SCPC25, SCPC50 and SCPC75 with pH measured in 50% ethanol. The conductivity dropped sharply after the iso-electric point and remained consistent in the pH range 6 − 8 (*p < 0.05).

On the other hand, the conductivity of SCPC's of all compositions decreased sharply from (1768 - 1961 μS cm^{-1}) at pH 2 to (12 - 30 μS cm^{-1}) at pH 4 (Fig. 2.2b). At pH > 4, minimal changes in the conductivity of the samples was measured, however the

conductivity of SCPC75 was significantly higher ($p < 0.05$) than that of SCPC50 or SCPC25. Comparable values of conductivity were measured for SCPC25 and SCPC50 in the pH range 4 - 9.

2.3.2.2   Effect of medium's ethanol concentration and SCPC composition

Figure 2.3a and Figure 2.3b show the respective zeta potential and conductivity values of various SCPC compositions measured in DI water and 50% ethanol at pH 7 as well as in 100% ethanol. Minimal effect of the suspension medium's ethanol concentration was measured on the zeta potential of the SCPC particles. On the other hand, the conductivity of all SCPC suspensions increased significantly ($p < 0.05$) with increasing ethanol concentration; the maximum conductivity value was measured in DI water and the minimum in 100% ethanol. Moreover, in all suspension media, the conductivity of SCPC75 was significantly higher ($p < 0.01$) than SCPC50 or SCPC25. Although, the average conductivity of SCPC50 was higher than that of SCPC25, the difference was not statistically significant.
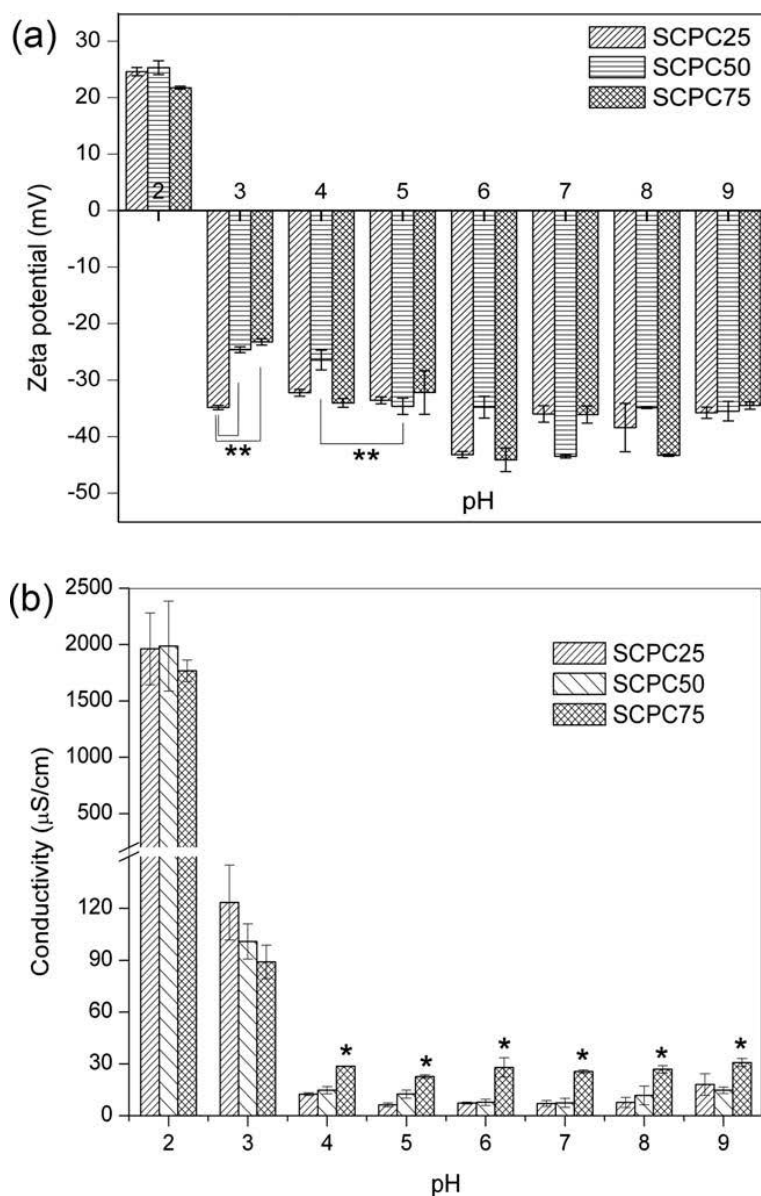
Figure 2.3: (a) Variation of zeta potential of SCPC25, SCPC50 and SCPC75 measured in 100% ethanol, 50% ethanol and DI water. Negative zeta potential values increased with increasing alcohol concentration for all the three SCPC compositions. (b) Variation of conductivity of SCPC25, SCPC50 and SCPC75 with change in alcohol concentration. The conductivity of the SCPC75 suspension was significantly higher than that of SCPC50 or SCPC25 in all solutions. (**p < 0.01)

2.3.3 EPD coating and SEM - EDX analyses

Among the various parameters tested, it was found that EPD carried out in 5 wt% SCPC50-ethanol suspension using 50 V for 2 min yielded a homogeneous and dense deposit on the Ti-6Al-4V samples. A greater uniformity of the SCPC50 coating was observed on the passivated Ti-6Al-4V samples as compared to that on the unmodified Ti-6Al-4V. SEM analyses of the SCPC50 coating treated at 600 ºC showed initial particles fusion (Figure 2.4a). As the treatment temperature increased to 700 ºC (Figure 2.4b) and 800 ºC (Figure 2.4c) the fusion between the particles significantly resulting in densification of the coating layer. Cross-sectional analysis of the SCPC50 layer coated on the Ti-6Al-4V decreased in the order 43.1 ± 5.7 µm > 35.6 ± 2.6 µm > 30.1 ± 4.6 µm after thermal treatment at 600, 700 and 800 ºC, respectively (Figure 2.4d-f). SEM analysis of the HA-coated Ti-6Al-4V disc showed a dense layer of HA marked by smooth splats along with round melted- and fused particles (Figure 2.5a). Various cracks (arrows) typical for HA-coated by plasma spraying could be seen traversing the surface. Cross-sectional analyses of the HA-coated samples showed densely packed HA layer; however considerable variation in coating thickness was observed; the average coating thickness was 29.7 ± 8.1 µm (Figure 2.5b).
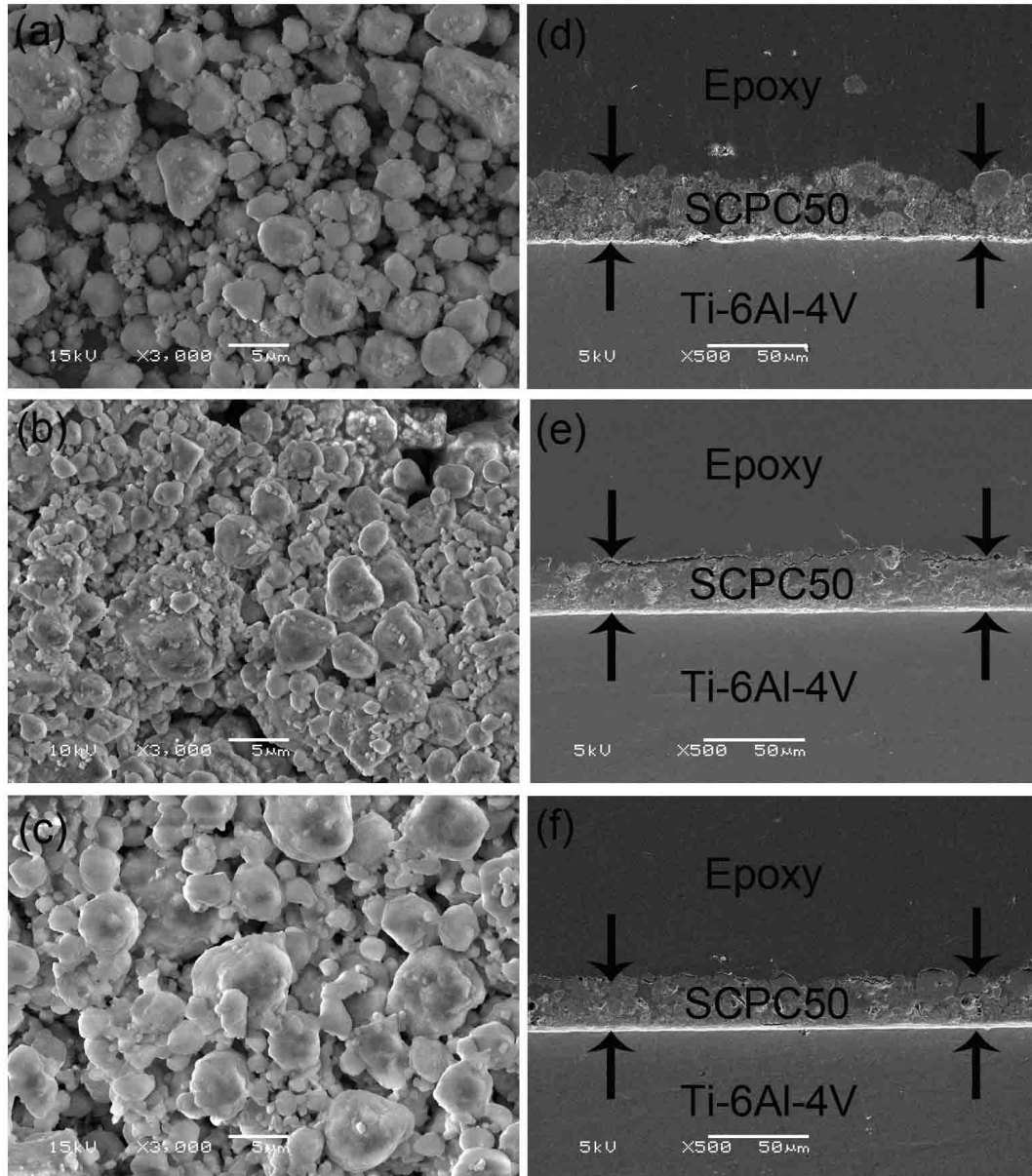
Figure 2.4: SEM images of SCPC50-coated Ti-alloy disc thermally treated at (a) 600 ºC for 3 hr (b) 700 ºC for 1 hr and (c) 800 ºC for 1 hr. Extensive necking and densification among the SCPC50 particles was seen at 800 ºC; SEM images of the cross-section showing a coating thickness of (d) 43.1 ± 5.7 μm, (e) 35.6 ± 2.6 μm and (f) 30.1 ± 4.6μm after thermal treatment at 600 ºC for 3 hr, 700 ºC for 1 hr and 800 ºC for 1 hr, respectively.
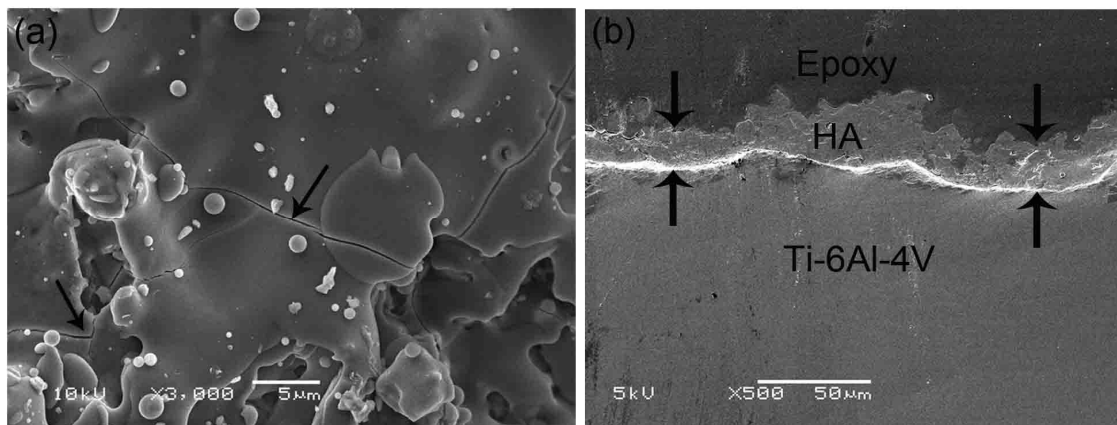
Figure 2.5: (a) SEM image showing the surface of HA-coated Ti-6Al-4V samples. Surface cracks were evident throughout the coating layer; (b) Cross-sectional image of the sample showing a dense HA layer of 29.7 ± 8.1 μm coating thickness.

2.3.4 XRD analysis

XRD analysis of the SCPC50 particles prepared by sintering at 850 ºC showed that SCPC50 was composed of β-rhenanite (β-NaCaPO$_4$) and α-cristobalite (α-SiO$_2$) solid solutions (Figure 2.6a). Moreover, no change in the crystallinity of SCPC50 was observed after EPD coating and thermal treatment at 800 ºC for 1 hr (Figure 2.6b). On the other hand, plasma-sprayed HA coating was composed of crystalline HA with trace amount of tri-calcium phosphate (Fig. 5c). A slight amorphous hump in the 2θ range of (27º – 35º) was observed indicating the presence of small amount of amorphous HA.
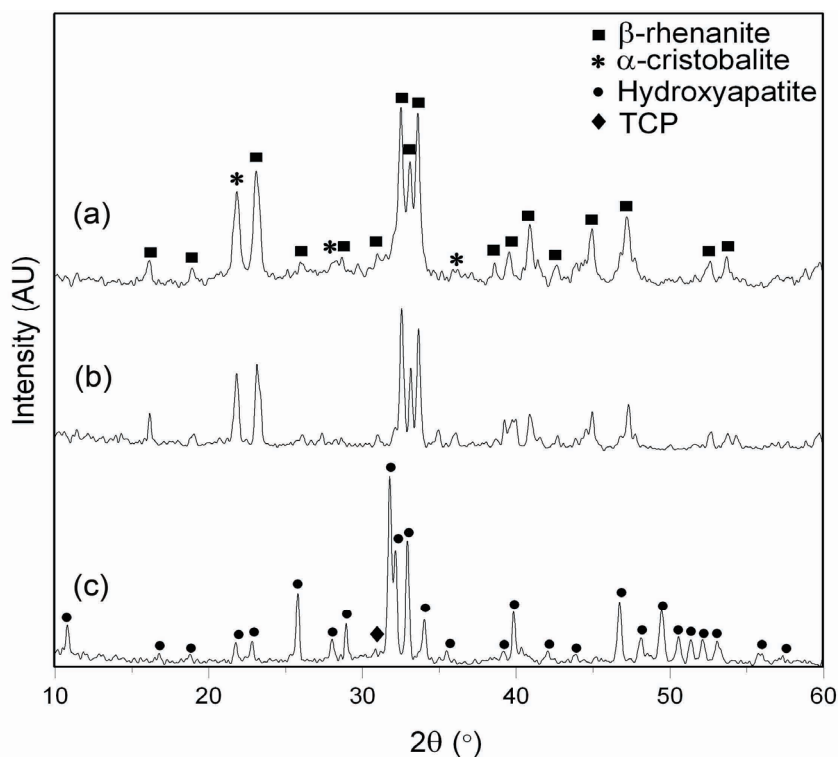
Figure 2.6: XRD analysis of SCPC50 (a) before coating and (b) after coating on Ti-6Al-4V and thermal treatment at 800 ℃ for 1 hr. After coating process SCPC50 maintained its crystalline structure of (β-rhenanite and α-cristobalite); (c) HA-coated Ti-6Al-4V was composed of crystalline hydroxyapatite with traces of tri-calcium phosphate.

2.3.5   Adhesion strength at the ceramic-metal interface

SCPC50-coated Ti-6Al-4V samples prepared in 5 wt% SCPC50-ethanol suspension and thermally treated at 600, 700 and 800 ℃ developed adhesion strength of 42.6 ± 3.6, 44.7 ± 8.7 and 47.2 ± 4.3 MPa, respectively, all of which exceeded the ASTM (F1147-05) requirement of 30 MPa. SEM analyses of the fractured surface indicated that the samples treated at 800 ℃ for 1 hr fractured either within the ceramic layer or at the interface of the ceramic with the polymer (Figure 2.7a and 2.7b). EDX analyses of the fractured surface confirmed the presence of SCPC50 particles embedded within the polymer matrix (Figure 2.7c).
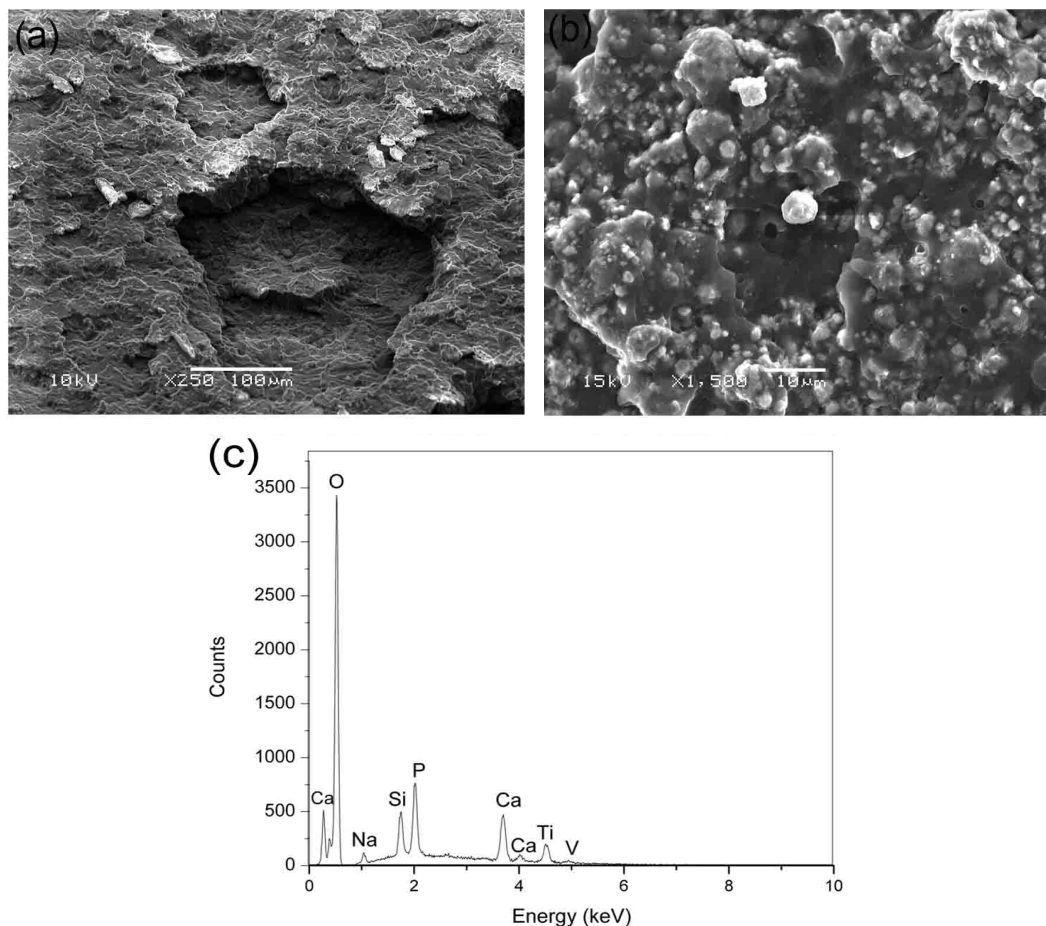
Figure 2.7: (a) SEM images of the fractured surface of SCPC50-coated Ti-6Al-4V after adhesion test showing extensive residual polymer on the surface of sample. (b) Higher magnification of the fractured surface showing SCPC50 particles embedded within the polymer matrix indicating that the fracture occurred either within the ceramic layer or at the ceramic/polymer interface. (c) EDX analysis of the fractured surface showed characteristic signals of Si, Ca, P and Na of SCPC50.

2.3.6   Interaction with physiological solution

2.3.6.1 Surface morphology analyses

SEM - EDX analyses of the SCPC50-coated Ti-6Al-4V discs after immersion in

PBS at 37 ℃ for 7 days showed the precipitation of a Ca-deficient hydroxyapatite

(CDHA) layer on the samples (Figure 2.8a) with an average Ca/P ratio of 1.4. Moreover,

the SCPC50 (*) layer was intact underneath the CDHA (■) layer (Figure 2.8b). Higher

magnification of the precipitated layer showed the presence of characteristic needle-like crystals of HA (Figure 2.8c). Weight analysis of the SCPC50-coated Ti-6Al-4V samples before and after immersion in PBS showed no significant weight loss at the end of the immersion period.
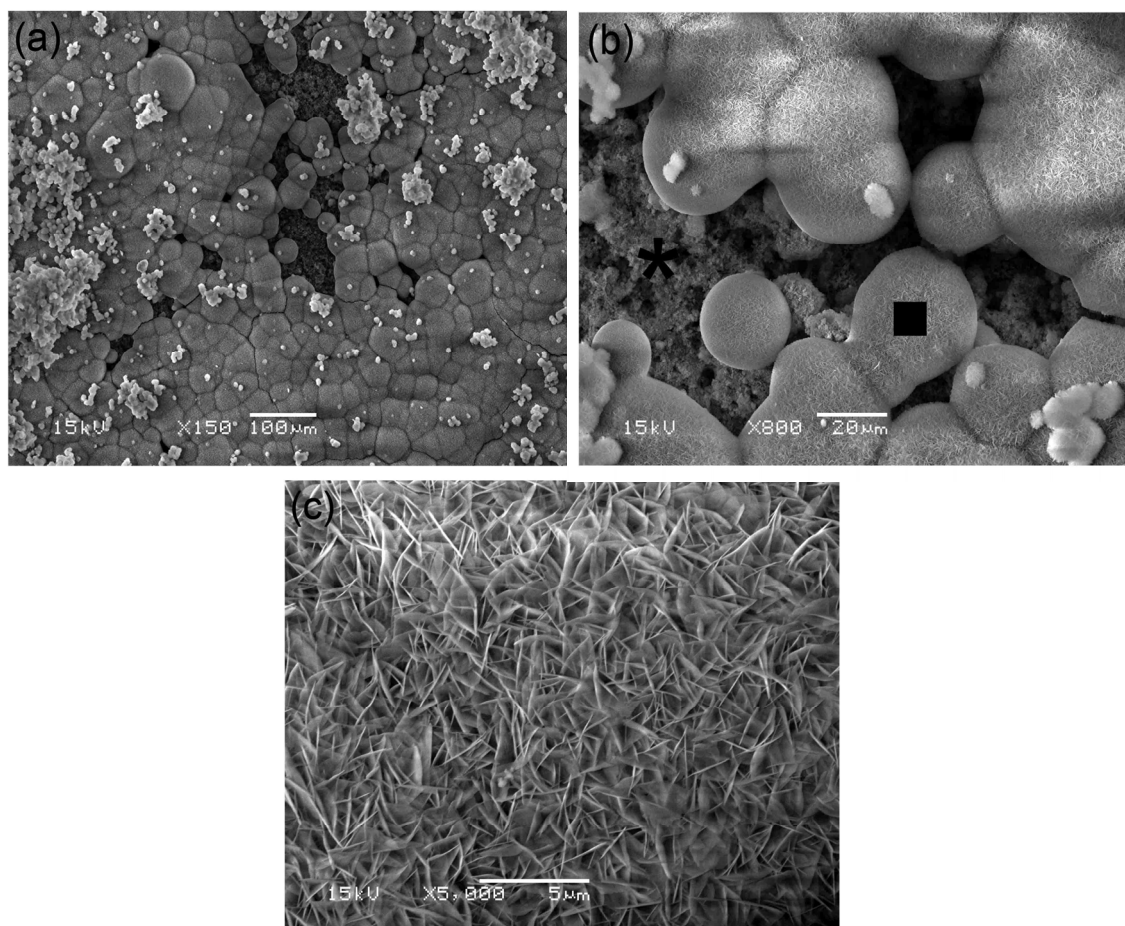
Figure 2.8: SEM images of SCPC50-coated Ti-6Al-4V disc pre-immersed in PBS for 7 days at 37 ºC showing (a) the presence of a uniform calcium-deficient HA (CDHA) layer over the SCPC50 coating; (b) SCPC50 coating (*) could be seen underneath the CDHA layer (■); (c) higher magnification showing the crystals of CDHA.

2.3.6.2 Dissolution analyses

ICP - OES analyses of the immersing solution showed a significant reduction (p <

0.01) in Ca concentration from 35.4 ± 1.7 ppm at day 1 to 9.8 ± 1.6 ppm at day 5 (Figure

2.9). However, no significant change in the Ca concentration was observed thereafter.

Contrary to the reduction in Ca concentration, an increase in Si concentration in the

immersing solution was observed in the first 4 days. The Si concentration in the medium

increased from 3.3 ± 0.9 ppm at day 1 to 5.0 ± 1.2 ppm at day 4 with minimal changes in

its concentration thereafter. The average P concentration (320.6 ± 6.4 ppm) in the

immersing solution showed no significant difference after all immersion periods.

Moreover, Ti ions were not detected in the immersing solution.
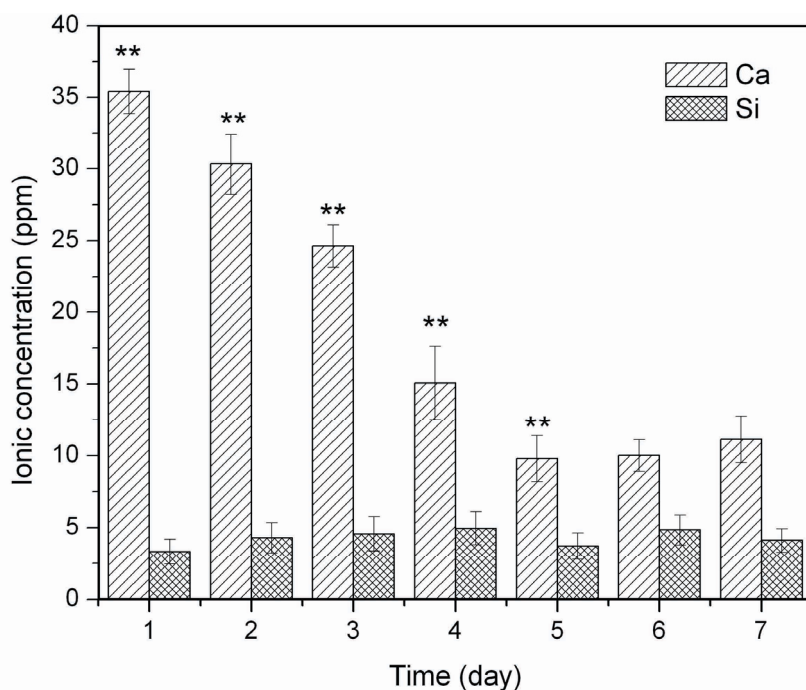
Figure 2.9: ICP-OES analyses of the immersing solution indicated initial rapid dissolution of Ca followed by a significant decrease due to the CDHA precipitation on the material surface. Minimal Si dissolution was observed indicating the stability of the coating layer. (**p < 0.01)

2.3.6.3 Measurement of adhesion strength after immersion

Mechanical tests showed that the adhesion strength acquired by the SCPC50-coated substrates after 2 days of immersion in PBS was 11.7 ± 3.9 MPa which was higher than the adhesion strength of 5.5 ± 2.7 MPa acquired by the HA-coated substrates, although the difference was not statistically significant. Further immersion of SCPC50-coated substrates in PBS for 7 days reduced the adhesion strength 6.4 ± 1.8 MPa. SEM – EDX analysis of the fractured surface showed that the fracture occurred at the interface of SCPC50 coating and the CDHA layer as indicated by the extensive presence of SCPC50 and residual CDHA on the fractured surface (Figure 2.10).
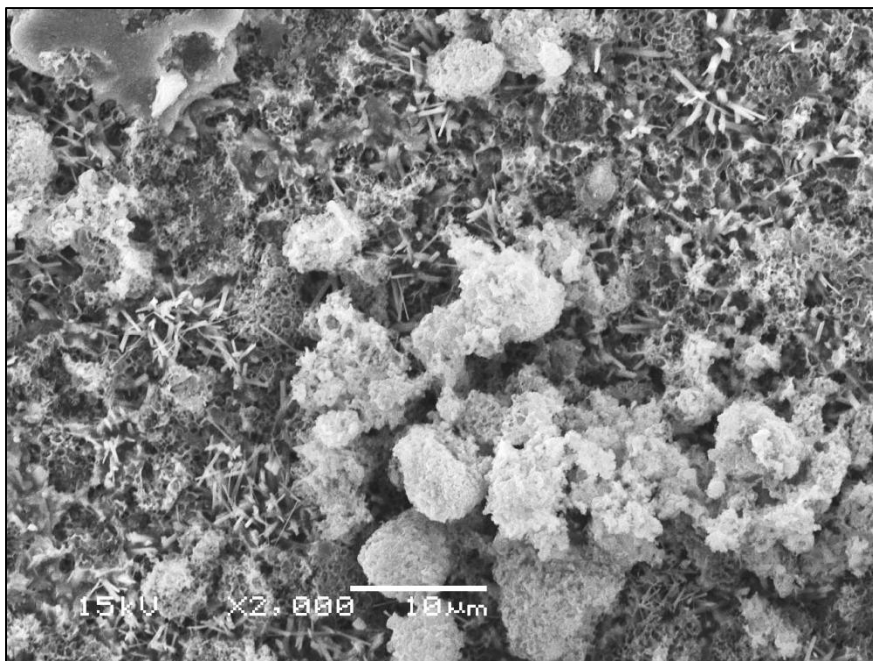
Figure 2.10: SEM image of the fractured surface of SCPC50-coated Ti-6Al-4V disc after PBS immersion showing the presence of CDHA crystals indicating that the failure occurred within the CDHA layer.

2.3.7   Bone cell response

Figure 2.11 shows the AP activity of the bone marrow mesenchymal stem cells measured on uncoated, HA-coated and SCPC50-coated Ti-6Al-4V discs after 14 days in culture. The alkaline phosphatase activity expressed by cells attached to the SCPC50-coated Ti-6Al-4V samples was (82.4 ± 25.6 nmoles p-NP/mg protein/min) which is significantly higher ($p < 0.05$) than that expressed by cells attached to the HA-coated Ti-6Al-4V (39.7 ± 7.1 nmoles p-NP/mg protein/min) or control uncoated Ti-6Al-4V samples (7.0 ± 3.4 nmoles p-NP/mg protein/min).
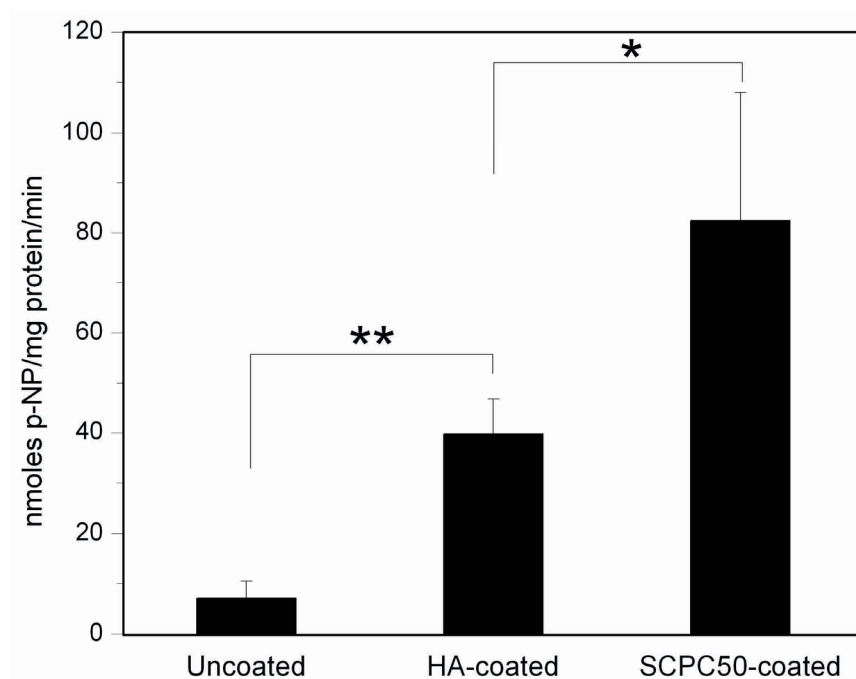
Figure 2.11: Bone marrow mesenchymal stem cells attached to SCPC50-coated Ti-6Al-4V substrate expressed significantly higher alkaline phosphatase activity than expressed by the cells attached to control (uncoated) or HA-coated substrates. (*$p < 0.05$; **$p < 0.01$)

2.4   Discussion

The broad objectives of this work were to develop a protocol to coat SCPC bioactive ceramic on Ti-6Al-4V orthopedic implant and to optimize the adhesion strength between the ceramic and metal. Moreover, the bioactivity of the SCPC-coated Ti-6Al-4V implant was evaluated *in vitro*. Zeta potential measurements indicated that SCPC50 particles suspended in pure ethanol acquired the most negative surface charge compared to other SCPC formulations. Moreover, the use of ethanol as a suspension medium demonstrated minimal conductivity allowing the SCPC50 particles to be the primary carrier for the electric charge. SCPC50-coated Ti-6Al-4V samples thermally treated at 800 ºC for 1 hr developed the highest adhesion strength of (47.2 ± 4.3 MPa) compared to the samples treated at lower temperatures. Fracture surface analyses showed that the failure occurred either at the interface between the ceramic coating and polymer or within the ceramic layer indicating the stability of the ceramic-metal interface. Bone marrow mesenchymal stem cells attached to SCPC50-coated Ti-6Al-4V samples expressed higher alkaline phosphatase activity than the cells attached to HA-coated or control uncoated Ti-6Al-4V samples. The strong stimulatory effect of SCPC50-coated Ti-6Al-4V implants indicates the superior bioactivity of the device compared to commercially available HA-coated or uncoated Ti-6Al-4V implant.

The key to successful coating by electrophoretic deposition was the creation of a stable SCPC suspension that maximized particle mobility under electric potential. A stable solution would be created when the particles carry maximum charge on their surface, such that the inter-particle repulsion is maximized. Measurement of zeta potential (Figure 2.2a) showed a switch in the charge of the SCPC particles between pH 2

and 3. The change in the sign of the charge indicates that the suspended particles passed through the iso-electric point (pH_{IEP}) at this pH range. The low iso-electric point of SCPC can be attributed to the presence of silica in the material. Previous reports have shown that the incorporation of Si in HA resulted in a shift of the iso-electric point from (pH_{IEP} = 5.5) for un-substituted HA to (pH_{IEP} = 3.8) for Si substituted HA.[117] Other studies on bioactive glass and pure silica[118,119] have reported the iso-electric point of the material to be at pH_{IEP} < 3, which was consistent with our findings. The high conductivity of the SCPC suspension at pH 2 can be attributed to the dominating role of H^+ (from HNO_3) that was added to adjust the pH. As the pH increased the conductivity of the solution decreased sharply. SCPC suspension with minimal conductivity is desirable because it enhances the current carrying capacity of the SCPC particles.

A strong correlation between the surface charge and the calcium phosphate content in SCPC material was observed. The surface charge at pH 3 increased in the order SCPC25 > SCPC50 > SCPC75 (Figure 2.2a). The highly polarized $P-O^-$ ^+Na bond in β-rhenanite solid solution facilitates the release of Na^+ ions exposing the negatively charged PO_4^{3-} groups on the material surface. The increase in the solution pH resulted in a further negative shift of the zeta potential of all samples due to the disruption of the silicate network and the ionization of SiO_4^{4-} groups. In the pH range 6 - 8, the zeta potential curve plateaus, attaining the most negative zeta potential value for all SCPC samples. Such a plateau can be attributed to the complete ionization of the surface SiO_4^{4-} groups in this pH range. Data in the literature showed that the negative zeta potential of quartz (SiO_2) increased in the pH range 4.5 - 6 and plateaued at pH > 6, attaining a maximum zeta potential of -35 to -45 mV in the pH range 6 – 10.[120] An increase in the

pH above 8 resulted in the decrease of the negative zeta potential of all SCPC samples. This was because of the increased ionic strength at pH 8 that compresses the electrical double layer resulting in a decrease of the zeta potential.[121] The magnitude of the zeta potential of SCPC50 particles (-43.5 ± 0.1 mV) suspended in ethanol was higher than the corresponding values reported for other bioactive materials such di-calcium phosphate anhydride (-4.8 ± 1.1 mV)[122] in similar suspending medium. In our study, the decrease in the suspension's conductivity correlated well with the decrease in the dielectric constant (ε) of the suspending medium. Dielectric constant represents the ability of a material to polarize in an electric field. The low polarization of pure ethanol ($\varepsilon = 24$) minimized its role in conductivity as compared to 50% ethanol ($\varepsilon = 38$) or DI water ($\varepsilon = 80$). Moreover, the lower polarizability of ethanol would further enhance the electric field strength and facilitate particle mobility during EPD coating. Therefore, among the different SCPC formulations and media tested, SCPC50 particles suspended in 100% ethanol was selected for the EPD coating process. Under these conditions the SCPC50 particles carried the most negative surface charge and the suspension had minimal conductivity thereby promoting maximum mobility of the particles and hence efficient EPD coating.

In addition to optimizing the SCPC suspension for EPD coating we also modified the surface chemistry of the Ti-6Al-4V substrate to enhance homogenous coating. Previous studies have shown that the passivation of Ti-6Al-4V in HNO_3 leads to the formation of a thick, homogeneous TiO_2 sub-surface layer characterized by high surface energy.[83] Moreover, the higher dielectric constant (ε) of the TiO_2 ($\varepsilon = 110$) as compared to its lower oxides, such as TiO ($\varepsilon = 40 - 50$), permits greater charge accumulation on the passivated Ti-6Al-4V substrate. A consequence of such high polarization of the TiO_2

surface is a stronger interaction with the charged SCPC50 particles and superior coating homogeneity. On the other hand, the mixture of oxides including TiO_2, TiO and Ti metal present on the unmodified Ti-6Al-4V contributes to non-uniform surface charge distribution on the material surface. During EPD coating, the variations in the surface charge distribution on Ti-6Al-4V surface due to the variation in the oxidation states of Ti result in a non-homogenous coating. Moreover, the formation of a thick film of TiO_2 on Ti-6Al-4V minimizes metal corrosion.[123,124] Previous studies on Ti-6Al-4V implants have reported the inhibitory role of the constituent metal ions on bone cell differentiation and debris induced osteolysis.[26] Based on these results, all Ti-6Al-4V samples were subjected to passivation treatment before EPD coating.

EPD coating of SCPC50 particles on Ti-6Al-4V substrate led to a uniform deposition of a densely packed SCPC50 coating layer. During EPD, particles from the bulk of the suspension migrate to the surface of Ti-6Al-4V anode and deposit to form the surface coating. Various theories have been proposed to explain the mechanism of particle deposition on the metal electrode.[125,126] Sarkar *et al* studied the EPD coating of positively charged alumina particles exhibiting zeta potential (ζ) of 80 mV when suspended in ethanol at pH 4.0.[126] They suggested that the cations (H^+) that co-migrate with the alumina particles react with the electrical double layer of alumina and reduce its thickness, thereby resulting in the coagulation of alumina on the metal. However, no experimental evidence for such a mechanism was offered. De *et al* later postulated a theoretical model to investigate the experimental data of Sarkar *et al*. Their model predicted that the concentration of H^+ in the vicinity of the metal electrode depletes due to charge neutralization, resulting in a local increase of pH from 4.0 to 7.2, the iso-electric

point (pH$_{iep}$) of alumina.[125] This facilitates the coagulation of alumina particles on the surface of the metal. It is interesting to note that the fate of cations described in these two studies is contradictory; while the former study suggests that the cations interact with alumina particles, the latter suggests that the cations discharge at the metal electrode. In a related work, Besra *et al* experimentally measured the pH of freshly deposited alumina obtained from the EPD coating of stainless steel using alumina particles suspended in water.[127] Their results showed that the pH of the alumina deposit increased from 4.5 in bulk suspension to 8.4 on the metal electrode, passing through the iso-electric point at 7.9. In any event, a common conclusion from these studies is that the reduction of the zeta potential of colloidal particles coagulates them onto the surface of the metal electrode. During EPD, the electric current is distributed between the negatively charged SCPC50 particles and the charged ions of the suspending medium. The applied electric field that motivates electrophoretic migration is much greater than the repulsive force between the negatively charged entities; therefore these species are attracted towards the positively charged Ti-6Al-4V electrode (anode). The coagulation of SCPC50 particles at the anode surface is caused due to the reduction of the zeta potential, most probably due to the discharge of electrons by anionic species (R-O$^-$) that reduce the pH towards the pH$_{iep}$ of SCPC50 (pH$_{iep}$ = 2 - 3).

Mechanical tests showed that the SCPC50-coated Ti-6Al-4V samples thermally treated at 800 ºC/1 hr developed adhesion strength of 47.2 ± 4.3 MPa which exceeded the ASTM standard requirement of 30 MPa (ASTM F1147-05). The high adhesion strength between the SCPC50 coating and the Ti-6Al-4V can be attributed to efficient sintering between the ceramic and the metal. For EPD coating, we used SCPC50 particles in the

size range (200 nm –10 µm). Due to their small size and greater electrophoretic mobility, the nano-size particles were deposited faster than the micro size particles onto the surface of Ti-6Al-4V substrate. The SCPC50 nano-particles provided a homogenous dense layer on the metal surface. Nano-particles are known to have a lower softening temperature than micro particles.[128] Therefore, upon thermal treatment the layer of nano-particles on Ti-6Al-4V served as an initiator for the strong bonding between the SCPC50 and the metal as well as among the SCPC50 particles. The enhanced softening of the SCPC50 layer resulted in a strong integration between the SCPC50 and metal as shown in the cross sectional analysis of the coated implants (Figure 2.4f). The atomic diffusion between the ceramic particles allowed for greater ceramic densification at the relatively low sintering temperature of 800 °C. Moreover, during the sintering process, the TiO_2 may react with SiO_2 and P_2O_5 of SCPC50 which would further enhance the bonding between the metal and the ceramic. Previous studies have reported the formation of Ti_5Si_3 and Ti_4P_3 compounds upon sintering silicate glass and Ti-6Al-4V.[129,130] It is also possible that the Ca of SCPC50 forms a covalent bond with the TiO_2 on the metal substrate. Such a hypothesis is based on previous studies that have shown that sintering powdered cp-Ti with HA at a temperature higher than 500 °C resulted in the formation of $CaTiO_3$ compound.[131,132] From a processing prospective, the use of lower temperature and/or slower rate of heating and cooling reduced the thermal stress at the ceramic-metal interface; thus contributing to the stability of the interface. It was interesting to note that the interface between Ti-6Al-4V and SCPC50 coating was intact for samples treated at various temperatures (600 - 800 °C). Analysis of the fractured surface, following the mechanical test, indicated that the fracture occurred within the SCPC50 coating layer or

at the polymer glue/ceramic interface. Moreover, adhesion strength between the SCPC50 layer and the Ti-6Al-4V substrate after 7 days of PBS immersion showed that the fracture occurred at the interface between the CDHA layer deposited on the ceramic surface and the underlying SCPC50 coating (Figure 2.10). The bioactivity of the coated implant was enhanced as evidenced by the formation of a HA layer similar to the mineral phase of bone after immersion in physiological solution. Moreover, cell culture studies demonstrated higher stimulatory effect on bone cell differentiation of the SCPC50-coated substrates compared to HA-coated or uncoated substrates. The AP activity is an essential initial marker for differentiation.[133] Figure 2.11 demonstrates that the AP activity on SCPC50-coated substrates was 2-fold higher than that expressed on the HA-coated substrates and 11-fold higher than that expressed on the uncoated substrates. The stimulatory effect of SCPC50 on osteoblastic gene expression has previously been reported.[104,108] These results indicate that the EPD coating process did not affect the superior bioactivity properties of SCPC50 previously reported in the literature.[103,104,108,116]

2.5 Conclusion

Successful coating of a uniform layer of bioactive SCPC50 on the surface of Ti-6Al-4V orthopedic implant was achieved using electrophoretic deposition. SCPC particles exhibited maximum zeta potential and minimal conductivity in pure ethanol. Moreover, the conductivity of the SCPC particles increased with the increasing silica content in the material. Mechanical tests showed that the interface between the SCPC50 coating and Ti-6Al-4V developed strong adhesion strength of 47.2 ± 4.3 MPa after thermal treatment at 800 ºC/1 hr. The strong adhesion between the SCPC50 coating and the Ti-alloy substrate persisted after 7 days of immersion in physiological solution.

Moreover, the SCPC50 layer enhanced the bioactivity properties of the implant as indicated by the formation of a biological hydroxyapatite layer and the strong stimulatory effect on the expression of alkaline phosphatase activity. Therefore, SCPC50 coating has the potential to expedite bone bonding to Ti-6Al-4V and enhance longevity of the implant. Future work to assess the effect of the SCPC50 coating on osteoblast activity would include gene expression and protein synthesis analyses.

CHAPTER 3: PRO-OSTEOGENIC RESPONSES BY A BIOACTIVE CERAMIC COATING

3.1 Introduction

Coating orthopedic Ti-6Al-4V implants with bioactive calcium phosphate ceramics provides an osteoconductive surface that stimulates direct bone bonding and minimizes the loosening of the implant.[52,134,135] Moreover, the bioactive ceramic coating facilitates proper transmission of a mechanical stimulus from the implant to the bone; an important phenomenon that alleviates stress shielding of the peri-prosthetic bone and impedes its resorption.[136,137] Plasma-sprayed hydroxyapatite (HA) coated Ti-6Al-4V has been widely used; however, the high temperature of the plasma during coating results in a partial decomposition of HA into undesirable phases of altered solubility and biocompatibility.[51,114] Moreover, the difference in the thermal expansion coefficient between ceramic and the metal substrate creates interfacial thermal stresses that result in poor adhesion.[57] Other studies have shown that the HA coating layer is often cracked and non-homogenous in both thickness and crystallinity which renders the coating prone to delamination.[57,138,139] The increase in the thickness of the HA layer decreases the shear strength of the implant making it more susceptible to failure at the metal-ceramic interface.

Recent approaches to improve the stability of the coated layer include the use of TiO_2, either as an intermediary layer between HA and the metal[75,76,140] or as a mixture with HA.[141] The incorporation of TiO_2 was found to reduce the decomposition of the HA

and enhance the Young's modulus, fracture toughness and shear strength of the HA coating layer.[75,140] The incorporation of carbon nano-tubes (CNT) within the HA layer has been proposed as a means of improving its mechanical strength.[78,80] CNT aided reinforcement of HA is reported to have produced a homogeneous coating with significant improvement in the crystallinity and toughness of HA coating.[78] However, the toxicity and long-term effects of CNT remains an on-going debate.[142] Coating techniques such as ion-beam-assisted deposition and magnetron sputtering have been employed to deposit thin ceramic coating of $0.1 - 10$ μm thickness,[44] however these processes are neither simple nor cost-effective. Electrophoretic Deposition (EPD) of bioactive ceramics on metal substrates favor low sintering temperature and slow heating and cooling cycles that minimize interfacial stresses between metal and ceramic and enhance adhesion strength.[143,144] Coating bioactive silica-calcium phosphate nanocomposite (SCPC50) on Ti-6Al-4V orthopedic implant using EPD showed the adhesion strength at the interface between the metal substrate and the bioactive ceramic to be 47 ± 4 MPa which exceeded the ASTM (F1147-05) requirement of 30 MPa as described in Chapter 2.

Cell responses to implants are known to be mediated by material-related parameters including: surface chemistry, surface charge, crystallinity and ion release. An increase in the negative surface charge of the HA coating by electric polarization enhances bone cell adhesion, and mineralization.[145] The enhancement of cell activity was attributed to the accumulation of Ca ions on the negatively charged HA surface after polarization treatment. Moura *et al* coated amorphous CaP onto rough Ti-6Al-4V surfaces and reported that a thin CaP coating with a thickness of 0.3-0.5 μm was insufficient to stimulate *in vitro* osteogenesis.[146] However, other studies reported

contradictory results and showed that 0.2 – 1.1 μm thick CaP coating stimulated cell proliferation and differentiation.[147,148] Gomes *et al* showed that coating Ti-6Al-4V with Si containing HA enhanced osteoblast proliferation, differentiation and matrix mineralization.[149] The stimulatory effect of the coating was attributed to the release of Si that resulted in a concentration of Si in the surrounding medium of 0.05 – 0.12 mM. In addition, none of the above studies addressed the effect of calcium phosphate coating on protein adsorption. Cell attachment to an implant is strongly governed by the amount, kind and conformation of proteins that adsorb onto the material's surface.[150-152]

Protein adsorption is determined by the physico-chemical characteristics of the implant material including zeta potential, surface chemistry, material crystallinity and surface area.[102,150,153,154] Previous studies of albumin adsorption to various bioactive and non-bioactive ceramics showed that materials exhibiting a higher negative zeta potential enhanced protein adsorption.[155] The selective adsorption of bioactive ceramics to certain proteins in serum has been reported.[156-158] . HA inhibits the adsorption of serum proteins less than 23.1 kD in size[156] while promoting the adsorption of attachment proteins such as fibronectin and vitronectin.[158] El-Ghannam *et al* showed that the formation of a CaP layer on bioactive glass enhanced the selective adsorption of fibronectin. On the other hand, porous HA adsorbed all kinds of serum proteins without any preference to fibronectin.[157] The reasons for the specificity of serum fibronectin to the HA surface layer that form on bioactive glass are not fully understood. Garcia *et al* investigated the effect of CaP crystallinity on protein adsorption and reported that the mere presence or crystallinity of the CaP layer does not affect the amount of adsorbed proteins.[159] Rather, it has been postulated that the substrate-induced fibronectin conformation can enhance cell adhesion.

In support of this idea, one study has shown that Si substitution in HA does not affect the amount of serum proteins adsorbed, suggesting that the enhanced cell response to Si-HA is most probably due to changes in the protein conformation.[160] Furthermore, Buchanan *et al* have demonstrated that attachment proteins such as fibronectin express a higher ratio of amide I/amide II FTIR bands after adsorption onto bioactive glass.[154] On the other hand, non-attachment proteins such as albumin showed higher amide II/amide I after adsorption on the same bioactive material.

The mechanism of action of bioactive ceramics includes up-regulation of the expression of osteoblastic genes such as collagen I, osteocalcin and osteopontin, and the increased product of such bone-associated proteins.[161,162] In particular, non-collagenous proteins such as osteopontin and osteocalcin are known to play important role in bone mineralization.[161,163] The literature suggests that the surface of implant materials can induce the expression of cytokines by osteoblasts that can promote potentially damaging inflammation and ostoclastogenesis.[164,165] Cytokines such as interleukin (IL)-6 and receptor activator for nuclear factor κ B ligand (RANKL) are well known to be expressed by activated osteoblasts and both promote osteoclast formation and/or activity. In contrast, IL-12 has been suggested to exert an inhibitory effect on osteoclast differentiation by blocking RANKL activity.[166] The objective of the present study is to investigate the responses of osteoblasts to SCPC50-coated Ti-6Al-4V implant material. The effect of SCPC50 coating on bone cell differentiation, mineralization and synthesis of pro-inflammatory/osteoclastogenic cytokines has been measured and correlated to the surface chemistry, protein adsorption and the dissolution of the material.

3.2 Materials and Methods

3.2.1 SCPC50 preparation and coating on Ti-6Al-4V implant

Bioactive SCPC50 containing 40.68% CaO, 20.34% P_2O_5, 19.49% Na_2O and 19.49% SiO_2 (in mol%) was prepared using a previously described powder metallurgy technique.[103,108] SCPC50 nano-particles were produced by grinding the ceramic powder in a PM-100 planetary ball mill (Retsch Technology, Newtown, PA) at 500 rpm for 24 hr. Medical grade Ti-6Al-4V ELI (ASTM F136-08e1) discs (1.3 cm dia x 0.5 cm thick) were coated with SCPC50 particles using EPD as described in Chapter 2. Briefly, the Ti-6Al-4V disc was immersed in a 10 wt% SCPC50 suspension in ethanol and coated using a voltage of 50 V for 30 sec (n = 25). The SCPC50-coated substrates were thermally treated at 800 ºC for 1 hr under argon.

3.2.2 Surface morphology and coating thickness analysis

The surface morphology of SCPC50-coated Ti-6Al-4V substrates was analyzed using a scanning electron microscope (SEM; JEOL USA Inc, Waterford, VA) equipped with an energy dispersive X-ray spectroscope (EDX; Oxford Instruments, Concord, MA) used under secondary electron imaging mode. To analyze the coating thickness, the samples were embedded in an epoxy solution and sectioned using a diamond saw. The fractured surface was ground on 1200 grit silicon carbide pad and polished on a micro-cloth using 50 nm alumina particles. Five measurements of the coating thickness were performed in seven (n = 7) different areas along the cross-section of the fractured surface using SEM. The data are presented as mean ± standard deviation of all measurements.

3.2.3   Protein adsorption analyses

3.2.3.1 Total protein adsorption

SCPC50-coated and uncoated Ti-6Al-4V samples (n = 5) were immersed in 6 mL of tissue culture medium (TCM) containing 10% FBS for 4 hr at 37 ºC. The samples were briefly rinsed and the total proteins adsorbed onto the samples were extracted in 3% Triton X-100 in PBS for 15 min. The concentration of the extracted protein was determined using Micro BCA protein assay kit (Thermo Scientific, Rockford, IL) as per the manufacturer's instructions. SCPC-coated and uncoated samples immersed in serum-free media served as control.

3.2.3.2 Protein conformation analyses

The secondary structure of the proteins adsorbed on SCPC50-coated and uncoated Ti-6Al-4V samples (n = 5) were analyzed by Fourier transform infrared spectroscopy (FTIR) using a Thermo Nicolet 6700 FTIR spectrometer (ThermoNicolet, Madison, WI) in the diffuse reflectance mode. Gold was used as the background for collecting the spectra. The baseline of the spectra was adjusted from 1460 to 1720 cm^{-1} to accommodate the amide I and amide II functional groups. The peak location and the ratio of the area under the peak for amide I and amide II functional groups in each spectra were determined.

3.2.3.3 Western blot analysis

SCPC50-coated and uncoated Ti-6Al-4V samples (n = 5) were immersed in 1 mL FBS for 4 hr at 37 ºC. The samples were rinsed briefly and the proteins adsorbed were extracted in a SDS-PAGE denaturing buffer, pooled, and boiled for 15 min. The volume of sample to be loaded for electrophoresis was determined based on the total amount of

protein absorbed by each sample. Equal amounts of protein were loaded onto an 8% polyacrylamide gel and separated by SDS-PAGE electrophoresis. The contents on the gel were electro-transferred onto a polyvinylidene difluoride membrane, blocked in 5% non-fat milk and incubated overnight with a mouse monoclonal antibody directed against fibronectin (Santa Cruz Biotech; 1:500 dilution) at 4 ℃. Immunoblots were then incubated with a horseradish peroxidase conjugated goat anti-mouse secondary antibody (Santa Cruz Biotech; 1:5000 dilution) for 2 hr at room temperature to visualize fibronectin bands as described elsewhere.[167]

3.2.4 Osteoblast cell line responses to SCPC50-coated Ti-6Al-4V

3.2.4.1 Cell culture system

MC3T3-E1 mouse osteoblast-like cells (ATCC; Manassas, VA) were cultured in Dulbecco's Modified Eagle Medium (DMEM) supplemented with 10% fetal bovine serum (FBS), 0.05% gentamycin and 0.1% amphotericin-B and incubated at 37 ℃ and 5% humidified CO_2. Ti-6Al-4V discs with and without SCPC50 coating (n = 5) were sterilized by immersion in pure ethanol for 30 min and dried under UV-irradiation. Upon 70-80% confluency, cells were trypsinized and seeded on the SCPC50-coated and uncoated Ti-6Al-4V samples at a density of 6 x 10^5 cells/sample in 6-well tissue culture polystyrene plates and incubated in a sufficient volume of cell culture media to cover the top surface of the implant disc (6 mL). After 2 days, the media was exchanged and supplemented with dexamethasone (10^{-8} M) and ascorbic acid (50 μg/mL), and the samples were incubated for another 2 days.

3.2.4.2 Gene expression analyses

After 4 days, total mRNA from each sample was extracted, pooled, and reverse transcribed to cDNA. Osteoblast phenotypic genes, collagen-I (Col-I), osteonectin (OSN), osteopontin (OPN) and osteocalcin (OCN) as well as the housekeeping gene glyceraldehyde-3-phosphate dehydrogenase (GAPDH) were used to amplify the cDNA fragments by semi-quantitative polymerase chain reaction (PCR) using specific primer pairs as previously described.[167-170] The PCR products were resolved by agarose gel electrophoresis (1.5 wt% gel containing trace amount of ethidium bromide) and visualized under UV-illumination. Quantitative real-time–PCR (qRT-PCR) analysis was also performed on each of the cDNA fragments using a SYBR green approach in a LightCycler (Roche, Indianapolis, IN) as previously described by our laboratory.[171] Gene amplification data analysis was performed with LightCycler software version 4.0 and normalized to the expression of GAPDH determined in parallel qRT-PCR analyses.

3.2.4.3 Osteogenic protein synthesis

The release of osteogenic proteins in the cell culture media (n = 6) was analyzed over 20 days using commercially available ELISA kits for osteopontin (R&D Systems, Minneapolis, MN) and osteocalcin (Biomedical Technologies, Stoughton, MA) according to the manufacturer's instructions. The media was exchanged every 2 days and stored at -80 ºC until further analysis. Cell culture media collected at every time point in the absence of cells served as control. After 20 days, the samples were immersed in 1% Triton X-100 for 15 min. The supernatant was collected, centrifuged briefly and analyzed for total protein using the micro BCA assay. The data are presented as ng/mL (OCN or OPN)/mg protein. Finally, the stability of the residual SCPC coating was evaluated by

immersion in 2 mL PBS for another 7 weeks (10 week total incubation period) at the end of which samples were embedded in an epoxy resin and residual coating layer thickness determined by SEM.

3.2.4.4 Immunological response

The production of the pro-inflammatory and/or osteoclastogenic cytokines, IL-6, IL-12p40 and RANKL, by MC3T3-E1 osteoblast-like cells was analyzed at 4 days of incubation (n = 5) using commercially available ELISA kits (R&D Systems, Minneapolis, MN) performed according to the directions provided by the manufacturer.

3.2.5   Spectroscopic and Imaging analyses

3.2.5.1 FTIR analyses of the osteoblast-like cell layer

The surface chemistry of SCPC50-coated and uncoated Ti-6Al-4V samples immersed for 4 days in TCM in the presence or absence of osteoblast-like cells was analyzed using FTIR as described above. Un-immersed SCPC50-coated and uncoated Ti-6Al-4V samples served as controls.

3.2.5.2 SEM - EDX analyses

The morphology of cells attached to one sample of SCPC50-coated and uncoated Ti-6Al-4V substrate was analyzed using SEM - EDX after 4 and 20 days of incubation. Moreover, EDX analyses of ten different regions on the substrate were carried out. Briefly, the samples were removed from the cell culture media, rinsed in PBS and fixed overnight in Karvonsky's fixative (Electron Microscopy Sciences, Hatfield, PA) at 4 ºC. The samples were subjected to serial ethanol dehydration followed by dehydration in hexamethyldisilazane for 15 min. After drying in a dessicator for 2 hr, the samples were coated with a 5 nm gold film.

3.2.6   Dissolution analyses

The dissolution of SCPC50-coated and uncoated Ti-6Al-4V samples were analyzed by measuring the ionic concentration of Ca, Si, P and Ti in the cell culture media using inductively coupled plasma – optical emission spectroscopy (ICP-OES; Perkin Elmer, Waltham, MA). The machine was operated under the conditions previously reported.[108]

3.2.7   Statistical analyses

The data are expressed as the means ± standard deviation and analyzed by one-way ANOVA using Fisher's LSD post-hoc test. A p-value of < 0.05 was considered statistically significant.

3.3   Results

3.3.1   Surface morphology and coating thickness

SEM imaging of the SCPC50-coated Ti-6Al-4V substrate showed that the surface was uniformly coated with SCPC50 nano-particles (Figure 3.1a). SCPC50 nano-particles appeared well sintered without any sign of surface cracking and demonstrated an average pore size of 50 ± 14 nm (inset; Figure 3.1a). Cross-section analyses showed that the thickness of the SCPC50 layer was 5.1 ± 0.08 μm (Figure 3.1b) (n = 7). Importantly, the interface between SCPC50 and Ti-6Al-4V was intact indicating strong adhesion.
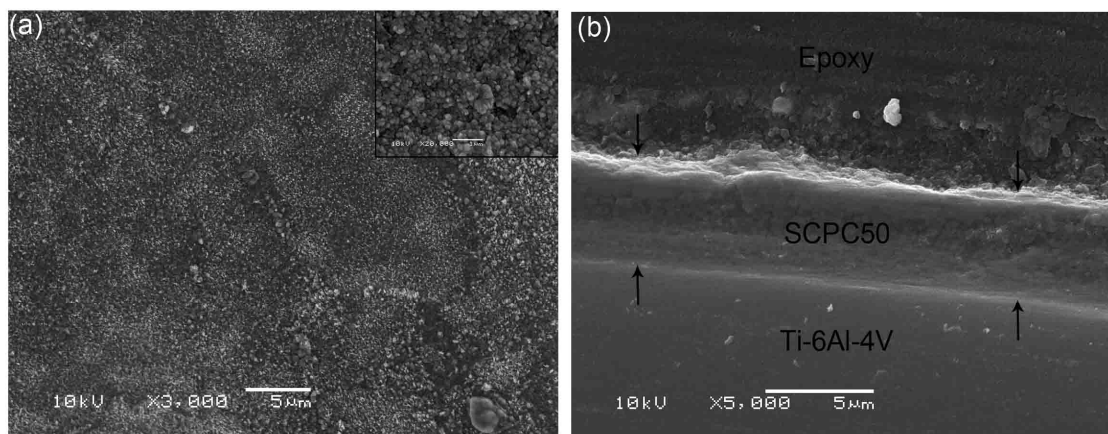
Figure 3.1: SEM images of the SCPC50-coated Ti-6Al-4V implant material showing (a) SCPC50 nano-particles on the surface of the metal substrate. The particles appeared well-sintered and showed the presence of nano-pores at high magnification (inset); (b) cross-section image showing a uniform thickness (5.1 ± 0.08 μm) of SCPC50 layer. The arrows point to the lower and upper interfaces of the SCPC50 coating layer with Ti-6Al-4V and epoxy resin, respectively.

3.3.2   Protein adsorption characteristics

3.3.2.1 Total protein and fibronectin adsorption

Measurement of total protein adsorption showed that SCPC50-coated Ti-6Al-4V substrates adsorbed 14.9 ± 1.2 μg of protein (n = 5) which was significantly higher ($p < 0.01$) than that adsorbed by uncoated Ti-6Al-4V substrates (8.9 ± 0.7 μg) (Figure 3.2a). Western blot analysis revealed extensive fibronectin adsorption by SCPC50-coated substrates (Figure 3.2b left lane) while uncoated Ti-6Al-4V substrates demonstrated only minimal adsorption (Figure 3.2b middle lane).
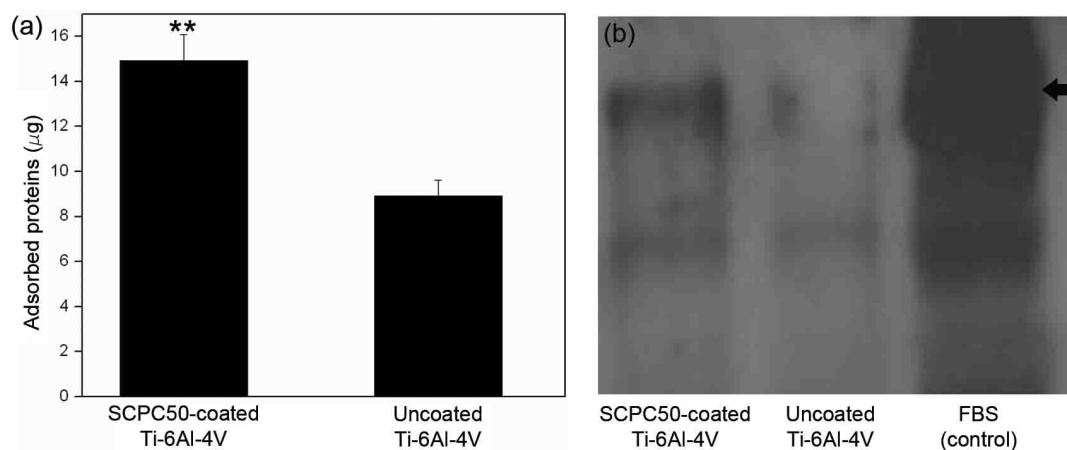
Figure 3.2: (a) Total protein analysis showed that SCPC50-coated Ti-6Al-4V samples adsorbed significantly higher (**$p < 0.01$) amount of serum proteins than uncoated Ti-6Al-4V samples. (b) Western blot analysis of the protein desorbed from SCPC50-coated (left lane) and uncoated (middle lane) Ti-6Al-4V samples showing evidence of fibronectin adsorption on the former substrate. Minimal fibronectin adsorption was observed on uncoated Ti-6Al-4V samples. The rightmost lane indicates a dark band at 205 kDa (arrow) resulting from fibronectin in FBS.

3.3.2.2 Protein conformation analysis

FTIR spectra of the proteins adsorbed on SCPC50-coated (Figure 3.3a) and uncoated (Figure 3.3b) Ti-6Al-4V substrates showed that the ratio of the area under the peak for the amide I and amide II spectra bands was significantly higher ($p < 0.05$) for SCPC50-coated substrate (5.0 ± 0.6) than uncoated substrate (2.2 ± 0.3). The center of the amide I band occurred at 1656 cm^{-1} on both substrates while the center of the amide II band appeared at 1542 and 1536 cm^{-1} on SCPC50-coated and uncoated Ti-6Al-4V samples, respectively. A distinct shoulder can be seen in the representative spectrum at 1600 cm^{-1} in the amide I region for samples from uncoated Ti-6Al-4V representing protein side chains (arrow; Figure 3.3b). In addition, it was found that the absorption intensity of the amide I and amide II bands on SCPC50-coated samples were 10- and 3-

fold higher, respectively, than the corresponding band intensities on the uncoated Ti-6Al-4V samples.
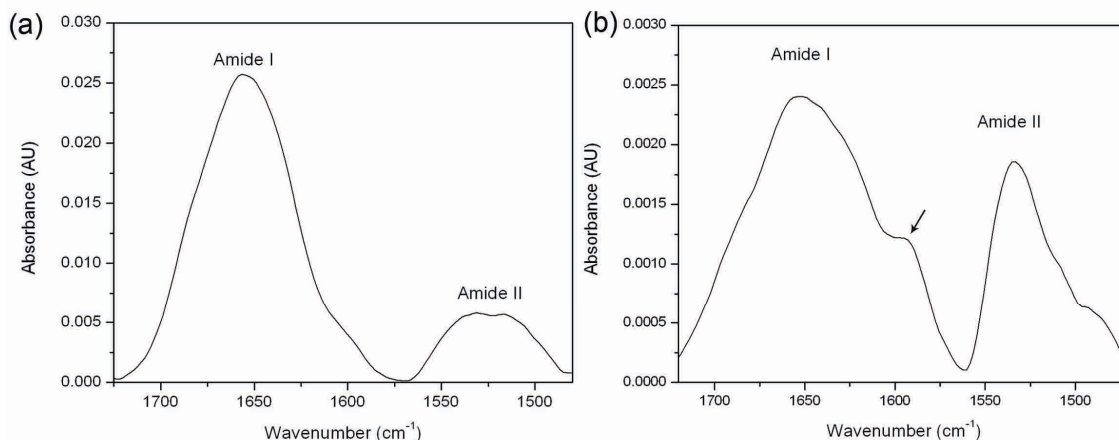
Figure 3.3: FTIR spectra of proteins adsorbed on (a) SCPC50-coated and (b) uncoated Ti-6Al-4V substrates after immersion in tissue culture medium for 4 h. Higher expression of amide I band was observed on SCPC50-coated substrate as compared to uncoated Ti-6Al-4V substrates. The high expression of amide I has been associated with enhanced cell activity. The arrow points to the shoulder representing protein side chains.

3.3.3 Bone cell phenotypic expression

3.3.3.1 Osteogenic protein synthesis

Cells attached to SCPC50-coated samples released significantly higher amounts of osteopontin (Figure 3.4a) and osteocalcin (Figure 3.4b) ($p < 0.05$) as compared to cells attached to uncoated Ti-6Al-4V samples throughout the experimental period. A significant increase ($p < 0.05$) in the synthesis of osteopontin was observed on both, SCPC50-coated and uncoated Ti-6Al-4V samples from day 16 to day 20. Minimal synthesis of osteocalcin was observed on either sample after 4 days of incubation, either due to the limitations of the detection limit of ELISA protocol or due to a delayed

osteocalcin secretion. Moderate levels of osteocalcin were synthesized by cells attached to SCPC50-coated or uncoated substrates until day 12; however significant ($p < 0.01$) changes in the osteocalcin levels were measured thereafter. Between day 16 and 20, a 3-fold increase in osteocalcin production was observed by cells attached to SCPC50-coated samples as compared to cells attached to uncoated Ti-6Al-4V samples.
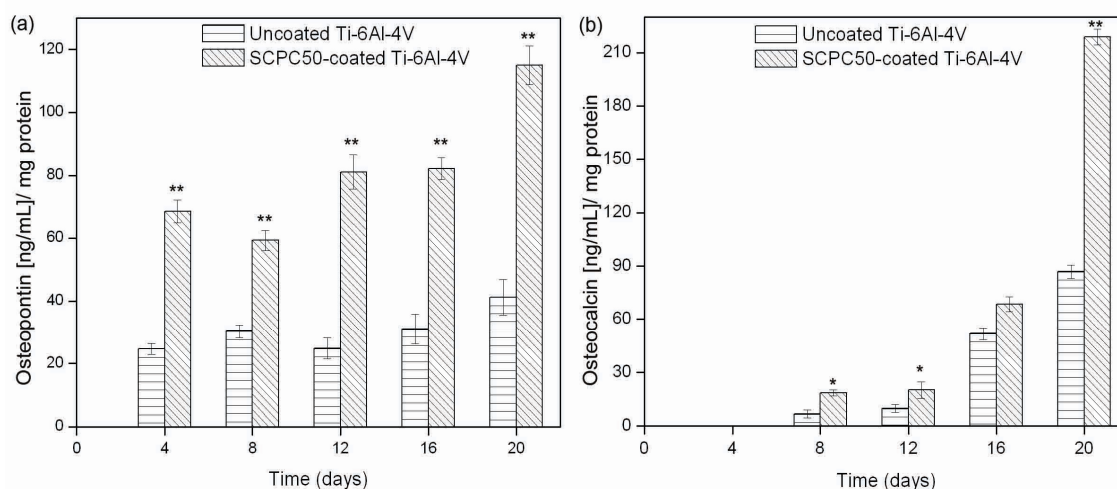
Figure 3.4: Concentrations of (a) osteopontin and (b) osteocalcin released by cells attached to SCPC50-coated and uncoated Ti-6Al-4V substrates after 4 - 20 days in culture. Cells attached to the SCPC50-coated substrates released significantly higher levels of osteopontin and osteocalcin throughout the experimental period. (*$p < 0.05$; **$p < 0.01$)

3.3.3.2 Measurement of gene expression

To determine whether enhanced levels of osteogenic protein production were due to changes in mRNA transcription, osteoblastic cells were attached to SCPC50-coated and uncoated Ti-6Al-4V for 4 days prior to isolation of total mRNA and analysis by quantitative real-time PCR. As shown in Figure 3.5d, cells attached to SCPC50-coated samples demonstrated 10.7-fold higher levels of mRNA encoding OCN than that

expressed by cells attached to uncoated Ti-6Al-4V. In contrast, cells attached to SCPC50-coated samples expressed significantly lower levels of mRNA encoding Col-I, OSN and OPN (Figure. 3.5a-c) suggesting that the increases in protein production of these products shown in Figure 3.4 are not due to increased transcription but may instead be due to changes in translation.
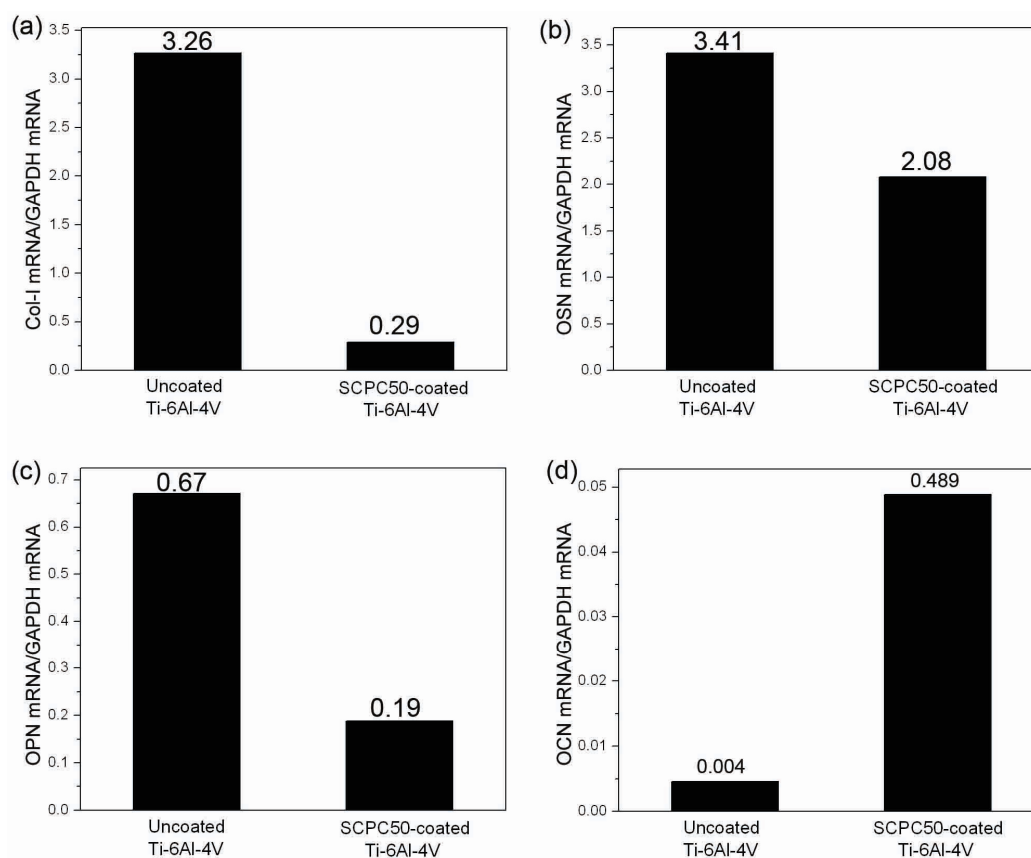
Figure 3.5: qRT-PCR analyses showing the levels of (a) Col-I; (b) OSN; (c) OPN and (d) OCN mRNA expressed by MC3T3-E1 cells after 4 days of incubation. Cells attached to uncoated Ti-6Al-4V substrates expressed higher levels of Col-I, OSN and OPN mRNA than that expressed by cells attached to the SCPC50-coated substrates. However, cells on SCPC50-coated substrate expressed higher level of OCN mRNA than the cells on uncoated Ti-6Al-4V substrate. The higher expression of OCN mRNA indicates the greater stimulatory effect of SCPC50 on cell differentiation.

3.3.3.2 Immunological response

Cells attached to SCPC50-coated Ti-6Al-4V substrates released significantly lower amount of the inflammatory and osteoclastogenic cytokines IL-6 ($p < 0.01$) and RANKL ($p < 0.05$) into the culture medium than that produced by cells attached to uncoated substrates (Figure 3.6). While the amount of IL-12p40 released by cells attached to SCPC50-coated samples tended to be lower than that released by cells attached to the uncoated Ti-6Al-4V, this decreased production was not statistically significant.
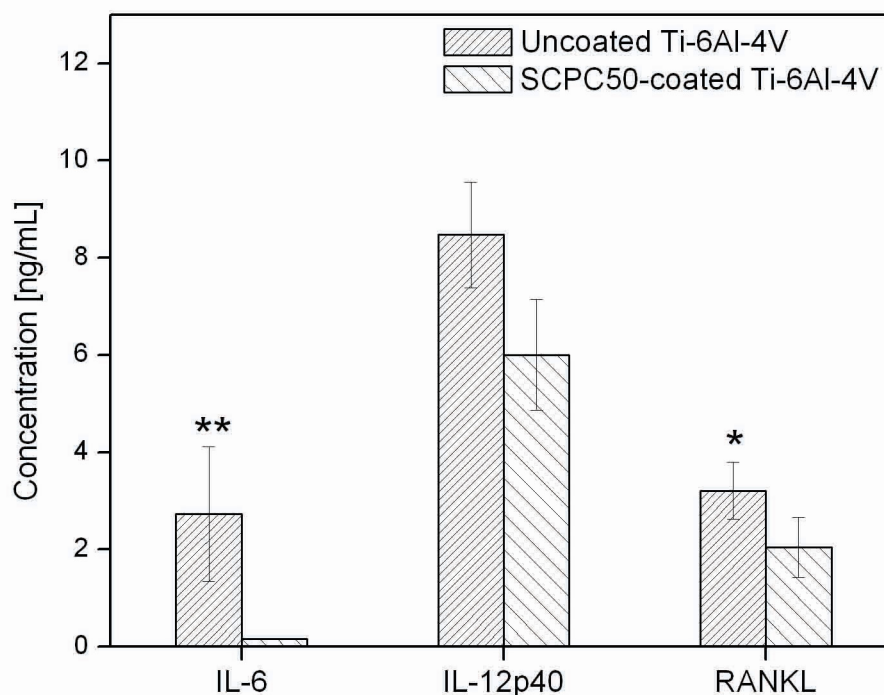
Figure 3.6: Measurements of the concentration of pro-inflammatory and osteoclastogenic cytokines showed that cells attached to SCPC50-coated Ti-6Al-4V released lower levels of IL-6, IL-12p40 and RANKL than those attached to the uncoated Ti-6Al-4V control. Lower expression of cytokines indicates low level immune response. (*$p < 0.05$; **$p < 0.01$)

3.3.4   Imaging and spectroscopic analyses

3.3.4.1 SEM - EDX analyses

SEM analyses of MC3T3-E1 cells after attached to SCPC50-coated or uncoated Ti-6Al-4V substrates showed complete surface coverage with a dense layer of cells on both samples after 4 days of incubation. Cells attached to the SCPC50-coated substrate showed early synthesis of calcified nodules (Figure 3.7a) while the cells attached to uncoated Ti-6Al-4V did not synthesize such nodules (Figure 3.7b). After 20 days of incubation, cells attached to the SCPC50-coated substrates produced a mineralized extracellular matrix populated with mature calcified nodules of 471.39 ± 96.08 nm diameter (Figure 3.7c). EDX analyses of the cell layer on the material surface showed a Ca/P ratio of 1.02 ± 0.23 with the presence of sulfur signal indicating biological mineralization. On the other hand, cells attached to uncoated Ti-6Al-4V substrates did not synthesize calcified nodules; however, spherical projections were observed on the cell layer (arrows; Figure 3.7d). The remarkable difference in the extent of mineralization between SCPC50-coated and uncoated Ti-6Al-4V substrate is noteworthy. Long-term immersion of SCPC50-coated samples in a physiologic solution showed that the thickness of the coating layer reduced from 5.1 ± 0.08 µm to 2.12 ± 0.38 µm after 10 weeks of immersion.
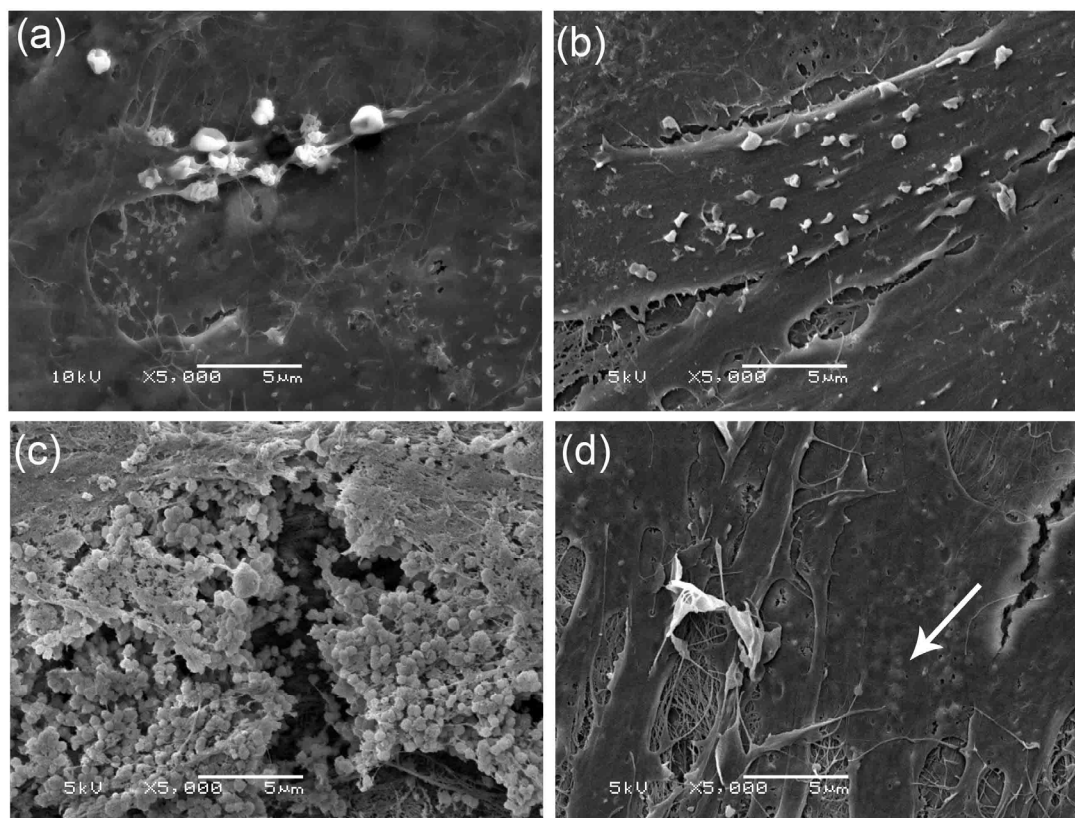
Figure 3.7: SEM images of MC3T3-E1 cells showed (a) the formation of calcified nodules on cells attached to SCPC50-coated substrates after 4 days of incubation. (b) Cell layer on the surface of control uncoated Ti-6Al-4V substrates did not show signs of calcification; (c) Cells attached to SCPC50-coated substrates produced mineralized extracellular matrix densely populated with calcified nodules after 20 days in culture. (d) Cells attached to the uncoated Ti-6Al-4V substrates did not show comparable mineralization under the same experimental conditions; however, a few spherical projections (arrow) were observed on the cell membrane.

3.3.4.2 FTIR analyses

Figure 3.8 shows the FTIR spectra of SCPC50-coated Ti-6Al-4V samples before and after immersion in TCM for 4 days in the presence or absence of cells. Unmodified (control) SCPC50-coated Ti-6Al-4V samples showed characteristic Si-O-Si stretching bands at 1075, 1160 and 1220cm^{-1} (Figure 3.8a). In addition, peaks representing P-O bending mode at 453 and 538 cm^{-1} and P-O stretching mode at 860 and 986 cm^{-1} were

observed. SCPC50-coated samples immersed in TCM in the absence of cells showed a diminished P-O stretching band at 860 cm^{-1}. New peaks at 850 and 1411 cm^{-1} corresponding to the symmetric stretching of O-C-O were noted (Figure 3.8b). On the other hand, SCPC50-coated samples immersed in TCM in the presence of cells showed evidence of HA formation. A characteristic triplet of peaks at 570 and 590 cm^{-1} corresponding to orthophosphate groups, along with a shoulder at 620 cm^{-1} corresponding to non-bridging O-H were observed (Figure 3.8c). Moreover, a sharp peak at 960 cm^{-1} corresponding to the PO$_4^{3-}$ group of HA was also observed. The presence of these bands indicates the formation of HA layer on SCPC-coated samples in the presence of cells. Uncoated Ti-6Al-4V samples immersed in TCM under similar experimental conditions did not show any HA formation (data not shown).
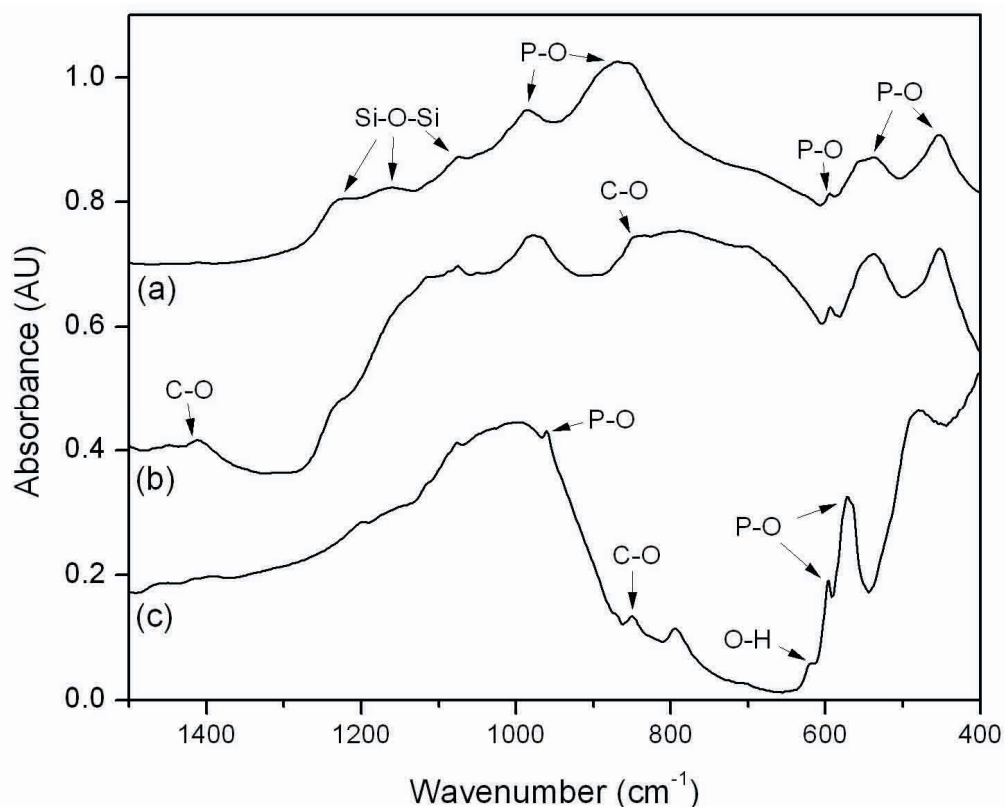
Figure 3.8: FTIR spectra of (a) unmodified SCPC50 coating layer on Ti-6Al-4V showing prominent peaks at 453, 538 and 978 cm^{-1} corresponding to the P-O groups and at 1075, 1160 and 1220 cm^{-1} corresponding to (Si-O-Si) structure; (b) After immersion in TCM for 4 days, the broad peak at 978 cm^{-1} representing P-O stretching band was diminished and new peaks at 850 and 1441 cm^{-1} corresponding to the O-C-O symmetric vibrations appeared. (c) SCPC50-coated samples with attached cells showed a characteristic triplet of peaks at 570, 590 and 620 cm^{-1} typical for hydroxyapatite.

3.3.5 Dissolution analyses

ICP - OES analyses of the cell culture media incubated with SCPC50-coated Ti-6Al-4V samples in the presence of cells showed that the Ca concentration in the media decreased significantly ($p < 0.01$) from 68.9 ± 6.9 ppm on day 2 to 38.2 ± 3.3 ppm on day 4 (Figure 3.9a). However, the Ca concentration in the medium increased thereafter and continued to increase to 74.2 ± 5.0 ppm on day 12 after which no significant change was measured. SCPC50-coated samples released 72.2 ± 6.1 ppm and 59.7 ± 2.4 ppm P after

incubation in media for 2 and 4 days, respectively which was significantly higher ($p <$ 0.05) than the corresponding values measured in media incubated with uncoated Ti-6Al-4V or media without substrate (control) (Figure 3.9b). However, a comparable P concentration among all substrates was measured thereafter. The release of Si was observed only in media incubated with the SCPC50-coated samples (Figure 3.9c). The Si concentration in the media increased marginally from 1.3 ± 0.2 ppm on day 2 to 1.9 ± 0.3 ppm on day 4, after which a sustained release in the range of 1.3 - 1.7 ppm was measured until day 12. A significant reduction ($p < 0.05$) in the Si concentration in the medium was measured after day 12, after which the SCPC50-coated samples continued to release Si in the range of $0.6 – 0.7$ ppm until day 20. The media of cells attached to uncoated Ti-6Al-4V or media without substrate showed comparable levels of Ca and P throughout the experimental period. Release of Ti from SCPC50-coated samples was not detected. However, uncoated Ti-6Al-4V samples released 4.3 ± 0.7 and 1.3 ± 0.5 ppb Ti after 2 and 4 days of incubation, respectively, after which no further release was detected.
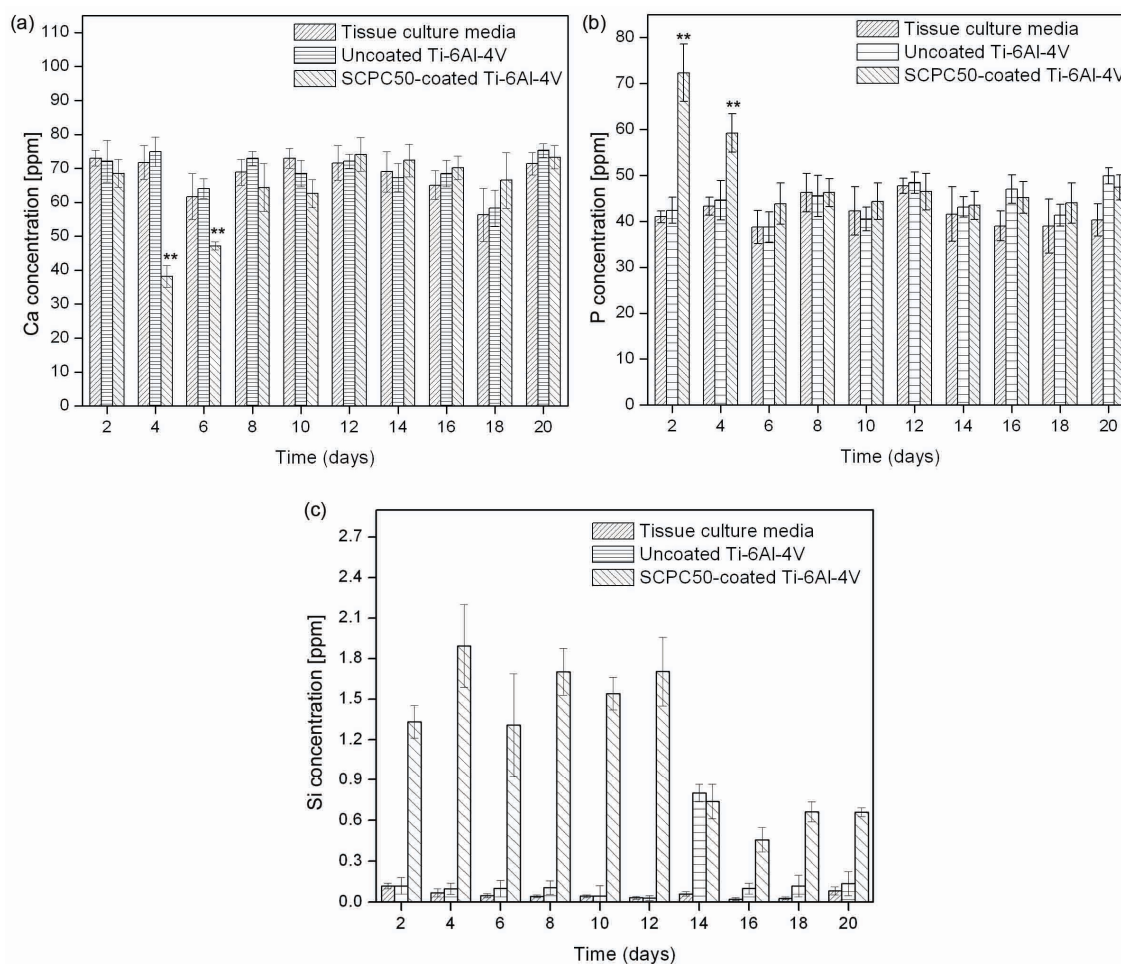
Figure 3.9: ICP-OES analyses of the tissue culture medium incubated with SCPC50-coated and uncoated Ti-6Al-4V samples in the presence of cells. (a) The concentration of Ca in the media incubated with SCPC50-coated samples decreased significantly after 4 days indicating Ca uptake by the SCPC50 surface. (b) On the other hand, the dissolution of SCPC50 coating significantly elevated the concentration of P in the tissue culture medium during the first 4 days of incubation. Minimal changes in the concentration of Ca and P were measured after 8 and 6 days, respectively. (c) The release of Si was observed only in TCM incubated with SCPC50-coated samples. A near-constant release of Si, in the concentration range of 1.3 − 1.8 ppm was measured up to 12 days of incubation, followed by a decrease in Si release thereafter. (**$p < 0.01$)

3.4   Discussion

Ti-6Al-4V coated with bioactive SCPC50 promoted osteoblast differentiation and deposition of mineralized bone matrix. MC3T3-E1 cells attached to SCPC50-coated Ti-6Al-4V showed up-regulated OCN mRNA after 4 days in culture and synthesized higher

amounts of osteocalcin and osteopontin proteins at all-time points as compared to uncoated Ti-6Al-4V substrates. Moreover, cells attached to the SCPC50-coated Ti-6Al-4V synthesized mineralized extracellular matrix after 4 days in culture as shown by FTIR and SEM analyses. The stimulatory effects of SCPC50 coating on cell differentiation and bone formation were accompanied by a decreased production of the inflammatory and osteoclastogenic cytokines, IL-6 and RANKL, indicating that such a coating minimizes the immune pro-resorptive functions of bone cells. On the other hand, cells attached to control uncoated Ti-6Al-4V implant material synthesized high levels of these soluble mediators and showed delayed osteoblast differentiation as indicated by a low expression of osteocalcin mRNA and a failure to produce mineralized bone matrix under the same experimental conditions. The strong stimulatory effect of SCPC50 coating on osteogenic functions correlates well with the selective adsorption of high quantities of serum proteins, in particular fibronectin, and the favorable conformation of the adsorbed protein onto the surface of the implant material. Another important factor that facilitated osteoblast differentiation was the dynamic changes in surface chemistry of SCPC50 coating as indicated by the uptake of Ca and release of P and Si. As such, the stimulatory effect on osteoblast differentiation and deposition of mineralized bone matrix of SCPC50-coated Ti-6Al-4V has the potential to enhance tissue integration and fixation of orthopedic implants.

The majority of serum proteins have low isoelectric point, such as albumin (pH_{iep} = 4.6), and are negatively charged at a physiological pH.[172] Previous studies have shown that the surface charge of SCPC50 is (-40.3 ± 1.76 mV), which is significantly higher than that reported for TiO_2 (15.0 - 30.2 mV) in water.[173,174] Ti-6Al-4V has a high

tendency to adsorb oxygen from the surrounding and form a TiO_2 surface layer.[175] Therefore, it is expected that negatively charged protein molecules are bound to the surface by electrostatic attraction. It is also possible that protein binding is mediated by Ca^{2+} ions adsorbed onto the surface of the material.[176] Therefore, based on the electrostatic adsorption mechanism, a lower serum protein adsorption onto SCPC50 surface is expected. However, our results showed a higher adsorption of serum proteins onto the SCPC50-coated substrates indicating that chemisorption is the primary mechanism of protein binding. The adsorbed protein was quantified using the detergent extraction which, based on previous work in our lab (not published), removes almost (95 - 98%) of the adsorbed proteins. The SCPC50 is composed of a solid solution of β– rhenanite (β-NaCaPO$_4$) and α-cristobalite (α-SiO$_2$).[103] Ca^{2+} present in the β-rhenanite phase of the SCPC50 serve as a bridge between the negatively charged substrate and serum proteins. The role of Ca^{2+} as a chelator and stabilizer for many different serum proteins, including albumin and fibronectin, is well established.[177,178] Previous reports from our lab have shown the ability of SCPC50 to up-take Ca^{2+} from physiologic solution and concentrate it onto the ceramic surface within 2 hr of immersion.[108] Therefore, the increase in Ca^{2+} concentration on the material surface could increase the number of binding sites for protein adsorption. Klinger *et al* incorporated Ca^{2+} on the surface of cp-Ti and studied the adsorption of human serum albumin (HSA) to the material.[179] It was found that the presence of Ca^{2+} on the surface of cp-Ti enhanced HSA adsorption more than two fold as compared to Ca^{2+} free surface. The presence of the α-cristobalite solid solution[103] as well as the amorphous silica-rich phase at the grain boundaries of SCPC50[180] can also play an important role in enhancing serum protein adsorption. In

aqueous solution, the deprotonation of silanol (Si-OH) groups into Si-O⁻ results in a

highly polar bond. The electronegative oxygen atom in Si-O⁻ can interact with the basic

amino acid residues in proteins such as guanidinium or NH_3^+, resulting in hydrogen

bonding (-N-H---O-) between the substrate and the protein.[181,182] Another material related

parameter that could contribute to the enhanced protein adsorption to SCPC50 is the high

surface area provided by the porosity of the surface. SEM analyses (Figure 3.1 inset)

showed that the surface of the SCPC50 coating is highly porous with an average pore size

of 50 ± 14 nm which provided a high surface area for protein binding.

Proteins adsorbed onto SCPC50-coated Ti-6Al-4V samples expressed a

significantly higher ratio of amide I/amide II bands as compared to that expressed by

proteins adsorbed onto the uncoated Ti-6Al-4V samples. Previous reports from our lab

have shown a correlation between the high expression of amide I and osteoblast

activity.[154] In contrast, high expression of amide II was associated with limited osteoblast

activity.[154] The amide I and amide II FTIR bands are primarily due to the stretching

vibrations of the C=O and bending vibrations of the N-H functional groups of the peptide

bond, respectively.[183,184] Both the C=O and the N-H bonds can interact with the Si-OH

groups and Ca-containing β-rhenanite in SCPC50 as shown in reactions 3.1 and 3.2:

$$O=C-N-H + Si-OH \longrightarrow (Si-O-H---N-C=O) \qquad (3.1)$$

$$H-N-C=O + Ca^{2+} \longrightarrow (-Ca-O-C-N-H) \qquad (3.2)$$
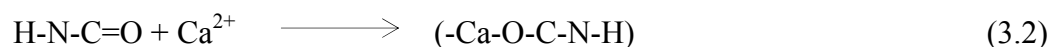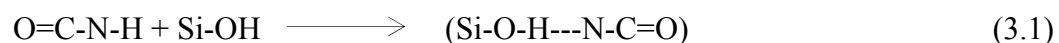
Protein adsorption according to equation (3.1) would results in the exposure of

C=O groups (amide I) on the material surface. Alternatively, protein adsorption

according to equation (3.2) would enhance the surface exposure of the -N-H groups and

hence the expression of amide II band. The enhanced expression of amide I band on

SCPC50-coated samples (Figure 3.3) indicates that the former binding mechanism dominates over the latter. On the other hand, the limited presence of negatively charged groups on uncoated Ti-6Al-4V substrates limits the expression of amide I band. Our results also showed that the intensity of the amide bands on SCPC50-coated Ti-6Al-4V substrates was higher than that of the amide bands on uncoated Ti-6Al-4V substrates. The difference in intensity is likely due to the significantly higher amount of protein adsorbed onto the former substrate.

ICP - OES analyses showed that SCPC50-coated Ti-6Al-4V substrates modified the chemical composition of the TCM by the uptake of Ca and the release of P and Si. SCPC50-coated samples seeded with cells absorbed Ca^{2+} from the TCM during the first 4 days of incubation (Figure 3.9a). The uptake of Ca^{2+} by SCPC50 can be attributed to the high surface area of SCPC50 rich in Si-OH groups.[108] A consequence of the Ca^{2+} uptake by the SCPC50 coating is an increase in the availability of Ca^{2+} for osteoblast activity. Ca^{2+} has been shown to change osteoblasts from a proliferative state to one that favors differentiation into mature bone forming cells.[185,186] Moreover, Ca^{2+} dependent proteins and gap-junctions are believed to participate in the signal transduction mechanisms that regulate osteoblast gene expression.[187] The dissolution of SCPC50 elevated the level of P during the first 4 days of incubation (Figure 3.9b). P plays an important role in cell differentiation by coordinating the expression and regulation of multiple factors necessary for bone mineralization, both at a transcriptional and at a post-translational stage.[188] Therefore, most studies in the literature use an exogenous P source, usually in the form of β–glycerophosphate, a component that does not exist in natural tissue.[189,190] In our study, we deliberately excluded β–glycerophosphate from the osteogenic media

and relied on SCPC50 to serve as a source for free P needed for bone formation. Recent reports from our lab have shown that the dissolution of SCPC50 elevates P level sufficiently enough to induce cell differentiation and mineralization of the extracellular matrix.[191] SCPC50-coated samples incubated with TCM also released Si in the concentration range of 1.3 – 1.9 ppm during the first 12 days of incubation (Figure 3.9c). Previous studies have shown that Si concentration in the range of 1 – 100 ppm range can stimulate osteoblast proliferation and differentiation.[149,192,193] Other reports have shown that Si is involved in the synthesis and stabilization of collagen and its presence is noted in the active growing front of new bone.[194] We have previously demonstrated the role of the α-cristobalite solid solution of SCPC50 in promoting guided cell adhesion and tissue regeneration by providing a preferential site for the deposition of extracellular matrix.[116] In the present study, cells attached to SCPC50-coated samples synthesized higher levels of OPN and OCN proteins as compared to the cells attached to uncoated Ti-6Al-4V samples. These proteins have critical roles in the mineralization of the extracellular matrix.[161,163] Indeed, a Ca/P ratio of 1.02 ± 0.23, the presence of sulfur, and the morphology of the calcified nodules observed on the extracellular matrix produced by cells attached to SCPC50-coated samples after 20 days, together with the enhanced synthesis of OCN protein indicate mineralized extracellular matrix. It is interesting to note that mineral formation occurred on SCPC50-coated samples only in the presence of cells, indicating that mineralization is cell-mediated. On the other hand, cells attached to uncoated Ti-6Al-4V samples demonstrated delayed onset of osteoblast differentiation. qRT-PCR results also showed that the expression levels of Col-I, OSN and OPN mRNA on uncoated Ti-6Al-4V substrates were significantly higher than the corresponding

levels on SCPC50 coated samples. Col-I and OSN genes are associated with cell-proliferation and pre-osseous matrix synthesis that precede cell differentiation and matrix mineralization.[97] The low expression of OPN mRNA on SCPC50-coated substrates may have been due to temporal variations in OPN gene which is known to decrease briefly post-proliferatively and then increase at the onset of matrix mineralization.[97] Taken together, the enhanced osteoblast differentiation and mineralization on the SCPC50-coated substrates can be attributed to the synergistic role of Ca uptake and SCPC50 ionic dissolution products. It is interesting to note that the stimulatory effect of SCPC50 on osteoblast activities was accompanied by minimal immune activation (Figure 3.6). This is in agreement with previous studies that have reported lower level immune response in actively differentiating osteoblasts.[195]

3.5 Conclusion

Bone cells attached to the SCPC50-coated Ti-6Al-4V substrates rapidly differentiated and produced mineralized bone matrix. Molecular biology assays demonstrated the SCPC50 surface up-regulated OCN mRNA expression and increased the production of OCN and OPN proteins. In contrast, cells attached to the uncoated Ti-6Al-4V substrates showed delayed differentiation and minimal bone-mineral formation. The enhanced osteogenic activity on SCPC50-coated Ti-6Al-4V substrates may be attributable to the enhanced protein adsorption and the dynamic changes in the surface chemistry of SCPC50 marked by Ca uptake and P and Si release, which would synergistically stimulate osteoblast differentiation and bone mineralization. Moreover, the enhanced osteogenic effects of SCPC50 layer were associated with decreases in the inflammatory and/or osteoclastogenic activities of osteoblast-like cells. Results of these

studies suggest that SCPC50 coating of Ti-6Al-4V implants has the potential to enhance

bone tissue integration and improve the fixation and longevity of the device.

CHAPTER 4: EFFECT OF SURFACE TOPOGRAPHY OF BIOACTIVE CERAMIC
COATING ON BONE CELL ACTIVITY

4.1 Introduction

Coating bioactive ceramics on Ti-6Al-4V orthopedic implants is a well-established method to enhance tissue integration and implant fixation.[77,101,114,145] Bioactive ceramic coating modifies both, the surface chemistry and the topography of the implant material. The enhancement effect of the calcium phosphate (CaP) surface chemistry on bone cell differentiation and tissue formation is well established.[108,116] Important material related bioactivity factors include: a CaP surface that is similar to the mineral phase of bone, enhanced protein adsorption, in particular cell attachment proteins, and the release of ions, such as Ca and Si, known to stimulate the metabolic activity of bone cells. The dynamic nature of bioactive ceramic surfaces, characterized by dissolution-precipitation reactions to and from the solution as well as cell-mediated resorption, can continuously alter the topography of the implant material. It is well established that the topography or surface patterning affects osteoblast activity, such as, adhesion, proliferation and differentiation; however, the exact effect on each function is debated.[196,197] It has been suggested that osteoblasts prefer smooth surface for proliferation and a rougher surface for differentiation related activities.[197-201] Li et al evaluated bone cell response to Ti substrates of varying roughness and showed that cell proliferation was highest on substrates with an average roughness (R_a) < 0.5 μm but decreased as the R_a value increased to 2.5 μm.[198] In contrast, the alkaline phosphatase

(AP) activity increased with increasing R_a values. Similar results were reported by Links *et al* who showed that an increase in the R_a of cp-Ti or Ti-6Al-4V substrates from 0.22 to 4.24 μm or from 0.23 to 3.20 μm, respectively, decreased cell proliferation while enhancing cell differentiation as measured by AP activity and osteocalcin synthesis.[199] Schneider *et al* analyzed osteoblast activity on grooved and roughened sand-blasted cp-Ti substrates and showed that after 3 days, cells attached to the rougher sandblasted substrate enhanced mineralization and up-regulated Cbfa1gene expression.[197] In a similar study, Balloni *et al* showed that cells on rough acid-etched Ti substrate expressed higher levels of differentiation associated genes including BMP-2, Runx2, collagen type I, bone sialoprotein, AP, osterix and osteocalcin after 15 days of culture than that expressed by cells on smother machined Ti substrate.[200] Other studies have found variable effects of surface roughness on cell proliferation and differentiation.[196,202,203] It was reported that an increase in the R_a value of cp-Ti substrates from 0.20 to 1.38 μm enhanced cell proliferation as well as osteocalcin synthesis, although AP activity decreased with increasing roughness.[196] Degasne *et al* showed that an increase in the R_a value of cp-Ti substrate from 0.30 to 0.94 μm was associated with an increase in cell proliferation.[202] Ramaglia *et al* reported that an increase in the roughness of cp-Ti discs from 318 to 762 nm had minimal effect on cell proliferation, although cell adhesion, collagen-I and integrin expression increased on substrates with higher roughness values.[203] Recent studies by Gittens *et al* have showed that nano-scale structures in combination with micro-scale roughness improve osteoblast differentiation and local factor production.[204]

The modifications in surface topography have been shown to control cell activity. Kim *et al* showed that an increase in the crystallinity and R_a of hydroxyapatite (HA)

coated cp-Ti substrates from 0.22 to 0.84 μm enhanced bone cell attachment to the substrate; however, AP activity and osteocalcin synthesis were not affected.[205] Moreover, they showed that HA coating layer prepared by sol-gel method and heat treated at 400 – 600 ˚C had undesirable higher dissolution rate that down-regulated cell proliferation and differentiation. The limited cell activity has been attributed to the instability of the implant surface. The dynamic surface instability of bioactive ceramics is difficult to measure and most studies have mainly focused on either the chemistry of the surface or the concentration of ions released from the substrate into physiological solutions. In case of bioactive materials characterized by a near chemically stable surface, such as stochiometric HA, data in the literature indicated that an increase in the R_a from 0.733 to 4.680 μm enhanced cell adhesion and proliferation.[206] Moreover, the AP activity of HA with R_a of 0.73 μm was almost double that on substrates with R_a of 2.86 or 4.68 μm after 8 days; however, at day 16, comparable AP activity was measured. It was speculated that the greater cell adhesion on rough HA was due to its higher surface area that enhances protein adsorption. In a separate study, it was shown that bone marrow cell proliferation on Ti-6Al-4V was higher than that on stochiometric HA discs of similar R_a.[207] However, comparable AP activity on both substrates was reported which might indicate higher AP activity per cell on the HA substrate. Other studies on various bioactive and non-bioactive materials have reported conflicting effects of surface topography and chemistry on cell behavior.[208,209] Dulgar-Tulloch *et al* evaluated cell response to nanophase alumina, titania and HA ceramic discs and showed that cell adhesion was dependent on the chemical composition and grain size of the material but not on surface roughness.[208] In addition, it was found that cells attached to ceramics of grain size of 200 nm

demonstrated greater proliferation than cells attached to ceramics of grain size 50 or 1500 nm, irrespective of the ceramic composition. The significant effect of surface chemistry on protein adsorption and cell response has prompted implanting the metal surface with ions such as Ca, Si, P to stimulate osteoblast activity.[201,210,211] Ca implantation on Ti substrates induced formation of integrin-rich adhesion plaques and changes in the cell shape from circular to elongated within 4 hr.[210] Park *et al* reported that the incorporation of Ca on machined and grit-blasted cp-Ti substrates enhanced cell proliferation irrespective of the substrate's roughness.[201] Moreover, cells attached to the Ca incorporated grit-blasted Ti substrates showed enhanced differentiation as indicated by higher levels of AP, osteopontin, and osteocalcin mRNA than cells attached to the other substrates. Bone cells attached to SCPC50-coated Ti-6Al-4V substrates have demonstrated enhanced osteoblast differentiation and low level immunogenic response as compared to the cells attached to uncoated Ti-6Al-4V substrates (described in Chapters 2 and 3). The objective of this study is to investigate the effect of substrate roughness on the characteristics of SCPC50 coating using atomic force microscopy (AFM). Moreover, bone cell morphology, cytoskeletal organization and proliferation have been correlated to the surface topography and ions released from the SCPC50-coated Ti-6Al-4V substrate.

4.2   Materials and Methods

4.2.1 Sample preparation

Bioactive SCPC50, in the size range of 100 – 500 nm, containing 40.68 % CaO, 20.34 % P_2O_5, 19.49 % Na_2O and 19.49 % SiO_2 (in mol %) was prepared following the methods described in the literature.[103,108] Ti-6Al-4V ELI (ASTM F136-08e1) discs of two different surface roughnesses were prepared by grinding the discs on 400 or 1200 grit silicon carbide (SiC) abrasive pad. The discs ground on the 1200 grit SiC were further

polished on a micro-cloth using 50 nm alumina particles until a mirror-finish was obtained. The samples were cleaned according to ASTM standard protocol F86-04 (Standard Practice for Surface Preparation and Marking of Metallic Surgical Implants) and passivated in 34% HNO_3 at 65 ºC for 40 min. SCPC50 nano-particles were coated on Ti-6Al-4V samples using EPD as previously described in chapter 3. Briefly, Ti-6Al-4V samples were immersed in a 10 wt% SCPC50 suspension in ethanol and coated using a voltage of 50 V for 10, 30, 60 or 90 s, with intermediate drying every 30 s. The coated samples were dried in a dessicator and thermally treated at 800 ºC for 1 hr under argon at a fixed heating and cooling rate of 2 ºC min^{-1}.

4.2.2 Surface topography analyses

The surface topography of the SCPC50-coated and uncoated Ti-6Al-4V samples was analyzed using Nanoscope IIIm Multimode atomic force microscope (AFM; Veeco Instruments, Plainview, NY). Ti-6Al-4V samples without SCPC50 coating but heat treated at 800 ºC for 1 hr were also analyzed. Images were obtained at two different resolutions, 5 μm x 5 μm and 40 μm x 40 μm, to characterize the nano- and the micro-roughness of the substrate, respectively. Data was acquired from 12 regions on 3 discs (4 regions/ disc) for every sample type in tapping mode using an integral cantilever attached with an uncoated silicon tip (n = 12). The force constant of the tip was 42 N m^{-1}, the resonant frequency was 320 kHz, the height was 10 - 15 μm and the radius of curvature was 8.0 nm. The R_a of the substrate was determined by image analysis using the inbuilt software (Nanoscope; Veeco Instruments, Plainview, NY). Dimensional analyses on 100 random regions of each sample type (n = 100) were performed using the 'linescan'

feature of the software to determine the peak diameter and peak-to-peak (PTP) distance as shown in Figure 4.1.
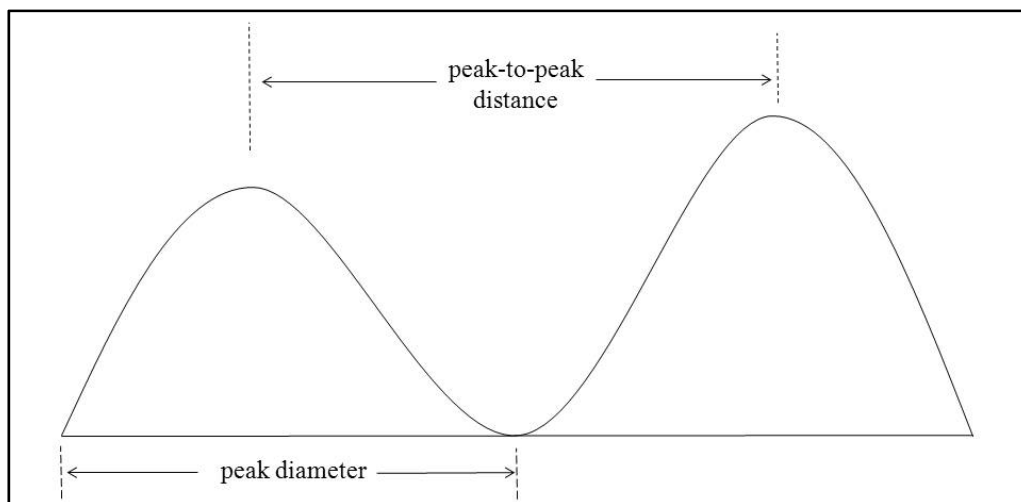
Figure 4.1: Schematic representation of peak diameter and peak-to-peak distance on SCPC50-coated and uncoated Ti-6Al-4V substrate.

4.2.3   Evaluation of bone cell response

4.2.3.1 Cell culture

MC3T3-E1 mouse osteoblast-like cells (ATCC; Manassas, VA) were cultured in Dulbecco's Modified Eagle Medium supplemented with 10% fetal bovine serum and 0.1% penicillin-streptomycin, and incubated at 37 ºC and 5% humidified CO_2. As Ti-6Al-4V (400 grit group) discs coated with SCPC50 for 30 and 60 s exhibited statistically significant differences in R_a, both, at the nano and at the micro level (see results), they were selected for cell culture studies. The samples were sterilized in pure ethanol for 20 min and dried under UV-irradiation. Upon 70 - 80% confluency, cells were trypsinized and seeded on the samples at a density of 5 x 10^4 cells/disc for 4, 8 or 24 hr. Uncoated Ti-6Al-4V (400 grit group) samples served as control.

4.2.3.2 Cell viability analysis

The viability of cells attached to 30 s and 60 s SCPC50 coated and uncoated Ti-6Al-4V substrates was determined using LIVE/DEAD cell viability assay (Invitrogen, Grand Island, NY) after 24 hr of incubation (n = 3). The samples were rinsed in phosphate buffer saline (PBS) and stained with 2 μM calcein AM and 4 μM ethidium homodimer-1 in PBS and incubated for 20 min at 37 °C in dark. Excess dye was removed by washing 3 times in PBS. 5 random fields on every sample were imaged using a confocal microscope. The percentage viability was calculated as the number of live cells divided by the total number of cells attached to the substrate.

4.2.3.3 Cell morphology analyses

At each time point (4, 8 or 24 hr), the morphology of cells attached to the 30 s and 60 s SCPC50 coated substrates as well as uncoated Ti-6Al-4V substrates were analyzed in duplicate using scanning electron microscopy (SEM). The samples were washed 3 times in pre-warmed PBS and fixed overnight in Karvonsky's fixative (Electron Microscopy Sciences, Hatfield, PA) at 4 °C. Cells were subjected to ethanol series dehydration followed by a final dehydration in hexamethyldisilazane. The samples were dried in a dessicator for 2 hr, coated with 5 nm gold film and analyzed using SEM. 10 images were obtained (5 images/disc) for every sample type. Cell spreading was quantified by measuring the area of 100 random cells (n = 100; 10 cells/image) using the Scandium platform image analysis software (Olympus Soft Imaging Solutions, Münster, Germany). Moreover, the shape of the cells was determined by a dimensionless shape factor value for circularity (area x 4Π / perimeter^2). A shape factor value approaching 1

represents circular shape (round cells) while values approaching 0 represents straight line (elongated cells).[212]

4.2.3.4 Cytoskeletal organization and cell proliferation analyses

The cytoskeletal organization of cells attached to 30 s and 60 s SCPC50 coated as well as the uncoated Ti-6Al-4V substrates were visualized in duplicate by staining the F-actin filaments with a fluorescent rhodamine phalloidin probe. Briefly, cells were washed 3 times in pre-warmed PBS and fixed in freshly prepared 4% paraformaldehyde for 15 min, permeabilized in 0.1% Triton X-100 for 1 min and blocked in 3% BSA (blocking buffer) for 30 min at room temperature. Cells were stained with TRITC conjugated phalloidin and Hoechst dye (Invitrogen, Grand Island, NY) in dilution ratios of 1:200 and 1:500, respectively, in blocking buffer for 20 min at room temperature under dark. At the end of the immersion period, the samples were washed 3 times in PBS and imaged using confocal microscope. The organization of actin filaments was scored as type I, II or III following the same method as suggested by Sinha *et al.*[212] Type I cells displayed faint staining with no discernible actin filaments; type II cells showed cortical filaments below the cell membrane with some radially oriented filaments; and type III cells had distinct well-formed filaments that oriented parallel to each other and along the long axis of the cell. The distribution of each cell type was determined by examining 100 cells (50 cells/disc) attached to every sample type (n = 100). To determine cell proliferation, 10 random fields on every sample type were imaged at 15X magnification (5 images/disc) and the number of cells (stained blue by Hoechst dye) was counted. The percentage increase in the number of cells was calculated by normalizing the average cell number at any given time to the average cell number on that sample type at the 4 hr time point.

4.2.4 Dissolution analyses

The release of ionic products from the dissolution of SCPC50 coated and uncoated Ti-6Al-4V substrate was analyzed by measuring the ionic concentration of Ca, Si, P, and Ti in TCM at every time point using Optima 2100 DV inductively coupled plasma-optical emission spectrometer (ICP – OES; Perkin Elmer, Waltham, MA). The machine was operated under conditions previously reported.[116]

4.2.5 Statistical analysis

One-way ANOVA was used to assess the statistical difference among the various treatment groups. Fisher's LSD post hoc test was conducted to ascertain the difference between individual groups. A p-value < 0.05 was considered statistically significant.

4.3 Results

4.3.1 Surface topography

The AFM images of the 1200-grit group Ti-6Al-4V substrates before and after coating are shown in Figure 4.2. The unmodified control surface ground on 1200 grit SiC and polished using 50 nm alumina particles appeared flat with minimal grooves or surface irregularities (Figure 4.2a). Thermal treatment of the sample at 800 ˚C for 1 hr increased the roughness of the substrate (Figure 4.2b), most probably due to the formation of TiO_2 at elevated temperatures. EDX analyses of the substrates indicated an O/Ti ratio of 3.92 ± 0.13 (n = 5) suggesting the presence of TiO_2 (data not shown). The surface topography of substrate coated with SCPC50 for 10 s (Figure 4.2c) appeared similar to uncoated heat-treated substrate; however, an increase in the coating duration to 30 s (Figure 4.2d) reduced the surface roughness of the substrate. An increase in the coating duration to 60 s (Figure 4.2e) or 90 s (Figure 4.2f) appeared to increase the

roughness of the substrate, and created pockets containing surface pits. Ti-6Al-4V substrates prepared on the 400-grit substrates prominently showed grooves created from grinding during surface finishing. (Figure 4.3a) Heat treatment of the substrate promoted the formation of fine TiO_2 grains (Figure 4.3b). The deposition of SCPC50 for 10 s (Figure 4.3c) or 30 s (Figure 4.3d) appeared to reduce surface roughness by filling in the grooves of the substrate. An increase in the coating duration to 60 s (Figure 4.3e) or 90 s (Figure 4.3f) appeared to deposit coarser particles and create regions of non-uniform distribution on the surface.
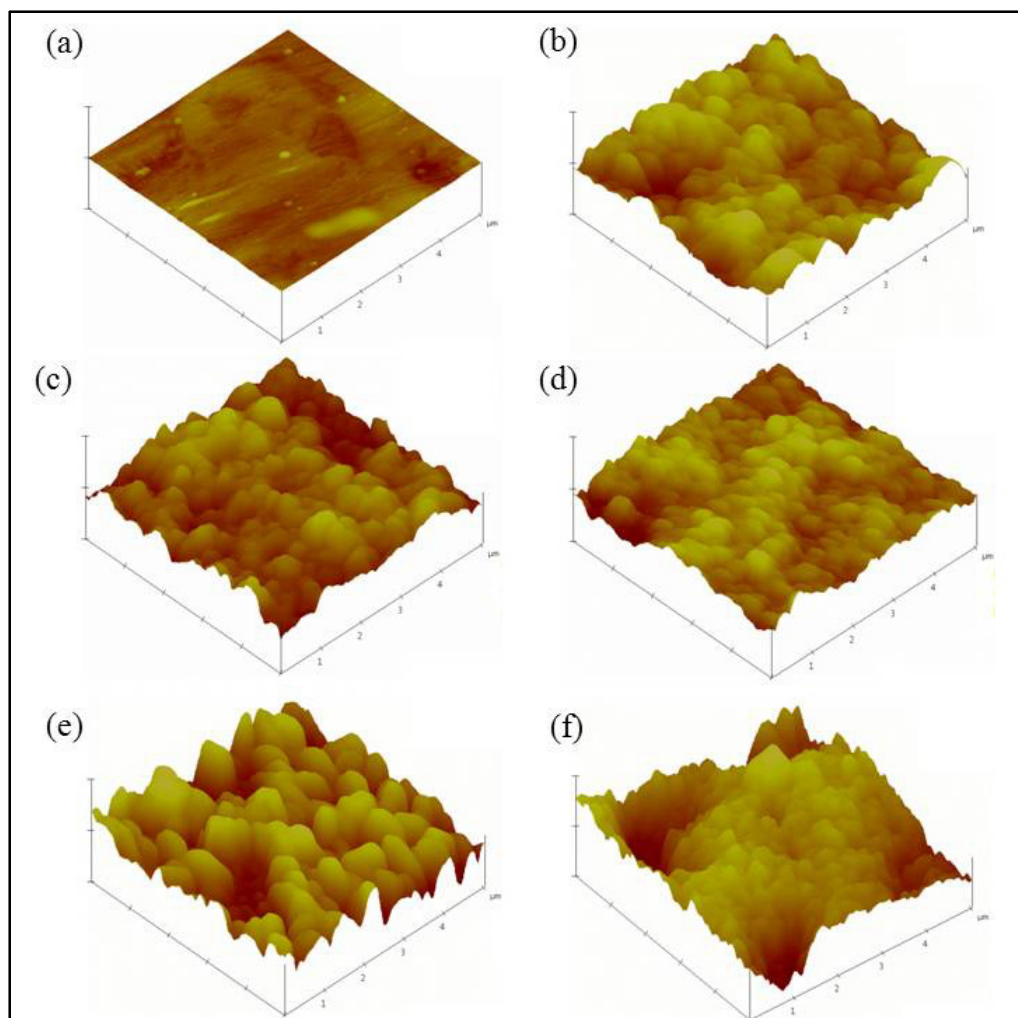
Figure 4.2: AFM images of the 1200-grit group SCPC50-coated and uncoated Ti-6Al-4V substrates (a) before and (b) after thermal treatment at 800 ˚C for 1 hr. The roughness of the substrate increased upon thermal treatment. Surface topography of SCPC50 on Ti-6Al-4V substrate after coating for (c) 10 s, (d) 30 s, (e), 60 s and (f) 90 s. The roughness appeared to decrease after 30 s of coating and increase at higher coating duration. The images were acquired at a resolution of 5 μm x 5 μm.
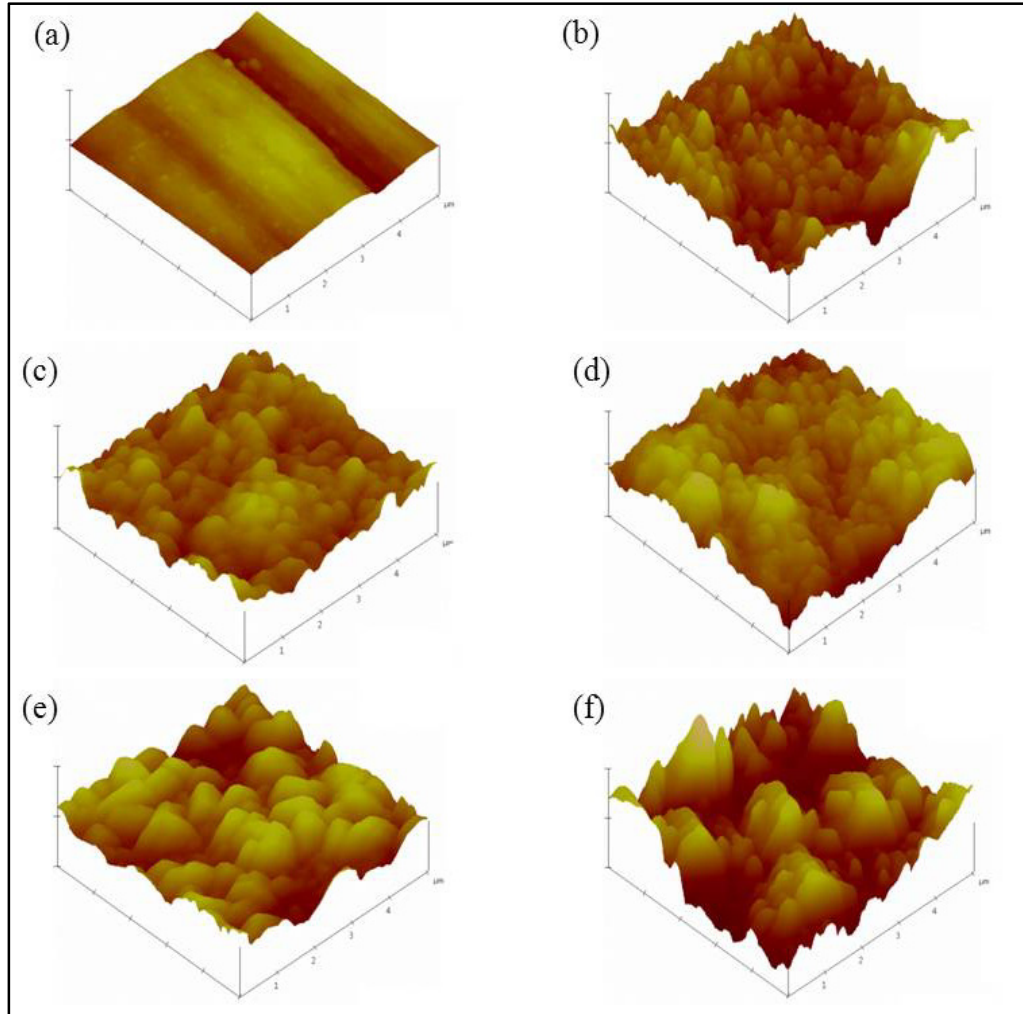
Figure 4.3: AFM images of the 400-grit group SCPC50-coated and uncoated Ti-6Al-4V substrates (a) before and (b) after thermal treatment at 800 ˚C/1 hr. The roughness of the substrate increased upon thermal treatment. Surface topography of SCPC50 on Ti-6Al-4V substrate after coating for (c) 10 s, (d) 30 s, (e), 60 s and, (f) 90 s. The roughness appeared to decrease after 30 s of coating and increase at higher coating duration. The images were acquired at a resolution of 5 μm x 5 μm

4.3.2 Surface roughness

4.3.2.1 Nano-roughness analyses (5 μm x 5 μm scans)

Surface topography analyses of uncoated Ti-6Al-4V substrates showed that the R_a of the samples ground on 1200 grit SiC (3.51 ± 0.70 nm) was significantly lower (p <

0.01) than those ground on 400 grit SiC (27.24 ± 6.68 nm) (Figure 4.4). Comparable R_a

values were measured before and after passivation treatment on each substrate. The R_a of

the 1200 grit group Ti-6Al-4V samples decreased slightly from (54.68 ± 11.81 nm) after

thermal treatment at 800 ˚C for 1 hr (control) to (52.96 ± 5.34 nm) and (46.43 ± 11.98

nm) after EPD coating for 10 s and 30 s, respectively (Figure 4.3). A significant increase

(p < 0.01) in R_a was measured upon increasing the coating duration to 60 s (74.13 ±

18.43 nm), followed by a slight decrease after 90 s of coating (62.44 ± 24.58 nm). On the

other hand, SCPC50 coating on the 400 grit polished Ti-6Al-4V substrates resulted in a

gradual increase of R_a with coating duration: 10 s (60.97 ± 7.42 nm) < 30 s (68.15 ±

18.74 nm) < 60 s (76.84 ± 15.99 nm) < 90 s (82.38 ± 21.23 nm).
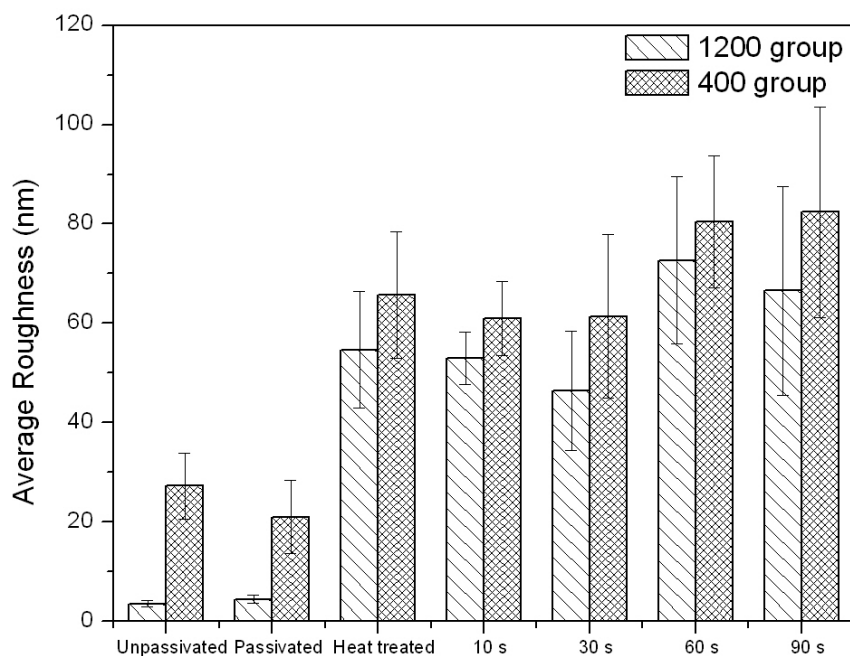
Figure 4.4: Nano-scale roughness analyses of uncoated and SCPC50-coated Ti-6Al-4V substrates at a resolution of 5 μm x 5 μm. The R_a of 400- and 1200-group Ti-6Al-4V substrates decreased with an increase in the coating duration up to 30 s to achieve minimal values. An increase in the coating duration from 30 to 60 s resulted in a significant increase in the R_a of the substrate.

4.3.2.2 Micro-roughness analyses (40 µm x 40 µm scans)

AFM analyses showed that the R_a of the Ti-6Al-4V substrates ground on 1200 grit SiC (8.01 ± 1.83 nm) was significantly lower ($p < 0.01$) than the substrates ground on the 400 grit SiC (82.89 ± 25.3 nm) (Figure 4.5). Comparable R_a values were measured before and after passivation treatment on each substrate. The R_a of the uncoated 1200 grit group Ti-6Al-4V substrate increased from (94.71 ± 14.46 nm) after heat treatment at 800 ˚C for 1 hr (control) to (159.68 ± 38.29 nm) and (132.55 ± 32.15 nm) after coating for 10 s and 30 s, respectively. An increase in the coating duration to 60 s increased the R_a significantly ($p < 0.01$) to (239.08 ± 54.73 nm); however, coating for 90 s decreased R_a significantly ($p < 0.01$) to (107.72 ± 11.14 nm). Similarly, the R_a on the (400 grit group) Ti-6Al-4V substrates increased significantly ($p < 0.01$) from (160.09 ± 21.02 nm) after heat treatment to (300.92 ± 32.75 nm) after coating with SCPC50 for 10 s. An increase in the coating duration to 30 s reduced R_a value significantly ($p < 0.01$) to (217.86 ± 54.57 nm); however, further increase in the coating duration to 60 or 90 s increased the R_a to (284.30 ± 37.33 nm) and (335.57 ± 47.64 nm), respectively.
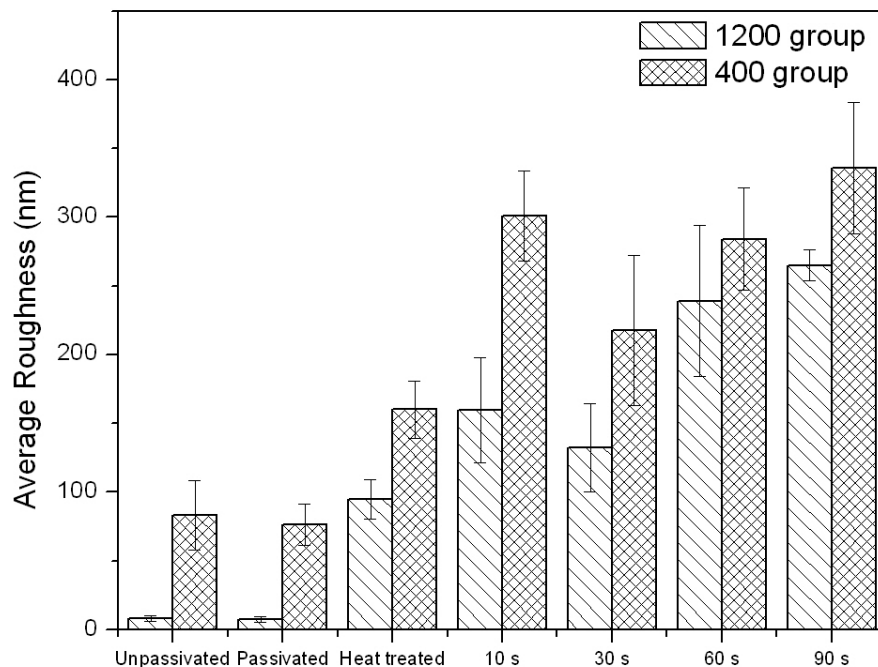
Figure 4.5: Micro-scale roughness analyses of uncoated and SCPC50-coated Ti-6Al-4V substrates at a resolution of 40 μm x 40 μm. The R_a of 400- and 1200-group Ti-6Al-4V substrates decreased with an increase in the coating duration to 30 s to achieve minimal values. An increase in the coating duration from 30 to 60 s resulted in a significant increase in the R_a of the substrate.

4.3.3 Peak diameter

The peak diameter of SCPC50 coated on (1200 grit group) Ti-6Al-4V substrates decreased with increasing coating duration: 10 s (452.06 ± 122.10 nm) > 30 s (403.78 ± 93.79 nm) > 60 s (387.44 ± 118.17) > 90 s (355.70 ± 107.34 nm) (Figure 4.6). The peak diameter of SCPC50 on all coated substrates was significantly smaller ($p < 0.05$) than that of heat treated uncoated Ti-6Al-4V substrates (498.89 ± 158.64 nm) obtained after thermal treatment (control). In contrast, the peak diameter of the 400 grit group SCPC50-coated substrates was significantly higher ($p < 0.01$) than that of heat-treated uncoated Ti-6Al-4V samples (277.04 ± 81.63 nm). The peak diameter of SCPC50 decreased with coating duration up to 60 s in the order: 10 s (538.51 ± 82.57 nm) > 30 s (519.71 ±

146.96 nm) > 60 s (420.04 ± 129.98 nm). Increase in the coating duration from 60 s to 90

s resulted in a significant increase (p < 0.05) of peak diameter (510.99 ± 154.18 nm).

Comparable peak diameter was measured on uncoated Ti-6Al-4V (without heat

treatment), for both 1200 and 400 grit group samples, before and after passivation

treatment.
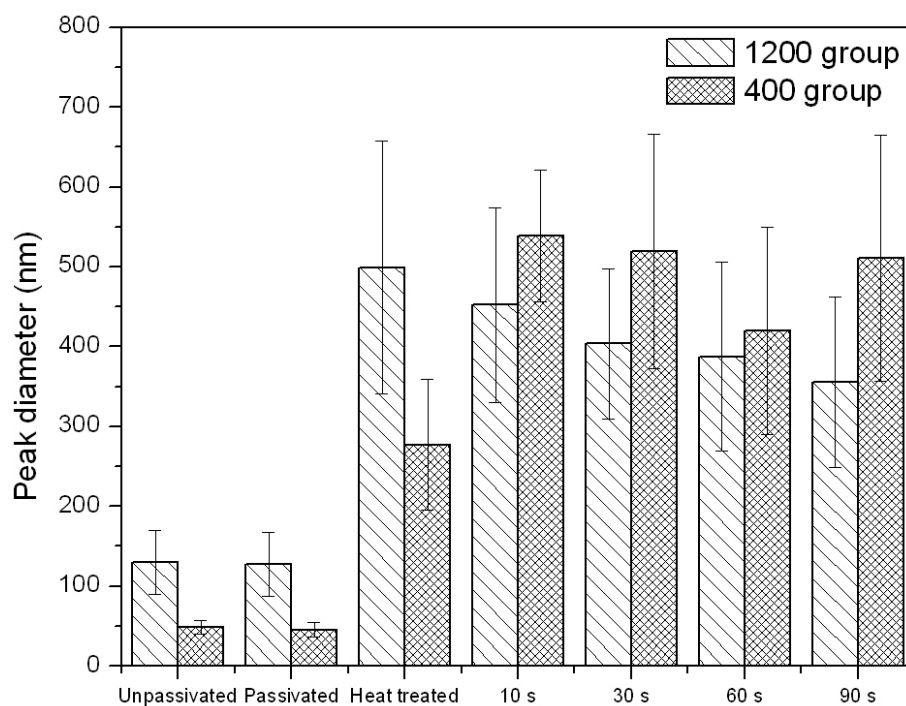
Figure 4.6: Peak diameter of uncoated and SCPC50-coated Ti-6Al-4V substrates as a function of coating duration. Higher peak diameter values at lower coating duration suggest that SCPC50 at the metal/ceramic interface experienced greater residual stresses leading to expansion of the material.

4.3.4 Peak-to-peak distance

Comparable PTP distance were measured on the 1200-grit group Ti-6Al-4V

substrates that had been heat-treated (330.19 ± 61.88 nm) or coated with SCPC50 for 10 s

(310.94 ± 76.33 nm) (Figure 4.7). An increase in the coating duration to 30 s resulted in a

significant decrease (p < 0.05) in the PTP distance (211.23 ± 55.04 nm), followed by a

significant increase (p < 0.05) upon increase to (274.22 ± 62.62 nm) and (277.40 ± 65.98

nm) after coating for 60 s and 90 s, respectively. PTP distance on the 400-grit group Ti-

6Al-4V substrates decreased with increasing coating duration in the order: 10 s (464.84 ±

67.38 nm) > 30 s (449.25 ± 100.00 nm) > 60 s (419.92 ± 77.01 nm) > 90 s (374.43 ±

72.53 nm). Moreover, the PTP distance on the control heat-treated substrate (220.94 ±

42.60 nm) was significantly lower (p < 0.01) than that on the SCPC50-coated substrates.

Comparable values of PTP distances were measured on both, 1200 and 400-grit group Ti-

6Al-4V substrates before and after passivation treatment.
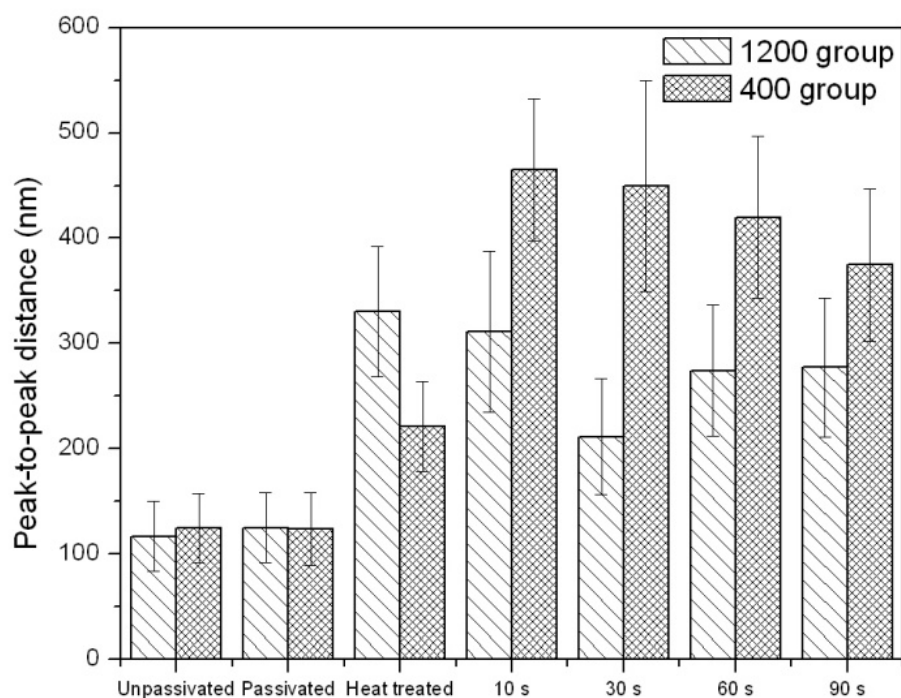
Figure 4.7: Peak-to-peak distance of uncoated and SCPC50-coated Ti-6Al-4V substrates as a function of coating duration. The PTP distances decreased with increasing coating duration on the 400-grit group substrates. On the other hand, the PTP distance on the 1200-grit group samples acquired minimal values after 30 s coating and increased at higher coating duration.

4.3.5 Analyses of cell response

4.3.5.1 Cell viability

Cell viability analyses using LIVE/DEAD assay showed a healthy population of live cells with intact cell membrane (green) attached to the uncoated (Figure 4.8a), 30 s SCPC50 coated Ti-6Al-4V substrates (Figure 4.8b) after 24 hr of incubation. On the other hand, fewer numbers of cells were seen attached to the 60 s SCPC50 coated substrate (Figure 4.8c). Nonetheless, negligible numbers of dead cells (red) were observed on all substrates indicating near 100% viability.
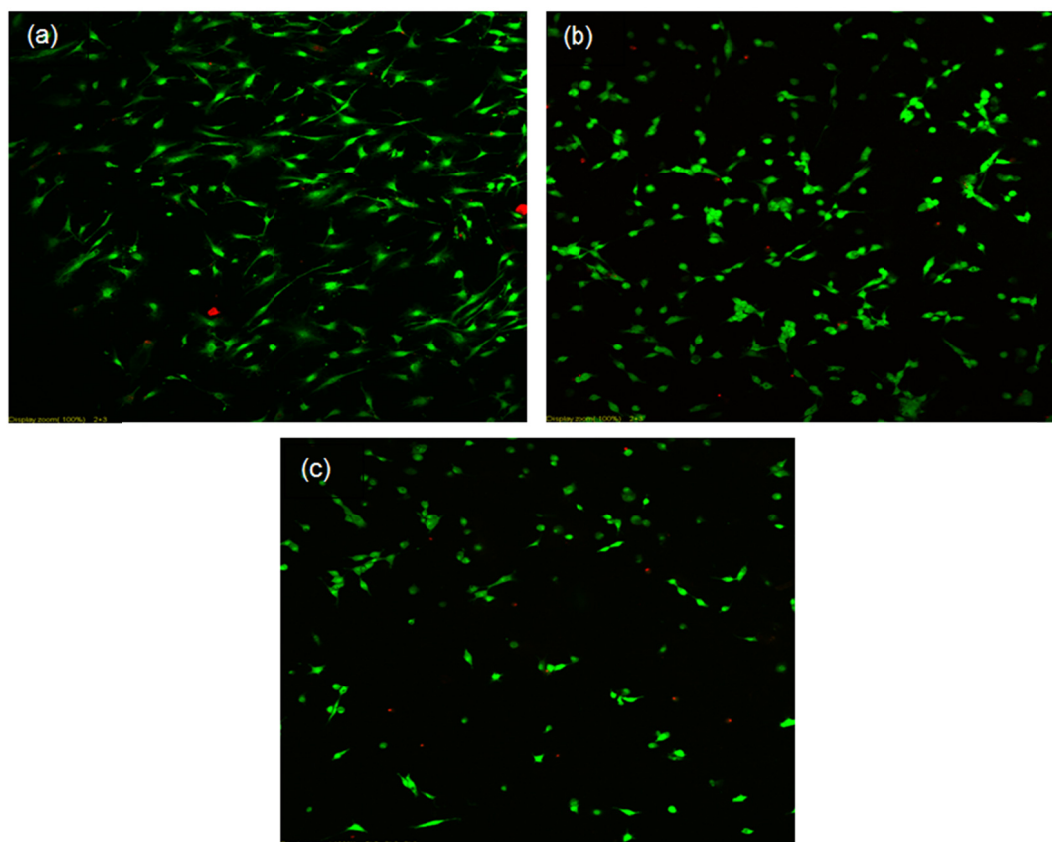
Figure 4.8: LIVE/DEAD analyses showing live cells (green) attached to (a) uncoated; (b) 30 s SCPC50 coated and (c) 60 s SCPC50 coated Ti-6Al-4V substrates after 24 hr of incubation. The minimal presence of dead cells (red) suggests near-complete viability.

4.3.5.2 Cell morphology

After 4 hr of incubation, cells attached to the uncoated Ti-6Al-4V substrates showed fully flattened and rounded morphology with limited cell-to-cell contact (Figure 4.9a). In contrast, cells attached to the Ti-6Al-4V substrates coated with SCPC50 for 30 s (Figure 4.9b) or 60 s (Figure 4.9c) showed less spreading and appeared polygonal in shape. Moreover, they formed multiple pseudopodia-like plasma-protrusions to adhere onto the SCPC50 coating and demonstrated extensive cell-to-cell contact. After 8 hr, cells attached to the uncoated Ti-6Al-4V substrates showed greater surface coverage with an increase in cell number (Figure 4.9d). In addition, the cells appeared to acquire a polygonal shape and developed greater cell-to-cell contacts. However, a distinct difference in cell morphology was noted between cells on the uncoated and SCPC50-coated substrates. Clusters of cells attached to the 30 s (Figure 4.9e) or 60 s (Figure 4.9f) coated SCPC50 substrates merged together in multiple regions. On the other hand, cells attached to the uncoated Ti-6Al-4V substrates appeared to resist such contact even when the cells were in close proximity. After 24 hr, cells attached to the uncoated Ti-6Al-4V substrates (Figure 4.9g) and 30 s coated SCPC50 substrate (Figure 4.9h) showed more cell-to-cell contact and surface coverage, with cells on the former substrate showing near-complete surface coverage. However, cells attached to 60 s coated SCPC50 substrate decreased in number and surface coverage, although they appeared more elongated than cells on other substrates (Figure 4.9i).
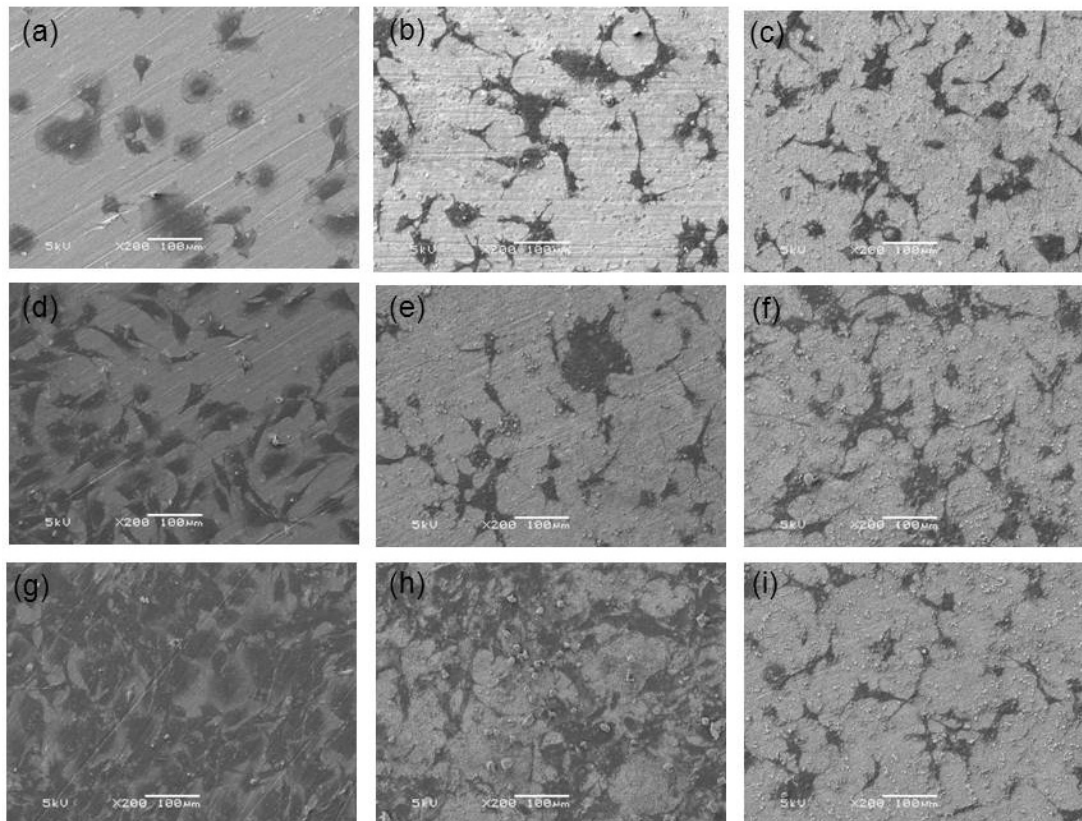
Figure 4.9: SEM images showing the morphology of bone cells attached to (a) uncoated, (b) 30 s SCPC50 coated and (c) 60 s SCPC50 coated substrates after 4 hr. More cells were attached to the SCPC50-coated substrates than to the uncoated substrates. After 8 hr, cells attached to the uncoated substrates showed higher proliferation rate than the cells attached to the (e) 30 s SCPC50 coated or (f) 60 s SCPC50 coated substrates. At the end of 24 hr, cells attached to the (g) uncoated substrates showed greater surface coverage than the cells attached to the (h) 30 s SCPC50 coated substrate. (i) In contrast, cells attached to the 60 s SCPC50 coated substrate reduced in number.

4.3.5.3 Cell spreading

Cells attached to the uncoated Ti-6Al-4V substrate showed significantly more spreading ($p < 0.05$) than cells attached to the 30 s and 60 s SCPC50-coated substrates throughout the experimental period (Figure 4.10). The area of cells attached to uncoated and 30 s coated SCPC50 substrates decreased slightly with culture time; however, the difference was not statistically significant. In contrast, cells attached to the 60 s-SCPC50

coated substrate showed a significant ($p < 0.05$) two-fold decrease in area as the culture time increased from 4 to 24 hr.
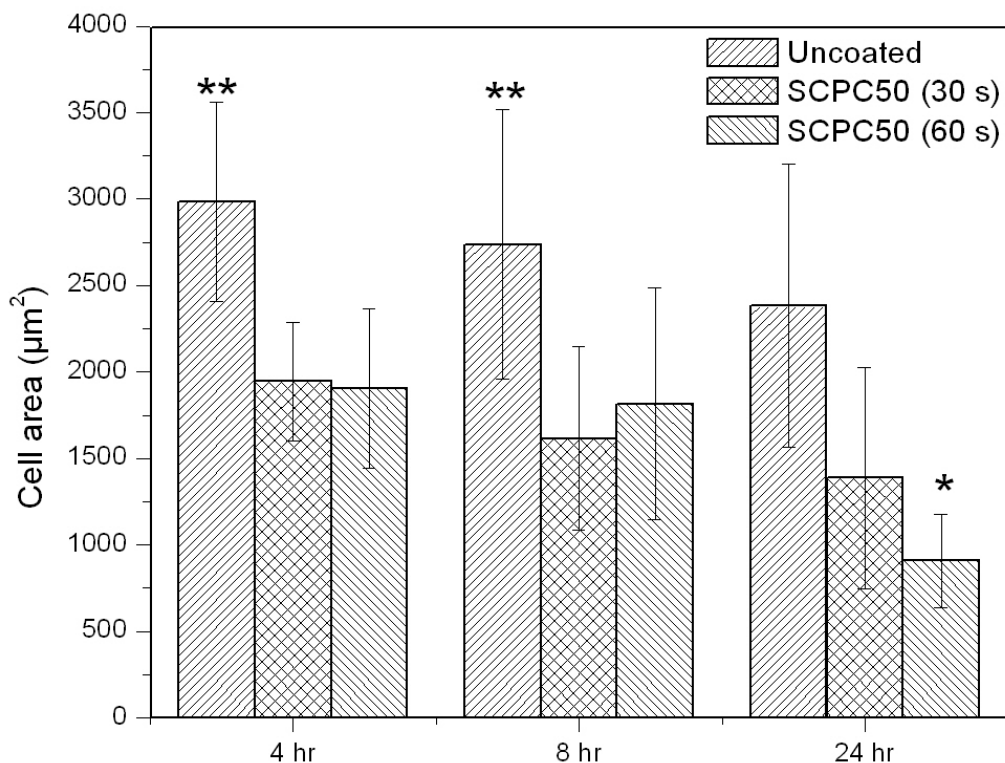
Figure 4.10: Quantitative estimation of cell spreading on the uncoated, 30 s SCPC50 coated and 60 s SCPC50 coated substrates. Cells attached to the uncoated Ti-6Al-4V substrates demonstrated greater spreading throughout the incubation period. (*$p < 0.05$; **$p < 0.01$)

4.3.5.4 Cell shape

Analyses of cell shape showed that cells attached to uncoated substrates were significantly more ($p < 0.05$) round than the cells attached to the SCPC50-coated substrates up to 8 hr of incubation (Figure 4.11). However, a comparable shape factor value was measured for cells attached to 30 s or 60 s SCPC50 coated substrates during the same time period. After 24 hr, cells attached to the uncoated and 60 s coated SCPC50

substrates became significantly ($p < 0.05$) more elongated while negligible change was observed in cells attached to the 30 s coated SCPC50 substrate.
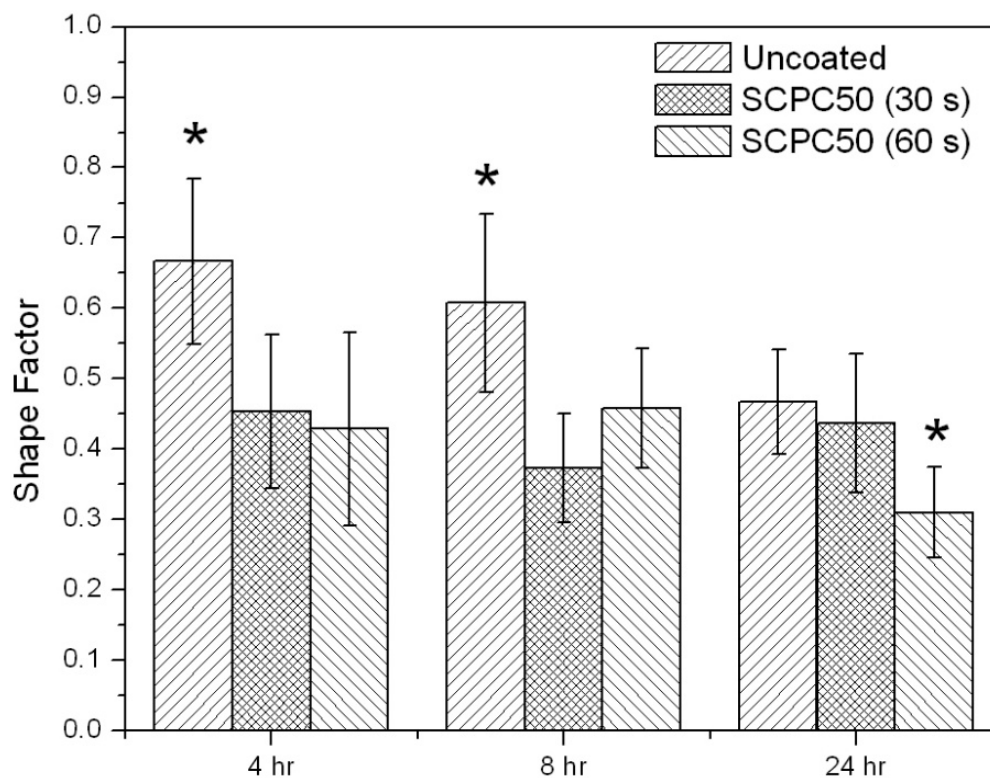
Figure 4.11: Shape factor analyses of bone cells attached to uncoated, 30 s SCPC50 coated and 60 s SCPC50 coated substrates. Cells attached to the uncoated Ti-6Al-4V substrate showed greater circularity than the cells attached to the SCPC50-coated substrates. After 24 hr of incubation, cells attached to the 60 s SCPC50 coated substrate exhibited lower shape factor value than cells attached to uncoated or 30 s SCPC50 coated substrates.

4.3.5.5 Cell proliferation

After 4 hr of incubation, the number of bone cells attached to the SCPC50-coated substrates were significantly higher ($p < 0.01$) than that attached to the uncoated Ti-6Al-4V substrates (Table 4.1). However, cells attached to the uncoated Ti-6Al-4V substrates

proliferated rapidly, increasing by 3.24- and 7.24-fold after 8 and 24 hr, respectively. Cells attached to the 30 s SCPC50 coated substrate showed slower proliferation rate than cells on uncoated Ti-6Al-4V substrates, increasing by 1.21- and 1.90-fold after 8 and 24 hr, respectively. Cells attached to the 60 s SCPC50 coated substrate increased in number by 1.38-fold after 8 hr; however, the proliferation rate decreased to 1.12-fold after 24 hr of incubation.

Substrate	4 hr		8 hr		24 hr	
	Cells/mm^2	Fold increase	Cells/mm^2	Fold increase	Cells/mm^2	Fold increase
Uncoated	10 ± 1	-	33 ± 7	3.30	76 ± 12	7.60
30 s SCPC50	65 ± 12	-	79 ± 24	1.21	124 ± 25	1.91
60 s SCPC50	49 ± 4	-	68 ± 11	1.38	55 ± 12	1.12

Table 4.1: Table showing the number of cells attached per unit area on uncoated, 30 s SCPC50 coated and 60 s SCPC50 coated substrate after 4, 8 and 24 hr of incubation.

4.3.5.6 Actin cytoskeletal organization

Cytoskeletal organization of cells attached to the uncoated Ti-6Al-4V substrates after 4 hr of incubation showed distinct actin filaments that were concentrated along the cell periphery in the form of lamellipodia (Figure 4.12a). In contrast, cells attached to 30 s (Figure 4.12b) or 60 s (Figure 4.12c) SCPC50-coated substrates showed diffused and less organized actin filaments; however, multiple points of focal contacts were noted on both surfaces. In addition, the cells also produced filopodia (arrows; Figure 4.12b) that

were intimately connected with the lamellipodia. After 8 hr of incubation, cells attached to the uncoated Ti-6Al-4V substrates showed a combination of parallel as well as radially oriented actin fibers (Figure 4.11d). Cells attached to 30 s (Figure 4.12e) and 60 s (Figure 4.12f) SCPC50-coated substrates showed improved cytoskeletal organization than that at 4 hr and demonstrated limited parallel actin organization. After 24 hr of incubation, cells attached to uncoated Ti-6Al-4V substrates exhibited robust and parallel actin fibers with well-defined polarization along the long axis of the cell (Figure 4.12g). In contrast, cells attached to the 30 s (Figure 4.12h) and 60 s (Figure 4.12i) SCPC50-coated substrates continued to exhibit under-developed cytoskeleton; however, cells on the former substrate showed more parallel actin organization than cells on the latter. The quality of actin filament organization was scored as I, II or III, with III being most organized and I being least organized. After 4 hr of incubation, 51% of the cells on uncoated Ti-6Al-4V substrates exhibited type II organization; however by 24 hr, 88% of the cells had progressed to type I organization (Table 4.2). On the SCPC50-coated substrates, approximately 60% cells exhibited type II organization after 4 hr. By 24 hr, only 32% of cells on the 30 s, and 14% cells on the 60 s SCPC50-coated substrate, exhibited type III organization. Cells attached to the 60 s SCPC50-coated substrate showed the most amount of type I actin fibers (31%) among all substrates after 24 hr of incubation.
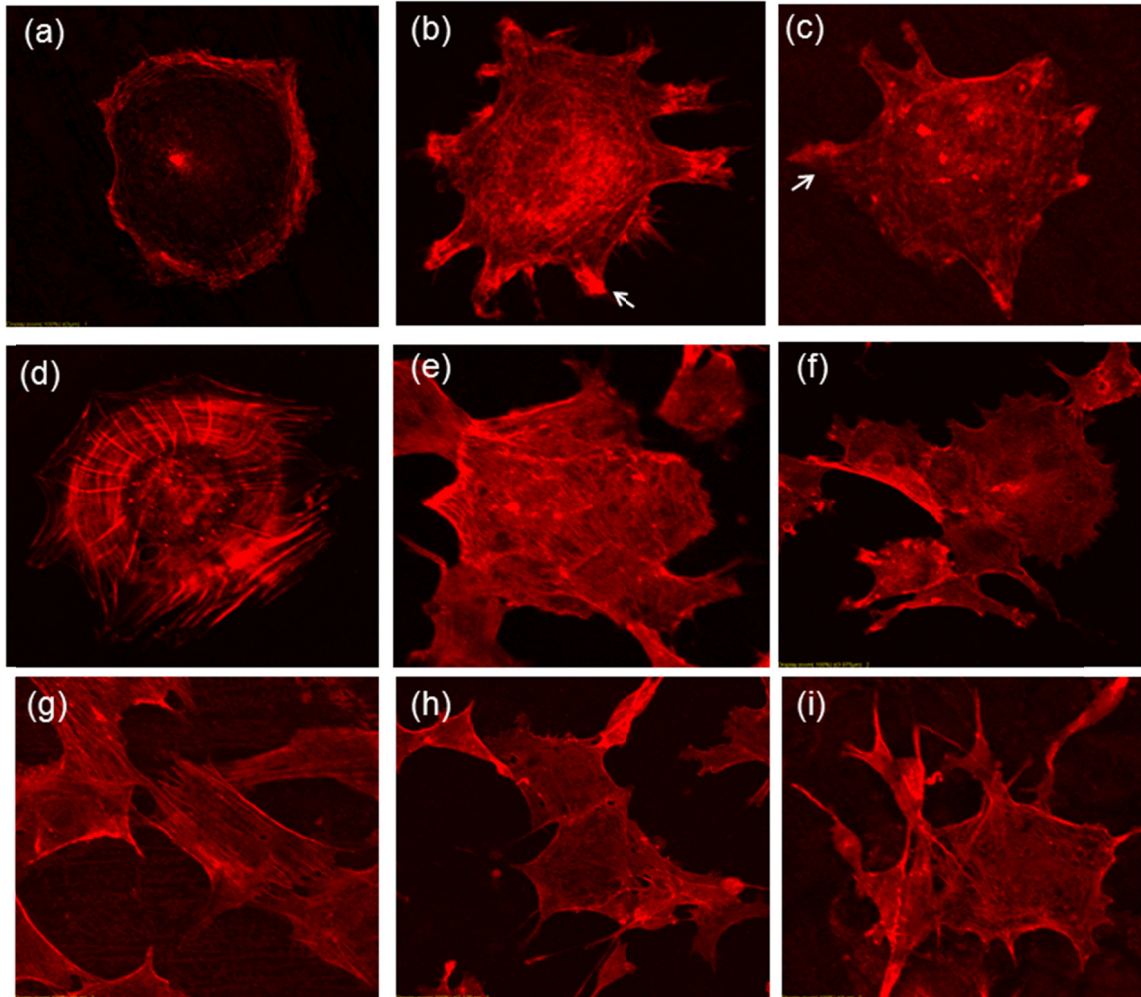
Figure 4.12: Actin filaments of bone cells attached to (a) uncoated; (b) 30 s SCPC50 coated and (c) 60 s SCPC50 Ti-6Al-4V substrate after 4 hr, 8 hr (d, e, f) and 24 hr of incubation (g, h, i). Cells attached to uncoated Ti-6Al-4V substrates developed well defined actin filaments that were parallel to the long axis of the cell. On the other hand, cells attached to the SCPC50-coated substrates showed enhanced focal point formation (arrows); however, they developed poorly organized actin filaments.

Actin distribution (%)

Substrate	4 hr			8 hr			24 hr		
	I	II	III	I	II	III	I	II	III
Uncoated	25.8	51.7	22.4	10.4	47.7	41.7	0	11.1	88.9
30 s SCPC50	41.2	58.8	0	28.7	43.6	27.7	13.5	54.1	32.4
60 s SCPC50	39.4	60.6	0	24.8	56.4	18.8	31.4	54.3	14.3

Table 4.2: Scoring of actin microfilaments as type I, II, or III on uncoated, 30 s SCPC50 coated and 60 s SCPC50 coated substrates after 4, 8 and 24 hr of incubation. The organization of actin improved in the order type I< II< III.

4.3.6 Dissolution analyses

ICP - OES analyses of the tissue culture medium incubated with cells for 24 hr showed Ca uptake by the SCPC50 coated substrates, with the 60 s SCPC50 coated substrate adsorbing significantly more Ca than the 30 s SCPC50 coated substrate (Figure 4.13a). In contrast to Ca adsorption, a release of P (Figure 4.13b) and Si (Figure 4.13c) from the SCPC50-coated substrates was observed. The 60 s SCPC50 coated substrate released significantly more P ($p < 0.05$) and Si ($p < 0.05$) than the 30 s-SCPC50 coated substrate. No dissolution of Ti ions was observed.
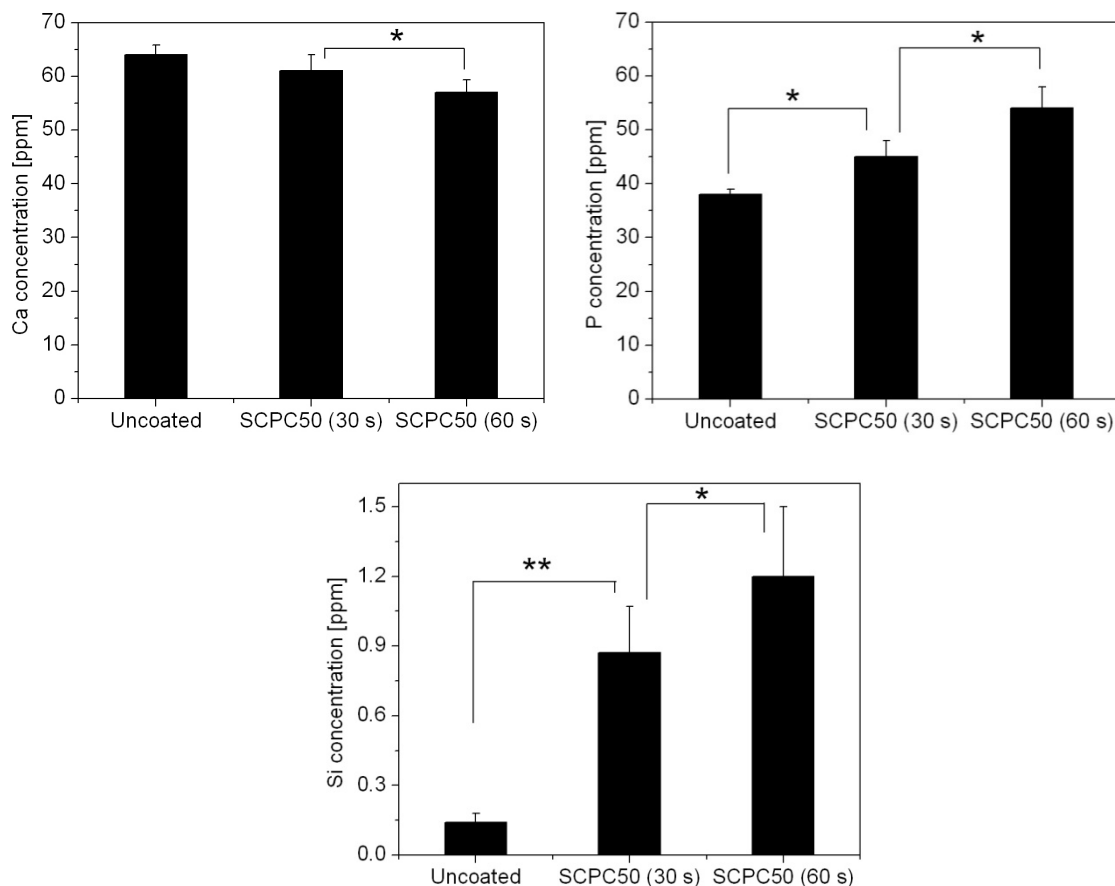
Figure 4.13: ICP - OES analyses of the tissue culture medium showed significantly greater Ca adsorption by the 60 s SCPC50 coated substrate than by the 30 s SCPC50 coated substrate. On the other hand, the 60 s SCPC50 coated substrate released significantly higher amount of P and Si than the 30 s SCPC50 coated substrate. (*p < 0.05; **p < 0.01)

4.4 Discussion

The objective of this study was to investigate the development of bioactive SCPC50 coating on Ti-6Al-4V substrates and analyze the effect of ceramic surface topography on bone cell attachment and proliferation. AFM analyses of the bioactive ceramic coating on the 400- as well as the 1200-grit polished Ti-6Al-4V substrates showed that the average roughness of the substrate increased initially after coating for 10 s but decreased after 30 s of coating. Increasing the coating duration in excess of 30 s

continued to enhance the average roughness of the substrate. Moreover, it was found that the peak diameter of sintered SCPC50 decreased with increasing coating duration. An increase in the surface roughness of the SCPC50-coated substrates was accompanied by a decrease in cell spreading, proliferation and poor actin cytoskeleton organization, although cell attachment was not affected. On the other hand, cells attached to the uncoated Ti-6Al-4V substrates showed significantly greater spreading, proliferation and developed well-defined actin cytoskeleton than the cells attached to the SCPC50-coated substrates. The decrease in cell proliferation with increasing surface roughness correlated well with the enhanced Ca-uptake and greater release of P and Si from and into the tissue culture medium, respectively, which indicates early onset of cell differentiation. The reduced cell proliferation of bone cells with increasing surface roughness of the SCPC50 coated substrates indicates the synergistic role of surface roughness and material dissolution on bone cell differentiation.

The topographical features of SCPC50 coated on the smooth 1200-grit polished Ti-6Al-4V substrates serve as a model to understand the mechanism of coating development when the inherent roughness of the metal substrate has minimal contribution. AFM analyses showed that after thermal treatment at 800 ˚C, the R_a of Ti-6Al-4V substrates increased significantly ($p < 0.01$) for both, 400- and 1200-grit polished substrates. EDX analyses showed that O:Ti ratio was 3.92 ± 0.13 after thermal treatment indicating the formation of TiO_2. Previous studies have shown that nanocrystalline TiO_2 undergoes densification and grain growth at temperatures ≥ 550 ˚C.[213] Therefore, the increase in the R_a of the Ti-6Al-4V substrates is attributed to the sintering and growth of TiO_2 nanocrystals layer on the metal surface. After SCPC50 coating for 10 s, the R_a of

the 1200-group Ti-6Al-4V substrate increased but decreased thereafter to achieve minimal values after 30 s coating, both at the nano- and at the micro-scale level. The decrease in R_a suggests that the deposition and sintering of SCPC50 particles after coating for 30 s coating is in a way such that they mitigate the changes in the surface topography of the substrate caused due to the grain growth of TiO_2. On the other hand, coating for 10 s does not deposit enough SCPC50 particles that could sufficiently fill in the valleys on the substrate surface. The deposition of ceramic layers on the metal substrate progressively reduces the electric field strength due to the interference by the ceramic particles which have lower electrical conductivity than metal.[69] The reduced electric field strength reduces the electrophoretic mobility of the SCPC50 particles during EPD and allows the deposition of larger particles on the substrate than what were deposited at lower coating duration. Consequently, the R_a of the surface increased significantly with an increase in the coating duration beyond 30 s. Analyses of coating topography also showed that the peak diameter of SCPC50 on the 400- or the 1200-grit polished Ti-6Al-4V substrate decreased with an increase in the coating duration. The greater peak diameter of SCPC50 in close proximity with the metal surface suggests that these particles underwent greater degree of expansion and/or melting during sintering as compared to the layers away from the metal surface. The high thermal expansion coefficient of Ti-6Al-4V causes greater expansion in the metal as compared to the ceramic upon heating. As a result, SCPC50 particles at the interface with the metal experiences enhanced thermal stresses which cause an increase in the peak diameter. It may also be possible that the slow rate of heating and cooling (2 ˚C min^{-1}) along with the relatively low softening temperature of SCPC50 (590 ˚C) [103] would cause some degree of

melting of the ceramic particles closest to the metal surface, since metals have higher thermal conductivity than ceramics. Higher peak diameter values were measured on the 400-grit substrates than the 1200-grit group substrates, most probably due to the higher roughness and higher hence surface area of the former substrate which enhanced melting of the ceramic particles.

LIVE/DEAD assay of bone cells attached to the SCPC50-coated and uncoated substrates (Figure 4.8) showed near 100 % viability indicating absence of measurable cytotoxicity of the material that could influence cell behavior. Therefore, the variations in cell attachment, cytoskeletal organization and proliferation are attributed mainly to the differences in roughness and surface chemistry of the substrates. However, it is prudent to mention that these two material related parameters are not constant due to the dynamic nature of the bioactive surface. The immediate dissolution-precipitation reactions at the SCPC50/biological fluid interface within 2 hr of immersion have resulted in the deposition of a hydroxyapatite surface layer.[108] Coating Ti-6Al-4V with SCPC50 resulted in an increase of the surface roughness (Figure 4.4 and 4.5) and enhancement of cell attachment compared to uncoated metal substrates (Table 4.1). As the amount of SCPC50 coating increased after longer coating time, the roughness of the surface significantly increased leading to an increase in the surface area of the substrate, however comparable numbers of cells were measured on both substrates. The latter observation strongly suggests that effect of SCPC50 surface chemistry on cell attachment override the effect of surface roughness. Therefore, the 8-fold increase in cell attachment on the SCPC50-coated substrates compared to uncoated substrate after 4 hr in culture emphasizes the synergistic effect of both surface chemistry and roughness. An increase in the surface

roughness modifies the topography of the substrate which increases the contact area and binding sites available for cell anchorage.[214] Moreover, the surface chemistry of the implant also influences cell attachment since it controls the type, amount, and conformation of proteins that adsorb onto the material.[153,154] SCPC50 coating is characterized by ionic and polar groups, such as Ca^{2+} and Si-OH, which facilitate the adsorption of serum proteins including fibronectin and induce a conformation that favors cell attachment (Figure 3.3a). Fibronectin is an important attachment protein that exhibits chemotactic and adhesive properties and facilitates integrin-mediated cell adhesion and spreading.[214,215] Other studies in the literature have reported enhanced cell attachment on HA as compared to carbonate apatite or uncoated Ti due to an increase in the surface polarity[216] as well as high adsorption of attachment proteins such as fibronectin and vitronectin.[158,217] Therefore, the enhanced cell attachment on the SCPC50-coated substrates is a combined effect of the high surface roughness and the modified surface chemistry of the material.

Cell morphology analyses showed comparable cell spreading and cell shape factor on the 30 s and the 60 s SCPC50-coated substrates up to 8 hr of incubation (Figure 4.10 and 4.11). However, after 24 hr, cells attached to the 60 s SCPC50-coated substrate showed less spreading and appeared more elongated than the cells attached to the 30 s SCPC50-coated substrate. In addition, cells attached to the 60 s SCPC50-coated substrate appeared to quit proliferation after 8 hr while cells attached to the 30 s SCPC50-coated substrate continued proliferating up to 24 hr (Table 4.1). The limited cell proliferation on the 60 s SCPC50-coated substrate could be attributed to two possible reasons; first, the increased micro- and/or the nano-roughness which provides physical barriers against

spreading and second, the early induction of cell differentiation by the chemical cues provided by the coating layer. The fact that there were no differences in cell spreading on the 30 s and 60 s SCPC50-coated substrates during the first 8 hr of incubation undermines the effect of surface roughness on cell spreading under the current experimental setup. Therefore, it is most likely that the exposure of attached cells to the 60 s SCPC50-coated substrates to the dissolution products of the bioactive coating enhanced the switch of cell function from spreading and proliferation to differentiation. ICP - OES analyses showed significantly higher adsorption of Ca and release of P and Si from and into the cell culture medium, respectively, by the 60 s SCPC50-coated substrates as compared to the 30 s SCPC50-coated substrates (Figure 4.13). The role of these ions on osteoblast function is well established in the literature.[93,188,193,218-223] Ca influx stimulates voltage-gated Ca channels which play an important role in osteoblast proliferation by accelerating the rate of entry of cells into the cell cycle.[220] Ca also regulates the signaling mechanism of bone morphogenetic protein-2 (BMP-2) and transforming growth factor-β (TGF-β) which are important growth factors associated with osteoblast differentiation.[218,222] Moreover, Ca plays a role in promoting the entry of P into the cell via type III sodium dependent phosphate transporters.[223] P plays an important role in cell differentiation by coordinating the expression and regulation of multiple factors necessary for bone mineralization, both at a transcriptional and at a post-translational stage.[188] In addition to stimulating differentiation, P can also induce apoptosis in osteoblasts by interfering with mitochondrial function.[93,221] Si plays a critical role in the synthesis and stabilization of collagen, particularly with the transcription of collagen type I gene and as a co-factor for prolyl hydroxylase, an enzyme involved with

collagen synthesis.[219] Moreover, Si, in the form of orthosilicic acid, has been reported to promote osteoblast differentiation by increasing osteocalcin synthesis.[193] Therefore, the enhanced solution-mediated ionic effects on cells attached to the 60 s-SCPC50 coated substrate resulted in the limited spreading and decreased proliferation.

The selective adsorption of fibronectin on the SCPC50 coating (Figure 3.2b) can contribute to the early and firm specific adhesion through integrin-RGD interaction known to trigger intracellular cascade reactions leading to cell differentiation. Data in the literature demonstrates that the nature of stimuli from the substrate and its microenvironment imposes morphological changes in the cell cytoskeleton that affects a multitude of processes including cell division, cell shape and cell migration.[224,225] In our study, visualization of the actin filaments (Figure 4.12) showed that after 4 hr, cells attached to the SCPC50-coated substrates formed multiple focal contacts (FC) with the substrate irrespective of the surface roughness. On the other hand, cells attached to the uncoated Ti-6Al-4V substrates showed minimal FC formation. FC are integrin-rich regions on the cell membrane that facilitate cell adhesion via attachment proteins. By the end of 24 hr, cells attached to the uncoated Ti-6Al-4V substrates developed well-organized cytoskeleton while those attached to the SCPC50-coated substrates showed poorly organized and diffused cytoskeleton. Similar results have been reported by Okumura *et al* who showed that cells attached to HA formed poor fiber bundles but those attached to cp-Ti developed well defined fibers with distinct polarity.[217] The variability in the degree of cell adhesion and cytoskeletal organization will impact the signal transduction and cell nucleus organization and ultimately modulate the gene expression characteristics. In contrast, cells attached to the uncoated Ti-6Al-4V substrates showed

enhanced spreading greater shape circularity due to the lower roughness and the absence of surface- or solution-related osteogenic stimulation. It is interesting to note that cell spreading on uncoated Ti-6Al-4V substrate was higher despite the lack of fibronectin adsorption. It has been suggested that osteoblast spreading on uncoated Ti metal is cooperatively, but not independently, mediated by interactions between the RGD domain of adhesive proteins other than fibronectin and vitronectin, and sialic acid residues.[226]

The inhibition of cell spreading and changes in the cell shape (from circular to elongated) may also be associated with apoptosis.[227] Previous studies have shown that HA suppresses osteoblast proliferation and enhances the expression of cell differentiation markers such as AP and osteocalcin.[94] Xie *et al* reported that osteoblasts attached to HA discs undergo transcriptional changes and up-regulate genes associated with cell differentiation within 24 hr of contact with material surface.[47] Therefore, the reduction in the cell number on the 60 s SCPC50-coated substrate after 24 hr of attachment may have been due to apoptosis-related initiation of cell differentiation. The lower concentration of P and Si ions available to cells attached to the 30 s SCPC50-coated substrate contributed to the delayed cell differentiation on this substrate. However, our results are contradictory to reports by Deligianni *et al* who showed that an increase in the roughness of stoichiometric HA enhanced cell proliferation.[206] Nonetheless, it should be pointed out that the high stability of stoichiometric HA in physiological solution resists material dissolution and therefore has a minimal stimulatory effect on osteoblast differentiation.

4.5 Conclusion

AFM analyses of SCPC50-coated substrates showed that the average roughness of the coating depended upon the duration of EPD coating as well as the surface topography

of the metallic substrate. The average roughness of the SCPC50 coating layer was minimal after EPD coating for 30 s, indicating that the deposition mechanism of the SCPC50 particles is in a way such that they preferentially deposit within the grooves of the metallic substrate and mitigate the irregularities of the metal's topography. It was also found that the SCPC50 diameter reduced with increasing coating duration which indicates that the thermal stresses on SCPC50 particles decreased with increasing coating layers. Bone cell attachment to the SCPC50-coated substrates was independent of the average roughness of the coating but depended on the surface chemistry of the substrate. On the other hand, an increase in the average roughness of the SCPC50-coated substrates was accompanied by a reduction in cell spreading, cell proliferation and poor actin cytoskeleton organization. Results of the study suggest that an increase in roughness of the SCPC50 coating in conjunction with enhanced material dissolution stimulates early cell differentiation.

CHAPTER 5: SUMMARY AND RECOMMENDATIONS FOR FUTURE WORK

5.1   Summary of findings

The development of a novel bioactive silica-calcium phosphate nanocomposite (SCPC) coating on Ti-6Al-4V orthopedic implants using electrophoretic deposition (EPD) has been described. *In vitro* studies have demonstrated the strong stimulatory effect of SCPC coating on, bone cell differentiation, mineralization and bone bonding ability of the orthopedic implant. The SCPC-coated Ti-6Al-4V implant has the potential to enhance bone-implant integration and improve the longevity of the device.

The attainment of a stable colloidal suspension is of prime importance to achieve efficient coating using EPD. Zeta potential and conductivity studies provided the basis for the selection of the optimum SCPC composition and suspension conditions for EPD coating. Maximum surface charge on SCPC particles and minimal conductivity of the suspension were achieved for SCPC50 particles containing 1:1 weight ratio of silica and calcium phosphate components suspended in pure ethanol. Under these conditions, SCPC50 particles acquired a zeta potential of -43 ± 0.2 mV which stabilized the colloidal suspension by enhancing the electrostatic repulsion between colloidal particles. Although the electrical conductivity of SCPC25 was slightly lower than that of SCPC50, the latter acquired significantly higher zeta potential in ethanol. On the other hand, SCPC75 demonstrated significantly greater conductivity than SCPC25 or SCPC50 in any suspending medium, which is attributed to the rapid disruption and ionization of the

silicate network in the material. The low conductivity of SCPC50 in ethanol (2 µS/cm) maximized the electric field strength and enhanced the electrophoretic mobility of the SCPC50 particles during EPD. A uniform SCPC50 coating on Ti-6Al-4V was achieved via EPD using a voltage of 50 V applied for 2 min in a 5 wt% SCPC50 suspension in pure ethanol. SEM analyses of the SCPC50 coated samples thermally treated at 600 - 800 ºC showed that the sintering between the particles increased as the thermal temperature was increased. XRD analyses of SCPC50 showed that the material was composed of β-rhenanite and α-cristobalite solid solutions and that the crystalline structure of the material did not change before or after coating. Mechanical tests carried out according to the ASTM F1147-05 protocol to measure the adhesion strength between the SCPC50 coating and Ti-6Al-4V substrate showed that ceramic coated substrates thermally treated at 800 ºC for 1 hr resulted in adhesion strength of 47 ± 4 MPa, a value higher than the ASTM requirement. Moreover, SEM - EDX analyses of the fractured surface indicated that the failure occurred at the interface of either the metal and polymer or the polymer and SCPC50 coating layer. However, the interface of SCPC50 coating with the Ti-6Al-4V substrate was always intact. Immersion of the SCPC50-coated Ti-6Al-4V samples in physiologic solution confirmed the bioactivity of the coated samples. The surface of the SCPC50-coated Ti-6Al-4V was covered with a Ca-deficient hydroxyapatite layer after immersion in phosphate buffer saline for 7 days. SCPC50-coated Ti-6Al-4V discs immersed in PBS for 2 days acquired higher adhesion strength (11.7 ± 3.9 MPa) than that acquired by commercially available hydroxyapatite coated Ti-6Al-4V samples (5.5 ± 2.7 MPa) treated under similar experimental conditions.

In vitro studies showed that bone cells attached to the SCPC50-coated Ti-6Al-4V substrates expressed significantly higher alkaline phosphatase activity (82.4 ± 25.6 nmoles p-NP/mg protein/min) than that expressed by the cells attached to the hydroxyapatite-coated (39.7 6 7.1 nmoles p-NP/mg protein/min) or uncoated Ti-6Al-4V substrates (7.0 6 3.4 nmoles p-NP/mg protein/min). SEM analyses of the bone cells attached to SCPC50-coated and uncoated Ti-6Al-4V substrates showed the synthesis of mineralized extracellular matrix by the cells attached to the ceramic coated substrates. Gene expression analyses using qRT-PCR revealed higher mRNA levels of osteonectin, osteopontin and collagen-I expressed by cells attached to the uncoated Ti-6Al-4V substrates after 4 days of incubation as compared to that expressed by cells attached to the SCPC50-coated substrates. However, cells attached to the SCPC50-coated substrate expressed 10-fold higher osteocalcin mRNA level than that expressed by cells attached to the uncoated Ti-6Al-4V substrate. The high expression of osteocalcin mRNA indicates that the cells attached to the SCPC50-coated substrate were in an advanced stage of differentiation since osteocalcin is expressed only post-proliferatively at the onset of bone matrix mineralization. In addition, bone cells attached to the SCPC50-coated substrates synthesized significantly higher amount of osteopontin and osteocalcin proteins which have important roles in bone matrix formation and remodeling. The enhancement of bone cell differentiation was accompanied by a low level immunological response as indicated by the lower release of pro-inflammatory and osteoclastogenic cytokines, IL-6, IL-12p40 and RANKL by bone cells attached to the SCPC50-coated substrates as compared to the uncoated Ti-6Al-4V substrates. The favorable pro-osteogenic responses of bone cells attached to the SCPC50-coated substrates were correlated to the high adsorption of serum

proteins, including fibronectin, by the SCPC50-coated substrates. However, it is not only the amount and nature of proteins adsorbed onto the implant that dictate cell response, the conformation acquired by these proteins plays an equally significant role. FTIR analyses of adsorbed protein layer showed that proteins adsorbed onto the SCPC50-coated substrates expressed higher ratio of amide I/amide II functional groups (5.0 ± 0.6) than that expressed by the proteins adsorbed onto the uncoated substrates (2.2 ± 0.3). The higher expression of amide I is associated with an active protein conformation that enhances cell activity. In addition to the proteins that enhanced cell activity on the SCPC50-coated substrates, the release of ionic dissolution products from the material modified the chemical composition of the medium and stimulated bone cell differentiation. ICP - OES analyses of the tissue culture medium showed that SCPC50-coated substrates withdrew Ca and released P and Si from and into the medium. These ions have the potential to stimulate bone cell differentiation by influencing cell signaling mechanisms and directly affecting cell activity at a transcriptional as well as post-translational stage. Moreover, FTIR and SEM - EDX analyses of the extracellular matrix produced by cells attached to the SCPC50-coated substrates demonstrated bone mineral formation as indicated by the Ca/P ratio of 1.02 ± 0.23 and the presence of sulfur in the matrix. On the other hand, bone matrix mineralization did not occur on uncoated Ti-6Al-4V substrates during the same time period. These results demonstrate the greater stimulatory activity of SCPC50 coating on bone cell differentiation bone matrix mineralization than uncoated Ti-6Al-4V substrate.

The surface roughness of the implant is known to affect cell response to the material. AFM analyses of the topographical characteristics of SCPC50-coated substrates

showed that the average roughness of the ceramic coating depends upon the surface topography of the metal substrate and can be controlled by the varying the duration of the EPD coating process. It was found that EPD coating carried out for 30 s produced a ceramic layer that exhibited minimum average roughness. An increase in the coating duration to 60 s resulted in a significant increase in the average roughness of the substrate, both at the nano- and at the micro-scale resolution. The variability in average roughness and the changes in SCPC50 peak diameter indicated that the SCPC50 particles are deposited preferentially in a manner that fills the grooves on the surface created during substrate preparation. *In vitro* analyses of bone cells attached to SCPC50-coated substrates of varying average roughness showed comparable number of cells attached to either substrate which suggests that cell attachment was dependent on the surface chemistry of the material rather than the average roughness. However, an increase in the roughness of the SCPC50-coated implant was accompanied by a decrease in cell proliferation and poor actin cytoskeleton development. Moreover, the increase in surface roughness caused greater release of P and Si and higher adsorption of Ca by the material. Thus, it is most likely that the decrease in cell proliferation with increasing surface roughness was a result of apoptosis which has been associated with the early onset of cell differentiation. These results suggest that variations in the surface roughness and dissolution profile of the SCPC50-coated substrate dominate over the effect of its surface chemistry in regulating bone cell activity.

5.2   Recommendations for future work

5.2.1   TEM analyses of SCPC50/Ti-6Al-4V interface

Mechanical tests carried out to determine the adhesion strength of SCPC50 coating with Ti-6Al-4V substrate showed that the coating developed adhesion strength of > 47 ± 4 MPa and that the fracture occurred away from the metal/ceramic interface. Therefore, there is a strong motivation to study the chemical bonding mechanism at the metal/ceramic interface to clearly delineate the reasons for the high adhesion strength. Thermal treatment at high temperature, such as 800 ºC, promotes atomic diffusion between the atoms of the metal and ceramic which strengthens the interface. TEM analysis of the SCPC50/Ti-6Al-4V interface can be carried out to ascertain the atomic interactions between SCPC50 and Ti-6Al-4V.

5.2.2   *In vivo* studies with SCPC50-coated Ti-6Al-4V implant

The results presented in this study strongly demonstrate the stimulatory effect of SCPC coating on bone cell differentiation and mineralization under *in vitro* conditions. The natural environment of the body is much more complicated, marked by the presence of many different types of cells, tissue fluids and proteins. As a continuation of this work, the osteo-integration of SCPC50-coated Ti-6Al-4V implant with living bone tissue should be evaluated under *in vivo* conditions. It is expected that the osteogenic stimulation provided by the SCPC50 coating would promote bone cell activity and foster bone bonding with the implant. In addition, pull-out tests should be carried out to ascertain the strength of bone-tissue integration.

5.2.3   Comparison of bone cell response between SCPC50 and other bioactive ceramic coatings

In the present study, the stimulatory effect of SCPC50-coated Ti-6Al-4V implant was evaluated at a molecular level and compared to that of control Ti-6Al-4V substrate without coating. The results showed that SCPC50 coating enhanced the cell differentiation of bone cells, as shown by elevated osteocalcin mRNA levels and higher synthesis of osteopontin and osteocalcin proteins. Comparison of alkaline phosphatase (AP) activity showed that bone cells attached to SCPC50-coated implants exhibited 2-fold higher AP activity than hydroxyapatite-coated implants. Therefore, there is merit in evaluating gene expression and protein syntheses by cells attached to SCPC50-coated implants and compare it to other commercially available bioactive ceramic coated implants, such as those coated with hydroxyapatite or biphasic ceramics. Moreover, in this study, gene expression was evaluated at one time point only, i.e. 4 days. Temporal variations in gene expression pattern can be evaluated at longer time points.

REFERENCES

1.	Moskowitz RW. Osteoarthritis: Diagnosis and medical/surgical management: Lippincott Williams & Wilkins; 2007.

2.	Kennon R. Hip and Knee Surgery: A Patient's Guide to Hip Replacement, Hip Resurfacing, Knee Replacement, and Knee Arthroscopy: Lulu. com; 2008.

3.	Siopack J, Jergesen H. Total hip arthroplasty. Western journal of medicine 1995;162(3):243.

4.	Hall MJ, DeFrances CJ, Williams SN, Golosinskiy A, Schwartzman A. National hospital discharge survey: 2007 summary. Natl Health Stat Report 2010;29:1-20.

5.	Merrill C, Elixhauser A, Research USAfH, Quality, Cost H. Hospital stays involving musculoskeletal procedures, 1997-2005: Agenty for Healthcare Research and Quality; 2007.

6.	Huo MH, Parvizi J, Bal BS, Mont MA. What's new in total hip arthroplasty. The Journal of Bone and Joint Surgery (American) 2009;91(10):2522-2534.

7.	Kurtz S, Ong K, Lau E, Mowat F, Halpern M. Projections of primary and revision hip and knee arthroplasty in the United States from 2005 to 2030. The Journal of Bone and Joint Surgery (American) 2007;89(4):780-785.

8.	Vidalain JP. Corailâ Hip System: A Practical Approach Based on 25 Years Experience: Springer Verlag; 2011.

9.	Konttinen YT, Zhao D, Beklen A, Ma G, Takagi M, Kivelä-Rajamäki M, Ashammakhi N, Santavirta S. The microenvironment around total hip replacement prostheses. Clinical orthopaedics and related research 2005;430:28.

10.	Bhatia SK. Engineering Biomaterials for Regenerative Medicine: Novel Technologies for Clinical Applications: Springer Verlag; 2011.

11.	Kevin J, Steven M, Edmund L, Kevin O, Thomas P, Daniel J. The epidemiology of revision total hip arthroplasty in the United States. The Journal of Bone and Joint Surgery (American) 2009;91(1):128-133.

12.	Huiskes R. Failed innovation in total hip replacement: diagnosis and proposals for a cure. Acta Orthopaedica 1993;64(6):699-716.

13.	Bonewald L. Osteocytes as multifunctional cells. Journal of musculoskeletal & neuronal interactions 2006;6(4):331.

14. Long M, Rack H. Titanium alloys in total joint replacement-a materials science perspective. BIOMATERIALS-GUILDFORD- 1998;19:1621-1639.

15. Fraker AC. Corrosion of metallic implants and prosthetic devices. ASM Handbook. 1987;13:1324-1335.

16. Buechel FF, Pappas MJ. Principles of Human Joint Replacement: Design and Clinical Application: Springer Verlag; 2011.

17. Shettlemore MG, Bundy KJ. Toxicity measurement of orthopedic implant alloy degradation products using a bioluminescent bacterial assay. Journal of biomedical materials research 1999;45(4):395-403.

18. Allen MJ, Myer B, Millett PJ, Rushton N. The effects of particulate cobalt, chromium and cobalt-chromium alloy on human osteoblast-like cells in vitro. JOURNAL OF BONE AND JOINT SURGERY-AMERICAN VOLUME- 1997;79:475-482.

19. Niinomi M. Mechanical properties of biomedical titanium alloys. Materials Science and Engineering: A 1998;243(1):231-236.

20. Ponader S, Von Wilmowsky C, Widenmayer M, Lutz R, Heinl P, Körner C, Singer RF, Nkenke E, Neukam FW, Schlegel KA. In vivo performance of selective electron beam-melted Ti-6Al-4V structures. Journal of Biomedical Materials Research Part A 2010;92(1):56-62.

21. Ingham E, Fisher J. Biological reactions to wear debris in total joint replacement. Proceedings of the Institution of Mechanical Engineers, Part H: Journal of Engineering in Medicine 2000;214(1):21-37.

22. Goodman SB. Wear particles, periprosthetic osteolysis and the immune system. Biomaterials 2007;28(34):5044-5048.

23. Anderson JM, Rodriguez A, Chang DT. Foreign body reaction to biomaterials. 2008. Elsevier. p 86-100.

24. Lalor P, Revell P, Gray A, Wright S, Railton G, Freeman M. Sensitivity to titanium. A cause of implant failure? Journal of Bone and Joint Surgery-British Volume 1991;73(1):25.

25. Lalor P, Revell P. T-lymphocytes and titanium aluminium vanadium (TiAlV) alloy: evidence for immunological events associated with debris deposition. Clinical materials 1993;12(1):57-62.

26. Thompson G, Puleo D. Ti-6Al-4V ion solution inhibition of osteogenic cell phenotype as a function of differentiation timecourse in vitro. Biomaterials 1996;17(20):1949-1954.

27. Cadosch D, Chan E, Gautschi OP, Meagher J, Zellweger R, Filgueira L. Titanium IV ions induced human osteoclast differentiation and enhanced bone resorption in vitro. Journal of Biomedical Materials Research Part A 2009;91(1):29-36.

28. Saldaña L, Barranco V, García-Alonso M, Vallés G, Escudero M, Munuera L, Vilaboa N. Concentration-dependent effects of titanium and aluminium ions released from thermally oxidized Ti6Al4V alloy on human osteoblasts. Journal of Biomedical Materials Research Part A 2006;77(2):220-229.

29. Case C, Langkamer V, James C, Palmer M, Kemp A, Heap P, Solomon L. Widespread dissemination of metal debris from implants. JOURNAL OF BONE AND JOINT SURGERY-BRITISH VOLUME- 1994;76:701-701.

30. Yang J, Merritt K. Production of monoclonal antibodies to study corrosion products of CO-CR biomaterials. Journal of biomedical materials research 1996;31(1):71-80.

31. Merrit K, Brown SA. Hypersensitivity to metallic biomaterials. In: Williams DF, editor. Systemic aspects of biocompatibility. Volume Vol. II. Boca Raton: CRC Press; 1981. p 33-57.

32. Spector M. Bone ingrowth into porous metals. Biocompatibility of orthopaedic implants 1982;2:89-128.

33. Wazen RM, Lefebvre LP, Baril E, Nanci A. Initial evaluation of bone ingrowth into a novel porous titanium coating. Journal of Biomedical Materials Research Part B: Applied Biomaterials 2010;94(1):64-71.

34. Davis JR. Handbook of materials for medical devices. Asm Intl; 2003. p 179-194.

35. Simmons CA, Meguid SA, Pilliar RM. Mechanical regulation of localized and appositional bone formation around bone-interfacing implants. Journal of biomedical materials research 2001;55(1):63-71.

36. Simmons CA, Meguid SA, Pilliar RM. Differences in osseointegration rate due to implant surface geometry can be explained by local tissue strains. Journal of orthopaedic research 2001;19(2):187-194.

37. Meding JB, Galley MR, Ritter MA. High survival of uncemented proximally porous-coated titanium alloy femoral stems in osteoporotic bone. Clinical Orthopaedics and Related Research® 2010;468(2):441-447.

38.   Patil N, Lee K, Goodman SB. Porous tantalum in hip and knee reconstructive surgery. Journal of Biomedical Materials Research Part B: Applied Biomaterials 2009;89(1):242-251.

39.   Smith T. The effect of plasma-sprayed coatings on the fatigue of titanium alloy implants. JOM Journal of the Minerals, Metals and Materials Society 1994;46(2):54-56.

40.   Pilliar RM. Concise encyclopedia of medical & dental materials. In: Williams DF, editor. Cambridge, MA: Pergamon Press and The MIT Press; 1990. p 312–319.

41.   Ducheyne P, Qiu Q. Bioactive ceramics: the effect of surface reactivity on bone formation and bone cell function. Biomaterials 1999;20(23-24):2287-2303.

42.   Hench LL, Wilson J. An introduction to bioceramics: World Scientific Pub Co Inc; 1993.

43.   Kokubo T. Bioactive glass ceramics: properties and applications. Biomaterials 1991;12(2):155-163.

44.   Groot K, Wolke JGC, Jansen J. Calcium phosphate coatings for medical implants. Proceedings of the Institution of Mechanical Engineers, Part H: Journal of Engineering in Medicine 1998;212(2):137-147.

45.   Ducheyne P, Cuckler JM. Bioactive ceramic prosthetic coatings. Clinical orthopaedics and related research 1992;276:102.

46.   Varanasi V, Saiz E, Loomer P, Ancheta B, Uritani N, Ho S, Tomsia A, Marshall S, Marshall G. Enhanced osteocalcin expression by osteoblast-like cells (MC3T3-E1) exposed to bioactive coating glass (SiO2-CaO-P2O5-MgO-K2O-Na2O system) ions. Acta biomaterialia 2009;5(9):3536-3547.

47.   Xie J, Baumann MJ, McCabe LR. Osteoblasts respond to hydroxyapatite surfaces with immediate changes in gene expression. Journal of Biomedical Materials Research Part A 2004;71(1):108-117.

48.   Xynos ID, Edgar AJ, Buttery LDK, Hench LL, Polak JM. Gene-expression profiling of human osteoblasts following treatment with the ionic products of Bioglass® 45S5 dissolution. Journal of biomedical materials research 2001;55(2):151-157.

49.   Lewandrowski KU. Tissue Engineering and Biodegradable Equivalents, Scientific and Clinical Applications: CRC Press; 2002.

50.   Fauchais P. Understanding plasma spraying. Journal of Physics D: Applied Physics 2004;37:R86.

51.   Sun L, Berndt CC, Gross KA, Kucuk A. Material fundamentals and clinical performance of plasma-sprayed hydroxyapatite coatings: A review. Journal of biomedical materials research 2001;58(5):570-592.

52.   Tanzer M, Kantor S, Rosenthall L, Bobyn JD. Femoral remodeling after porous-coated total hip arthroplasty with and without hydroxyapatite-tricalcium phosphate coating: a prospective randomized trial. The journal of arthroplasty 2001;16(5):552-558.

53.   Nilsson KG, Kärrholm J, Carlsson L, Dalén T. Hydroxyapatite coating versus cemented fixation of the tibial component in total knee arthroplasty:: Prospective randomized comparison of hydroxyapatite-coated and cemented tibial components with 5-year follow-up using radiostereometry. The Journal of arthroplasty 1999;14(1):9-20.

54.   Hermida JC, Bergula A, Dimaano F, Hawkins M, Colwell Jr CW, D'Lima DD. An in vivo evaluation of bone response to three implant surfaces using a rabbit intramedullary rod model. Journal of orthopaedic surgery and research 2010;5(1):57.

55.   Landor I, Vavrik P, Sosna A, Jahoda D, Hahn H, Daniel M. Hydroxyapatite porous coating and the osteointegration of the total hip replacement. Archives of orthopaedic and trauma surgery 2007;127(2):81-89.

56.   D'Antonio JA, Capello WN, Manley MT, Geesink R. Hydroxyapatite femoral stems for total hip arthroplasty: 10-to 13-year followup. Clinical orthopaedics and related research 2001;393:101.

57.   Yang YC, Chang E. Influence of residual stress on bonding strength and fracture of plasma-sprayed hydroxyapatite coatings on Ti-6Al-4V substrate. Biomaterials 2001;22(13):1827-1836.

58.   Nieh T, Jankowski A, Koike J. Processing and characterization of hydroxyapatite coatings on titanium produced by magnetron sputtering. Journal of Materials Research 2001;16(11):3238-3245.

59.   Wei M, Ruys A, Swain M, Milthorpe B, Sorrell C. Hydroxyapatite-coated metals: interfacial reactions during sintering. Journal of Materials Science: Materials in Medicine 2005;16(2):101-106.

60.   Ergun C, Doremus R, Lanford W. Hydroxylapatite and titanium: Interfacial reactions. Journal of Biomedical Materials Research Part A 2003;65(3):336-343.

61.   Breme J, Zhou Y, Groh L. Development of a titanium alloy suitable for an optimized coating with hydroxyapatite. Biomaterials 1995;16(3):239-244.

62.   Kim HW, Kim HE, Salih V, Knowles JC. Hydroxyapatite and titania sol–gel composite coatings on titanium for hard tissue implants; mechanical and in vitro biological performance. Journal of Biomedical Materials Research Part B: Applied Biomaterials 2005;72(1):1-8.

63.   Stoch A, Długoń E, Lejda W, Trybalska B, Stoch G, Adamczyk A. Sol–gel derived hydroxyapatite coatings on titanium and its alloy Ti6Al4V. Journal of molecular structure 2005;744:633-640.

64.   Chai C, Ben-Nissan B. Bioactive nanocrystalline sol-gel hydroxyapatite coatings. Journal of Materials Science: Materials in Medicine 1999;10(8):465-469.

65.   Best S, Porter A, Thian E, Huang J. Bioceramics: past, present and for the future. Journal of the European Ceramic Society 2008;28(7):1319-1327.

66.   Kelly P, Arnell R. Magnetron sputtering: a review of recent developments and applications. Vacuum 2000;56(3):159-172.

67.   Nelea V, Morosanu C, Iliescu M, Mihailescu I. Microstructure and mechanical properties of hydroxyapatite thin films grown by RF magnetron sputtering. Surface and Coatings Technology 2003;173(2):315-322.

68.   Surmenev RA, Surmeneva MA, Evdokimov KE, Pichugin VF, Peitsch T, Epple M. The influence of the deposition parameters on the properties of an rf-magnetron-deposited nanostructured calcium phosphate coating and a possible growth mechanism. Surface and Coatings Technology 2010.

69.   Besra L, Liu M. A review on fundamentals and applications of electrophoretic deposition (EPD). Progress in materials science 2007;52(1):1-61.

70.   Zhitomirsky I. Cathodic electrodeposition of ceramic and organoceramic materials. Fundamental aspects. Advances in colloid and interface science 2002;97(1-3):279-317.

71.   Ōhshima H. Electrical phenomena at interfaces: fundamentals, measurements, and applications: CRC; 1998.

72.   Zheng X, Huang M, Ding C. Bond strength of plasma-sprayed hydroxyapatite/Ti composite coatings. Biomaterials 2000;21(8):841-849.

73.   Gu Y, Khor K, Cheang P. In vitro studies of plasma-sprayed hydroxyapatite/Ti-6Al-4V composite coatings in simulated body fluid (SBF). Biomaterials 2003;24(9):1603-1611.

74. Chen M, Liu D, You C, Yang X, Cui Z. Interfacial characteristic of graded hydroxyapatite and titanium thin film by magnetron sputtering. Surface and Coatings Technology 2007;201(9-11):5688-5691.

75. Albayrak O, El-Atwani O, Altintas S. Hydroxyapatite coating on titanium substrate by electrophoretic deposition method: Effects of titanium dioxide inner layer on adhesion strength and hydroxyapatite decomposition. Surface and Coatings Technology 2008;202(11):2482-2487.

76. Cannillo V, Lusvarghi L, Sola A. Production and characterization of plasma-sprayed TiO2-hydroxyapatite functionally graded coatings. Journal of the European Ceramic Society 2008;28(11):2161-2169.

77. Lin S, LeGeros RZ, LeGeros JP. Adherent octacalciumphosphate coating on titanium alloy using modulated electrochemical deposition method. Journal of Biomedical Materials Research Part A 2003;66(4):819-828.

78. Balani K, Anderson R, Laha T, Andara M, Tercero J, Crumpler E, Agarwal A. Plasma-sprayed carbon nanotube reinforced hydroxyapatite coatings and their interaction with human osteoblasts in vitro. Biomaterials 2007;28(4):618-624.

79. Hahn BD, Lee JM, Park DS, Choi JJ, Ryu J, Yoon WH, Lee BK, Shin DS, Kim HE. Mechanical and in vitro biological performances of hydroxyapatite–carbon nanotube composite coatings deposited on Ti by aerosol deposition. Acta biomaterialia 2009;5(8):3205-3214.

80. Kaya C, Singh I, Boccaccini AR. Multi-walled Carbon Nanotube-Reinforced Hydroxyapatite Layers on Ti6Al4V Medical Implants by Electrophoretic Deposition (EPD). Advanced Engineering Materials 2008;10(1-2):131-138.

81. Sayes CM, Wahi R, Kurian PA, Liu Y, West JL, Ausman KD, Warheit DB, Colvin VL. Correlating nanoscale titania structure with toxicity: a cytotoxicity and inflammatory response study with human dermal fibroblasts and human lung epithelial cells. Toxicological Sciences 2006;92(1):174.

82. Manjubala I, Sampath Kumar T. Effect of TiO2-Ag2O additives on the formation of calcium phosphate based functionally graded bioceramics. Biomaterials 2000;21(19):1995-2002.

83. El-Ghannam A, Starr L, Jones J. Laminin-5 coating enhances epithelial cell attachment, spreading, and hemidesmosome assembly on Ti-6Al-4V implant material in vitro. Journal of biomedical materials research 1998;41(1):30-40.

84. Suzuki O, Nakamura M, Miyasaka Y, Kagayama M, Sakurai M. Bone formation on synthetic precursors of hydroxyapatite. The Tohoku journal of experimental medicine 1991;164(1):37.

85.   Kamakura S, Sasano Y, Homma H, Suzuki O, Kagayama M, Motegi K. Implantation of octacalcium phosphate (OCP) in rat skull defects enhances bone repair. Journal of dental research 1999;78(11):1682.

86.   Hahn BD, Park DS, Choi JJ, Yoon WH, Ryu J, Kim DY. Effects of Zr/Ti ratio and post-annealing temperature on the electrical properties of lead zirconate titanate (PZT) thick films fabricated by aerosol deposition. Journal of Materials Research 2008;23(01):226-235.

87.   Fazan F, Marquis P. Dissolution behavior of plasma-sprayed hydroxyapatite coatings. Journal of Materials Science: Materials in Medicine 2000;11(12):787-792.

88.   Dinda G, Shin J, Mazumder J. Pulsed laser deposition of hydroxyapatite thin films on Ti–6Al–4V: Effect of heat treatment on structure and properties. Acta biomaterialia 2009;5(5):1821-1830.

89.   Puleo DA, Huh WW. Acute toxicity of metal ions in cultures of osteogenic cells derived from bone marrow stromal cells. Journal of Applied Biomaterials 1995;6(2):109-116.

90.   Wang JY, Wicklund BH, Gustilo RB, Tsukayama DT. Titanium, chromium and cobalt ions modulate the release of bone-associated cytokines by human monocytes/macrophages in vitro. Biomaterials 1996;17(23):2233-2240.

91.   Teitelbaum SL. Bone resorption by osteoclasts. Science 2000;289(5484):1504.

92.   Thian ES, Huang J, Best SM, Barber ZH, Brooks RA, Rushton N, Bonfield W. The response of osteoblasts to nanocrystalline silicon-substituted hydroxyapatite thin films. Biomaterials 2006;27(13):2692-2698.

93.   Adams CS, Mansfield K, Perlot RL, Shapiro IM. Matrix regulation of skeletal cell apoptosis. Journal of Biological Chemistry 2001;276(23):20316-20322.

94.   Shu R, McMullen R, Baumann M, McCabe L. Hydroxyapatite accelerates differentiation and suppresses growth of MC3T3-E1 osteoblasts. Journal of Biomedical Materials Research Part A 2003;67(4):1196-1204.

95.   Zhu L, Ye X, Tang G, Zhao N, Gong Y, Zhao Y, Zhao J, Zhang X. Biomimetic coating of compound titania and hydroxyapatite on titanium. Journal of Biomedical Materials Research Part A 2007;83(4):1165-1175.

96.   Stephansson SN, Byers BA, García AJ. Enhanced expression of the osteoblastic phenotype on substrates that modulate fibronectin conformation and integrin receptor binding. Biomaterials 2002;23(12):2527-2534.

97.   Lian JB, Stein GS. Concepts of osteoblast growth and differentiation: basis for modulation of bone cell development and tissue formation. Critical Reviews in Oral Biology & Medicine 1992;3(3):269-305.

98.   Muller J, Huaux F, Lison D. Respiratory toxicity of carbon nanotubes: How worried should we be? Carbon 2006;44(6):1048-1056.

99.   Lam CW, James JT, McCluskey R, Hunter RL. Pulmonary toxicity of single-wall carbon nanotubes in mice 7 and 90 days after intratracheal instillation. Toxicological Sciences 2004;77(1):126.

100.   Wang J, de Boer J, de Groot K. Proliferation and differentiation of osteoblast-like MC3T3-E1 cells on biomimetically and electrolytically deposited calcium phosphate coatings. Journal of Biomedical Materials Research Part A 2009;90(3):664-670.

101.   Knabe C, Howlett CR, Klar F, Zreiqat H. The effect of different titanium and hydroxyapatite-coated dental implant surfaces on phenotypic expression of human bone-derived cells. Journal of Biomedical Materials Research Part A 2004;71(1):98-107.

102.   El-Ghannam A, Hamazawy E, Yehia A. Effect of thermal treatment on bioactive glass microstructure, corrosion behavior, ζ potential, and protein adsorption. Journal of Biomedical Materials Research 2001;55(3):387-395.

103.   El-Ghannam AR. Advanced bioceramic composite for bone tissue engineering: Design principles and structure–bioactivity relationship. Journal of Biomedical Materials Research Part A 2004;69(3):490-501.

104.   El-Ghannam A, Ning C, Mehta J. Cyclosilicate nanocomposite: A novel resorbable bioactive tissue engineering scaffold for BMP and bone-marrow cell delivery. Journal of Biomedical Materials Research Part A 2004;71(3):377-390.

105.   El-Ghannam A, Ahmed K, Omran M. Nanoporous delivery system to treat osteomyelitis and regenerate bone: Gentamicin release kinetics and bactericidal effect. Journal of Biomedical Materials Research Part B: Applied Biomaterials 2005;73(2):277-284.

106.   El-Ghannam A, Jahed K, Govindaswami M. Resorbable bioactive ceramic for treatment of bone infection. Journal of Biomedical Materials Research Part A 2010;94(1):308-316.

107.   El-Ghannam A, Ricci K, Malkawi A, Jahed K, Vedantham K, Wyan H, Allen LD, Dréau D. A ceramic-based anticancer drug delivery system to treat breast cancer. Journal of Materials Science: Materials in Medicine 2010:1-10.

108. Gupta G, Kirakodu S, El-Ghannam A. Dissolution kinetics of a Si-rich nanocomposite and its effect on osteoblast gene expression. Journal of Biomedical Materials Research Part A 2007;80(2):486-496.

109. Revell P, Al-Saffar N, Kobayashi A. Biological reaction to debris in relation to joint prostheses. Proceedings of the Institution of Mechanical Engineers, Part H: Journal of Engineering in Medicine 1997;211(2):187-197.

110. Maloney W, Smith R, Castro F, Schurman D. Fibroblast response to metallic debris in vitro. Enzyme induction cell proliferation, and toxicity. The Journal of bone and joint surgery. American volume 1993;75(6):835.

111. Goldring S, Clark C, Wright T. The problem in total joint arthroplasty: aseptic loosening. The Journal of bone and joint surgery. American volume 1993;75(6):799.

112. Puleo D, Nanci A. Understanding and controlling the bone-implant interface. Biomaterials 1999;20(23-24):2311-2321.

113. Yang C, Lin R, Wang B, Lee T, Chang E, Hang Y, Chen P. In vitro and in vivo mechanical evaluations of plasma-sprayed hydroxyapatite coatings on titanium implants: The effect of coating characteristics. Journal of Biomedical Materials Research 1997;37(3):335-345.

114. Gross KA, Berndt CC. Thermal processing of hydroxyapatite for coating production. Journal of Biomedical Materials Research 1998;39(4):580-587.

115. Li H, Khor K, Cheang P. Impact formation and microstructure characterization of thermal sprayed hydroxyapatite/titania composite coatings. Biomaterials 2003;24(6):949-957.

116. El-Ghannam A, Ning C. Effect of bioactive ceramic dissolution on the mechanism of bone mineralization and guided tissue growth in vitro. Journal of Biomedical Materials Research Part A 2006;76(2):386-397.

117. Botelho C, Lopes M, Gibson I, Best S, Santos J. Structural analysis of Si-substituted hydroxyapatite: zeta potential and X-ray photoelectron spectroscopy. Journal of Materials Science: Materials in Medicine 2002;13(12):1123-1127.

118. Radice S, Kern P, Bürki G, Michler J, Textor M. Electrophoretic deposition of zirconia-Bioglass® composite coatings for biomedical implants. Journal of Biomedical Materials Research Part A 2007;82(2):436-444.

119. Lu HH, Pollack SR, Ducheyne P. Temporal zeta potential variations of 45 S 5 bioactive glass immersed in an electrolyte solution. Journal of Biomedical Materials Research 2000;51(1):80-87.

120. Schwarz S, Lunkwitz K, Keßler B, Spiegler U, Killmann E, Jaeger W. Adsorption and stability of colloidal silica. Colloids and Surfaces A: Physicochemical and Engineering Aspects 2000;163(1):17-27.

121. Szymczyk A, Fievet P, Mullet M, Reggiani J, Pagetti J. Comparison of two electrokinetic methods-electroosmosis and streaming potential-to determine the zeta-potential of plane ceramic membranes. Journal of Membrane Science 1998;143(1-2):189-195.

122. Gbureck U, Probst J, Thull R. Surface properties of calcium phosphate particles for self setting bone cements. Biomolecular engineering 2002;19(2-6):51-55.

123. Tengvall P, Lundström I. Physico-chemical considerations of titanium as a biomaterial. Clinical materials 1992;9(2):115-134.

124. Solar RJ, Pollack SR, Korostoff E. In vitro corrosion testing of titanium surgical implant alloys: an approach to understanding titanium release from implants. Journal of Biomedical Materials Research 1979;13(2):217-250.

125. De D, Nicholson PS. Role of ionic depletion in deposition during electrophoretic deposition. Journal of the American Ceramic Society 1999;82(11):3031-3036.

126. Sarkar P, Nicholson PS. Electrophoretic deposition (EPD): mechanisms, kinetics, and application to ceramics. Journal of the American Ceramic Society 1996;79(8):1987-2002.

127. Besra L, Uchikoshi T, Suzuki TS, Sakka Y. Experimental verification of pH localization mechanism of particle consolidation at the electrode/solution interface and its application to pulsed DC electrophoretic deposition (EPD). Journal of the European Ceramic Society 2010;30(5):1187-1193.

128. Lu K. Sintering of nanoceramics. International Materials Reviews 2008;53(1):21-38.

129. Donald I. Preparation, properties and chemistry of glass-and glass-ceramic-to-metal seals and coatings. Journal of materials science 1993;28(11):2841-2886.

130. Lopez-Esteban S, Saiz E, Fujino S, Oku T, Suganuma K, Tomsia AP. Bioactive glass coatings for orthopedic metallic implants. Journal of the European Ceramic Society 2003;23(15):2921-2930.

131. Manik S, Pradhan S, Pal M. Nanocrystalline $CaTiO_3$ prepared by soft-chemical route. Physica E: Low-dimensional Systems and Nanostructures 2005;25(4):421-424.

132. Ning C, Zhou Y. On the microstructure of biocomposites sintered from Ti, HA and bioactive glass. Biomaterials 2004;25(17):3379-3387.

133. El-Ghannam A, Ducheyne P, Shapiro I. Formation of surface reaction products on bioactive glass and their effects on the expression of the osteoblastic phenotype and the deposition of mineralized extracellular matrix. Biomaterials 1997;18(4):295-303.

134. LeGeros RZ. Properties of osteoconductive biomaterials: calcium phosphates. Clinical Orthopaedics and Related Research 2002;395:81.

135. Geesink R, de Groot K, Klein C. Bonding of bone to apatite-coated implants. Journal of Bone and Joint Surgery-British Volume 1988;70(1):17.

136. Reikerås O, Gunderson RB. Excellent results of HA coating on a grit-blasted stem: 245 patients followed for 8-12 years. Acta Orthopaedica 2003;74(2):140-145.

137. Wong M, Eulenberger J, Schenk R, Hunziker E. Effect of surface topology on the osseointegration of implant materials in trabecular bone. Journal of Biomedical Materials Research 1995;29(12):1567-1575.

138. Gross KA, Berndt CC, H H. Amorphous phase formation in plasma-sprayed hydroxyapatite coatings. Journal of Biomedical Materials Research 1998;39:407-414.

139. Yang C, Wang B, Lee T, Chang E, Chang G. Intramedullary implant of plasma-sprayed hydroxyapatite coating: An interface study. Journal of Biomedical Materials Research 1997;36(1):39-48.

140. Li H, Khor K, Cheang P. Titanium dioxide reinforced hydroxyapatite coatings deposited by high velocity oxy-fuel (HVOF) spray. Biomaterials 2002;23(1):85-91.

141. Lu YP, Li MS, Li ST, Wang ZG, Zhu RF. Plasma-sprayed hydroxyapatite+ titania composite bond coat for hydroxyapatite coating on titanium substrate. Biomaterials 2004;25(18):4393-4403.

142. Zhao Y, Xing G, Chai Z. Nanotoxicology: Are carbon nanotubes safe? Nature Nanotechnology 2008;3(4):191-192.

143. Javidi M, Javadpour S, Bahrololoom M, Ma J. Electrophoretic deposition of natural hydroxyapatite on medical grade 316L stainless steel. Materials Science and Engineering: C 2008;28(8):1509-1515.

144. Wang C, Ma J, Cheng W, Zhang R. Thick hydroxyapatite coatings by electrophoretic deposition. Materials Letters 2002;57(1):99-105.

145. Bodhak S, Bose S, Bandyopadhyay A. Electrically polarized HAp-coated Ti: In vitro bone cell–material interactions. Acta Biomaterialia 2010;6(2):641-651.

146. Moura CCG, Souza MA, Dechichi P, Zanetta-Barbosa D, Teixeira CC, Coelho PG. The effect of a nanothickness coating on rough titanium substrate in the osteogenic properties of human bone cells. Journal of Biomedical Materials Research Part A 2010;94(1):103-111.

147. Hao J, Kuroda S, Ohya K, Bartakova S, Aoki H, Kasugai S. Enhanced osteoblast and osteoclast responses to a thin film sputtered hydroxyapatite coating. Journal of Materials Science: Materials in Medicine 2011:1-11.

148. Peng P, Kumar S, Voelcker NH, Szili E, Smart RSC, Griesser HJ. Thin calcium phosphate coatings on titanium by electrochemical deposition in modified simulated body fluid. Journal of Biomedical Materials Research Part A 2006;76(2):347-355.

149. Gomes PS, Botelho C, Lopes MA, Santos JD, Fernandes MH. Evaluation of human osteoblastic cell response to plasma-sprayed silicon-substituted hydroxyapatite coatings over titanium substrates. Journal of Biomedical Materials Research Part B: Applied Biomaterials 2010;94(2):337-346.

150. Roach P, Farrar D, Perry CC. Surface tailoring for controlled protein adsorption: effect of topography at the nanometer scale and chemistry. Journal of the American Chemical Society 2006;128(12):3939-3945.

151. Yang Y, Cavin R, Ong JL. Protein adsorption on titanium surfaces and their effect on osteoblast attachment. Journal of Biomedical Materials Research Part A 2003;67(1):344-349.

152. Keselowsky BG, Collard DM, Garcia AJ. Surface chemistry modulates focal adhesion composition and signaling through changes in integrin binding. Biomaterials 2004;25(28):5947-5954.

153. Keselowsky BG, Collard DM, García AJ. Surface chemistry modulates fibronectin conformation and directs integrin binding and specificity to control cell adhesion. Journal of Biomedical Materials Research Part A 2003;66(2):247-259.

154. Buchanan LA, El-Ghannam A. Effect of bioactive glass crystallization on the conformation and bioactivity of adsorbed proteins. Journal of Biomedical Materials Research Part A 2010;93(2):537-546.

155. Krajewski A, Piancastelli A, Malavolti R. Albumin adhesion on ceramics and correlation with their Z-potential. Biomaterials 1998;19(7-9):637-641.

156. Boyd A, Burke G, Duffy H, Holmberg M, O'Kane C, Meenan B, Kingshott P. Sputter deposited bioceramic coatings: surface characterisation and initial protein adsorption studies using surface-MALDI-MS. Journal of Materials Science: Materials in Medicine 2011:1-14.

157. El-Ghannam A, Ducheyne P, Shapiro I. Effect of serum proteins on osteoblast adhesion to surface-modified bioactive glass and hydroxyapatite. Journal of Orthopaedic Research 1999;17(3):340-345.

158. Kilpadi KL, Chang PL, Bellis SL. Hydroxylapatite binds more serum proteins, purified integrins, and osteoblast precursor cells than titanium or steel. Journal of Biomedical Materials Research 2001;57(2):258-267.

159. García AJ, Ducheyne P, Boettiger D. Effect of surface reaction stage on fibronectin-mediated adhesion of osteoblast-like cells to bioactive glass. Journal of Biomedical Materials Research 1998;40(1):48-56.

160. Botelho C, Brooks RA, Kawai T, Ogata S, Ohtsuki C, Best SM, Lopes M, Santos J, Rushton N, Bonfield W. In vitro analysis of protein adhesion to phase pure hydroxyapatite and silicon substituted hydroxyapatite. Key Engineering Materials 2005;284:461-464.

161. Cowles E, DeRome M, Pastizzo G, Brailey L, Gronowicz G. Mineralization and the expression of matrix proteins during in vivo bone development. Calcified Tissue International 1998;62(1):74-82.

162. Stein GS, Lian JB, Owen TA. Relationship of cell growth to the regulation of tissue-specific gene expression during osteoblast differentiation. The FASEB Journal 1990;4(13):3111.

163. Lian J, McKee M, Todd A, Gerstenfeld LC. Induction of bone-related proteins, osteocalcin and osteopontin, and their matrix ultrastructural localization with development of chondrocyte hypertrophy in vitro. Journal of Cellular Biochemistry 1993;52(2):206-219.

164. Boyle WJ, Simonet WS, Lacey DL. Osteoclast differentiation and activation. Nature 2003;423(6937):337-342.

165. Haynes DR, Crotti T, Zreiqat H. Regulation of osteoclast activity in peri-implant tissues. Biomaterials 2004;25(20):4877-4885.

166. Amcheslavsky A, Bar-Shavit Z. Interleukin (IL)-12 mediates the anti-osteoclastogenic activity of CpG-oligodeoxynucleotides. Journal of Cellular Physiology 2006;207(1):244-250.

167. Alexander EH, Bento JL, Hughes Jr FM, Marriott I, Hudson MC, Bost KL. Staphylococcus aureus and Salmonella enterica serovar Dublin induce tumor necrosis factor-related apoptosis-inducing ligand expression by normal mouse and human osteoblasts. Infection and Immunity 2001;69(3):1581.

168. Tropel P, Noël D, Platet N, Legrand P, Benabid AL, Berger F. Isolation and characterisation of mesenchymal stem cells from adult mouse bone marrow. Experimental Cell Research 2004;295(2):395-406.

169. Chackalaparampil I, Peri A, Nemir M, Mckee MD, Lin PH, Mukherjee BB, Mukherjee AB. Cells in vivo and in vitro from osteopetrotic mice homozygous for c-src disruption show suppression of synthesis of osteopontin, a multifunctional extracellular matrix protein. Oncogene 1996;12(7):1457.

170. Windahl SH, Vidal O, Andersson G, Gustafsson J, Ohlsson C. Increased cortical bone mineral content but unchanged trabecular bone mineral density in female ERbeta (-/-) mice. J Clin Invest 1999;104(7):895-901.

171. McCall SH, Sahraei M, Young AB, Worley CS, Duncan JA, Ting JPY, Marriott I. Osteoblasts Express NLRP3, a Nucleotide-Binding Domain and Leucine-Rich Repeat Region Containing Receptor Implicated in Bacterially Induced Cell Death. Journal of Bone and Mineral Research 2008;23(1):30-40.

172. Chaiyasut C, Tsuda T. Isoelectric points estimation of proteins by electroosmotic flow: pH relationship using physically adsorbed proteins on silica gel. Chromatography 2001;22(2):91-96.

173. Ji Z, Jin X, George S, Xia T, Meng H, Wang X, Suarez E, Zhang H, Hoek EMV, Godwin H. Dispersion and stability optimization of TiO2 nanoparticles in cell culture media. Environmental Science & Technology 2010;44:7309–7314.

174. Murdock RC, Braydich-Stolle L, Schrand AM, Schlager JJ, Hussain SM. Characterization of nanomaterial dispersion in solution prior to in vitro exposure using dynamic light scattering technique. Toxicological Sciences 2008;101(2):239-253.

175. Ask M, Lausmaa J, Kasemo B. Preparation and surface spectroscopic characterization of oxide films on Ti6Al4V. Applied Surface Science 1989;35(3):283-301.

176. Steinberg D, Klinger A, Kohavi D, Sela MN. Adsorption of human salivary proteins to titanium powder. I. Adsorption of human salivary albumin. Biomaterials 1995;16(17):1339-1343.

177. Amphlett GW, Hrinda ME. The binding of calcium to human fibronectin. Biochemical and Biophysical Research Communications 1983;111(3):1045-1053.

178. Scott BJ, Bradwell A. Identification of the serum binding proteins for iron, zinc, cadmium, nickel, and calcium. Clinical Chemistry 1983;29(4):629.

179. Klinger A, Steinberg D, Kohavi D, Sela M. Mechanism of adsorption of human albumin to titanium in vitro. Journal of Biomedical Materials Research 1997;36(3):387-392.

180. Liu X, EI-Ghannam A. Effect of processing parameters on the microstructure and mechanical behavior of silica-calcium phosphate nanocomposite. Journal of Materials Science: Materials in Medicine 2010;21(7):2087-2094.

181. Kawano M, Hwang J. Influence of Guanidine, Imidazole, and Some Heterocyclic Compounds on Dissolution Rates of Amorphous Silica. Clays and Clay Minerals 2011;58(6):757.

182. Fournier AC, McGrath KM. Porous protein–silica composite formation: manipulation of silicate porosity and protein conformation. Soft Matter 2011;7(10):4918-4927.

183. Chittur KK. FTIR/ATR for protein adsorption to biomaterial surfaces. Biomaterials 1998;19(4-5):357-369.

184. Roach P, Farrar D, Perry CC. Interpretation of protein adsorption: surface-induced conformational changes. Journal of the American Chemical Society 2005;127(22):8168-8173.

185. Dvorak MM, Riccardi D. Ca2+ as an extracellular signal in bone. Cell Calcium 2004;35(3):249-255.

186. Maeno S, Niki Y, Matsumoto H, Morioka H, Yatabe T, Funayama A, Toyama Y, Taguchi T, Tanaka J. The effect of calcium ion concentration on osteoblast viability, proliferation and differentiation in monolayer and 3D culture. Biomaterials 2005;26(23):4847-4855.

187. Anselme K. Osteoblast adhesion on biomaterials. Biomaterials 2000;21(7):667-681.

188. Beck Jr GR. Inorganic phosphate as a signaling molecule in osteoblast differentiation. Journal of cellular biochemistry 2003;90(2):234-243.

189. Boskey AL, Guidon P, Doty SB, Stiner D, Leboy P, Binderman I. The mechanism of β-glycerophosphate action in mineralizing chick limb-bud mesenchymal cell cultures. Journal of Bone and Mineral Research 1996;11(11):1694-1702.

190. Chung CH, Golub EE, Forbes E, Tokuoka T, Shapiro IM. Mechanism of action of β-glycerophosphate on bone cell mineralization. Calcified Tissue International 1992;51(4):305-311.

191. Gupta G, Kirakodu S, El-Ghannam A. Effects of exogenous phosphorus and silicon on osteoblast differentiation at the interface with bioactive ceramics. Journal of Biomedical Materials Research Part A 2010.

192. Arumugam MQ, Ireland D, Brooks RA, Rushton N, Bonfield W. The effect orthosilicic acid on collagen type I, alkaline phosphatase and osteocalcin mRNA expression in human bone-derived osteoblasts in vitro. Key Engineering Materials 2006;309:121-124.

193. Reffitt D, Ogston N, Jugdaohsingh R, Cheung H, Evans B, Thompson R, Powell J, Hampson G. Orthosilicic acid stimulates collagen type 1 synthesis and osteoblastic differentiation in human osteoblast-like cells in vitro. Bone 2003;32(2):127-135.

194. Carlisle EM. Silicon as an essential trace element in animal nutrition. Ciba Found Symp 1986;121:123-139.

195. Gori F, Hofbauer LC, Dunstan CR, Spelsberg TC, Khosla S, Riggs BL. The expression of osteoprotegerin and RANK ligand and the support of osteoclast formation by stromal-osteoblast lineage cells is developmentally regulated. Endocrinology 2000;141(12):4768.

196. Mustafa K, Wroblewski J, Lopez BS, Wennerberg A, Hultenby K, Arvidson K. Determining optimal surface roughness of TiO2 blasted titanium implant material for attachment, proliferation and differentiation of cells derived from human mandibular alveolar bone. Clinical Oral Implants Research 2001;12(5):515-525.

197. Schneider G, Perinpanayagam H, Clegg M, Zaharias R, Seabold D, Keller J, Stanford C. Implant surface roughness affects osteoblast gene expression. Journal of Dental Research 2003;82(5):372-376.

198. Li LH, Kong YM, Kim HW, Kim YW, Kim HE, Heo SJ, Koak JY. Improved biological performance of Ti implants due to surface modification by micro-arc oxidation. Biomaterials 2004;25(14):2867-2875.

199. Lincks J, Boyan B, Blanchard C, Lohmann C, Liu Y, Cochran D, Dean D, Schwartz Z. Response of MG63 osteoblast-like cells to titanium and titanium alloy is dependent on surface roughness and composition. Biomaterials 1998;19(23):2219-2232.

200. Balloni S, Calvi EM, Damiani F, Bistoni G, Calvitti M, Locci P, Becchetti E, Marinucci L. Effects of titanium surface roughness on mesenchymal stem cell

commitment and differentiation signaling. The International Journal of Oral & Maxillofacial Implants 2009;24(4):627.

201. Park JW, Suh JY, Chung HJ. Effects of calcium ion incorporation on osteoblast gene expression in MC3T3-E1 cells cultured on microstructured titanium surfaces. Journal of Biomedical Materials Research Part A 2008;86(1):117-126.

202. Degasne I, Basle M, Demais V, Hure G, Lesourd M, Grolleau B, Mercier L, Chappard D. Effects of roughness, fibronectin and vitronectin on attachment, spreading, and proliferation of human osteoblast-like cells (Saos-2) on titanium surfaces. Calcified Tissue International 1999;64(6):499-507.

203. RAMAGLIA L, POSTIGLIONE L, DI SPIGNA G, CAPECE G, SALZANO S, ROSSI G. Sandblasted-acid-etched titanium surface influences in vitro the biologicalbehavior of SaOS-2 human osteoblast-like cells. Dental Materials Journal 2011(0):1103100122.

204. Gittens RA, McLachlan T, Olivares-Navarrete R, Cai Y, Berner S, Tannenbaum R, Schwartz Z, Sandhage KH, Boyan BD. The effects of combined micron-/submicron-scale surface roughness and nanoscale features on cell proliferation and differentiation. Biomaterials 2011.

205. Kim HW, Kim HE, Salih V, Knowles JC. Sol-gel-modified titanium with hydroxyapatite thin films and effect on osteoblast-like cell responses. Journal of Biomedical Materials Research Part A 2005;74(3):294-305.

206. Deligianni DD, Katsala ND, Koutsoukos PG, Missirlis YF. Effect of surface roughness of hydroxyapatite on human bone marrow cell adhesion, proliferation, differentiation and detachment strength. Biomaterials 2001;22(1):87-96.

207. Korovessis PG, Deligianni DD. Role of surface roughness of titanium versus hydroxyapatite on human bone marrow cells response. Journal of Spinal Disorders & Techniques 2002;15(2):175.

208. Dulgar-Tulloch A, Bizios R, Siegel R. Human mesenchymal stem cell adhesion and proliferation in response to ceramic chemistry and nanoscale topography. Journal of Biomedical Materials Research Part A 2009;90(2):586-594.

209. Zheng Z, Zhang L, Kong L, Wang A, Gong Y, Zhang X. The behavior of MC3T3-E1 cells on chitosan/poly-L-lysine composite films: Effect of nanotopography, surface chemistry, and wettability. Journal of Biomedical Materials Research Part A 2009;89(2):453-465.

210. Nayab SN, Jones FH, Olsen I. Effects of calcium ion implantation on human bone cell interaction with titanium. Biomaterials 2005;26(23):4717-4727.

211. Shie MY, Ding SJ, Chang HC. The role of silicon in osteoblast-like cell proliferation and apoptosis. Acta Biomaterialia 2011.

212. Sinha RK, Morris F, Shah SA, Tuan RS. Surface composition of orthopaedic implant metals regulates cell attachment, spreading, and cytoskeletal organization of primary human osteoblasts in vitro. Clinical Orthopaedics and Related Research 1994;305:258.

213. Hahn H, Logas J, Averback R. Sintering characteristics of nanocrystalline TiO 2. Journal of Materials Research 1990;5(3):609-614.

214. Jäger M, Zilkens C, Zanger K, Krauspe R. Significance of nano-and microtopography for cell-surface interactions in orthopaedic implants. Journal of Biomedicine and Biotechnology 2007;2007.

215. Ogura N, Kawada M, Chang WJ, Zhang Q, Lee SY, Kondoh T, Abiko Y. Differentiation of the human mesenchymal stem cells derived from bone marrow and enhancement of cell attachment by fibronectin. Journal of Oral Science 2004;46(4):207-213.

216. Redey SA, Nardin M, Bernache–Assolant D, Rey C, Delannoy P, Sedel L, Marie PJ. Behavior of human osteoblastic cells on stoichiometric hydroxyapatite and type A carbonate apatite: role of surface energy. Journal of Biomedical Materials Research 2000;50(3):353-364.

217. Okumura A, Goto M, Goto T, Yoshinari M, Masuko S, Katsuki T, Tanaka T. Substrate affects the initial attachment and subsequent behavior of human osteoblastic cells (Saos-2). Biomaterials 2001;22(16):2263-2271.

218. Zayzafoon M. Calcium/calmodulin signaling controls osteoblast growth and differentiation. Journal of Cellular Biochemistry 2006;97(1):56-70.

219. Carlisle E, Berger J, Alpenfels W. A silicon requirement for prolyl hydroxylase activity. Fed Proc 1981. p 886.

220. Madgwick S, Levasseur M, Jones KT. Calmodulin-dependent protein kinase II, and not protein kinase C, is sufficient for triggering cell-cycle resumption in mammalian eggs. Journal of Cell Science 2005;118(17):3849-3859.

221. Meleti Z, Shapiro I, Adams C. Inorganic phosphate induces apoptosis of osteoblast-like cells in culture. Bone 2000;27(3):359-366.

222. Scherer A, Graff JM. Calmodulin differentially modulates Smad1 and Smad2 signaling. Journal of Biological Chemistry 2000;275(52):41430-41438.

223. Schmid C, Keller C, Schläpfer I, Veldman C, Zapf J. Calcium and insulin-like growth factor I stimulation of sodium-dependent phosphate transport and proliferation of cultured rat osteoblasts. Biochemical and Biophysical Research Communications 1998;245(1):220-225.

224. Dalby MJ, Gadegaard N, Tare R, Andar A, Riehle MO, Herzyk P, Wilkinson CDW, Oreffo ROC. The control of human mesenchymal cell differentiation using nanoscale symmetry and disorder. Nature Materials 2007;6(12):997-1003.

225. Woodring PJ, Hunter T, Wang JYJ. Regulation of F-actin-dependent processes by the Abl family of tyrosine kinases. Journal of Cell Science 2003;116(13):2613-2626.

226. Matsuura T, Hosokawa R, Okamoto K, Kimoto T, Akagawa Y. Diverse mechanisms of osteoblast spreading on hydroxyapatite and titanium. Biomaterials 2000;21(11):1121-1127.

227. Ingber DE, Dike L, Hansen L, Karp S, Liley H, Maniotis A, McNamee H, Mooney D, Plopper G, Sims J. Cellular tensegrity: exploring how mechanical changes in the cytoskeleton regulate cell growth, migration, and tissue pattern during morphogenesis. International Review of Cytology 1994;150:173-224.

APPENDIX: PUBLISHED WORK

Society For
Biomaterials

Electrophoretic deposition of bioactive silica-calcium phosphate nanocomposite on Ti-6Al-4V orthopedic implant

Aniket, Ahmed El-Ghannam

Department of Mechanical Engineering and Engineering Science, The University of North Carolina at Charlotte, Charlotte, North Carolina

Abstract: Bioactive silica-calcium phosphate nanocomposite (SCPC) has been coated on Ti-6Al-4V implant employing an electrophoretic deposition (EPD) technique. The effects of composition and pH of the suspending medium on the zeta potential of three different SCPC formulations; SCPC25, SCPC50 and SCPC75 were analyzed. The average zeta potential of SCPC50 in pure ethanol was more negative than that of SCPC25 or SCPC75; however, the difference was not statistically significant. Discs of Ti-6Al-4V were passivated, coated with SCPC50 (200 nm–10 μm) and thermally treated at 600–800°C to produce a coating thickness in the range of 43.1 ± 5.7 to 30.1 ± 4.6 μm. After treatment at 600, 700, and 800°C, the adhesion strength at the SCPC50/Ti-6Al-4V interface was 42.6 ± 3.6, 44.7 ± 8.7, and 47.2 ± 4.3 MPa, respectively. SEM-EDX analyses of SCPC50-coated Ti-6Al-4V preimmersed in PBS for 7 days showed the formation of a Ca-deficient hydroxyapatite surface layer. ICP-OES analyses of the immers-ing solution ($n = 6$) showed an increase in the ionic concentration of Si from 3.3 ± 0.9 to 5.0 ± 1.2 ppm between days 1 and 4; after which no significant change in the Si concentration was measured. Bone marrow mesenchymal stem cells attached to the SCPC50-coated implants expressed significantly higher ($p < 0.05$) alkaline phosphatase activity (82.4 ± 25.6 nmoles p-NP/mg protein/min) than that expressed by cells attached to HA-coated or uncoated implants. Results of the study suggest that bioactive SCPC50 can efficiently be coated on Ti-6Al-4V using EPD. The SCPC50 coating has the potential to enhance bone integration with the orthopedic implant. © 2011 Wiley Periodicals, Inc. J Biomed Mater Res Part B: Appl Biomater 99B: 369–379, 2011.

Key Words: electrophoretic deposition, zeta potential, bioactive silica-calcium phosphate nanocomposite, Ti-6Al-4V orthopedic implant, adhesion strength

INTRODUCTION

Tissue integration between bone and orthopedic biomaterials is essential for implant fixation and long-term stability. Host tissue response against metal implants results in the formation of a nonadherent fibrous capsule.[1–4] Fibrous encapsulation of the implant is a nonideal interface for two reasons: first, the fibrous capsule does not properly transfer the mechanical signal from metal to bone. Second, it allows micro-motion, the range of which would increase by time causing implant loosening. To enhance tissue integration, metal implants are coated with bioactive ceramics such as calcium phosphates.[5–7] Hydroxyapatite (HA) coating provides an osteoconductive surface that promotes rapid and direct bone bonding with the Ti-6Al-4V implants. Despite the commercial success, there are many shortcomings associated with the HA-coated metals due to plasma spraying technique. The high temperature involved in the coating process results in the decomposition of HA into various undesirable phases including tri-calcium phosphate, tetra-calcium phosphate, calcium oxide, and oxy-hydroxyapatite.[8–10] Moreover, several studies have shown that Ti-6Al-4V catalyzes the decomposition of HA at high temperature.[11,12]

Silica–calcium phosphate nanocomposite (SCPC) is a novel bioactive resorbable ceramic that has the ability to bond to bone and expedite bone formation. Previous reports have demonstrated the superior bone regenerative capability, mechanical properties, and resorbability of SCPC as compared with hydroxyapatite or bioactive glass.[13,14] The enhanced bioactivity of the SCPC has been attributed to its unique phase composition, modified nanocrystalline structure, and high porosity.[13–16] SCPC demonstrated the formation of a surface apatite layer within 2 h of immersion in simulated body fluid.[13] Moreover, SCPC developed the apatite surface layer in the presence of serum proteins.[14,15] Real time RT-PCR analyses demonstrated that SCPC up-regulated osteoblastic gene expression significantly higher than HA.[13] In vivo studies have shown rapid bone formation and graft material resorption in critical size bone defects implanted with SCPC. In contrast, similar defects implanted with bioactive glass granules showed bone formation but minimal graft resorption.[15] Moreover, SCPC has demonstrated its ability as a potential drug-delivery vehicle for rh-BMP2, gentamicin, vancomycin, and 5-fluorouracil.[14,17–19]

Correspondence to: A. El-Ghannam; e-mail: arelgha@uncc.edu

Promotion of pro-osteogenic responses by a bioactive ceramic coating

Aniket,[1] Amy Young,[2] Ian Marriott,[2] Ahmed El-Ghannam[1]

[1]Department of Mechanical Engineering and Engineering Science, University of North Carolina at Charlotte, Charlotte, North Carolina 28223
[2]Department of Biology, University of North Carolina at Charlotte, Charlotte, North Carolina 28223

Abstract: The objective of this study was to analyze the responses of bone-forming osteoblasts to Ti-6Al-4V implant material coated with silica-calcium phosphate nanocomposite (SCPC50). Osteoblast differentiation at the interface with SCPC50-coated Ti-6Al-4V was correlated to the adsorption of high amount of serum proteins, high surface affinity to fibronectin, Ca uptake from and P and Si release into the medium. SCPC50-coated Ti-6Al-4V adsorbed significantly more serum protein ($p < 0.05$) than control uncoated substrates. Moreover, Western blot analysis showed that the SCPC50 coating had a high affinity for serum fibronectin. Protein conformation analyses by FTIR showed that the ratio of the area under the peak for amide I/amide II bands was significantly higher ($p < 0.05$) on the surface of SCPC50-coated substrates than that on the surface of the control uncoated substrates. Moreover, ICP – OES analyses indicated that SCPC50-coated substrates withdrew Ca ions from, and released P and Si ions into, the tissue culture medium, respectively. In conjunction with the favor-

able protein adsorption and modifications in medium composition, MC3T3-E1 osteoblast-like cells attached to SCPC50-coated substrates expressed 10-fold higher level of mRNA encoding osteocalcin and had significantly higher production of osteopontin and osteocalcin proteins than cells attached to the uncoated Ti-6A1-4V substrates. In addition, osteoblast-like cells attached to the SCPC50-coated substrates produced significantly lower levels of the inflammatory and osteoclastogenic cytokines, IL-6, IL-12p40, and RANKL than those attached to uncoated Ti-6A1-4V substrates. These results suggest that SCPC50 coating could enhance bone integration with orthopedic and maxillofacial implants while minimizing the induction of inflammatory bone cell responses. © 2012 Wiley Periodicals, Inc. J Biomed Mater Res Part A: 00A:000–000, 2012.

Key Words: bioactive silica-calcium phosphate nanocomposite, ceramic coating, protein adsorption, osteoblast differentiation, orthopedic implant

INTRODUCTION

Coating orthopedic Ti-6Al-4V implants with bioactive calcium phosphate (CaP) ceramics provides an osteoconductive surface that stimulates direct bone bonding and minimizes the loosening of the implant.[1–3] Moreover, the bioactive ceramic coating facilitates proper transmission of a mechanical stimulus from the implant to the bone; an important phenomenon that alleviates stress shielding of the periprosthetic bone and impedes its resorption.[4,5] Plasma-sprayed hydroxyapatite (HA) coated Ti-6Al-4V has been widely used; however, the high temperature of the plasma during coating results in a partial decomposition of HA into undesirable phases of altered solubility and biocompatibility.[6,7] Moreover, the difference in the thermal expansion coefficient between ceramic and the metal substrate creates interfacial thermal stresses that result in poor adhesion.[8] Other studies have shown that the HA coating layer is often cracked and nonhomogenous in both, thickness and crystallinity, which renders the coating prone to delamination.[8–10] Electrophoretic deposition (EPD) of bioactive ceramics on metal substrates favors low sintering temperature and slow heating and cooling cycles that minimize interfacial stresses between metal and ceramic and enhance adhesion strength.[11–13] Coating bioactive silica-calcium phosphate nanocomposite (SCPC50) on Ti-6Al-4V orthopedic implant using EPD showed the adhesion strength at the interface between the metal substrate and the bioactive ceramic to be 47 ± 4 MPa which exceeded the ASTM (F1147-05) requirement of 30 MPa.[11]

Cell attachment to an implant is strongly governed by the amount, kind and conformation of proteins that adsorb onto the material's surface.[14–16] Protein adsorption is determined by the physicochemical characteristics of the implant material including zeta potential, surface chemistry, material crystallinity and surface area.[14,17–19] An increase in the negative zeta potential of bioactive ceramics was found to reduce protein adsorption.[18,20] The selective adsorption of certain proteins in serum to bioactive ceramics has been

Correspondence to: A. El-Ghannam; e-mail: arelgha@uncc.edu

Effect of Bioactive Surface Coating on Protein Adsorption, Bone Cell Differentiation and Immune Response

Aniket, Ian Marriott and Ahmed El-Ghannam
The University of North Carolina at Charlotte, Charlotte, NC

Proceedings of the 2011 Annual Meeting of the Society for Biomaterials, Orlando, FL

Statement of Purpose: Bioactive ceramic coating promotes bone bonding and fixation of orthopedic implants. Protein adsorption mediates cell-material interaction and so it plays an important role in tissue responses to implant materials. An ideal implant surface should therefore be able to selectively bind attachment proteins, expose their active sites for specific cell adhesion, and trigger an intracellular cascade reaction that leads to bone deposition. The objective of the present study is to coat the surface of medical grade Ti-6Al-4V implant material with a bioactive silica-calcium phosphate nanocomposite (SCPC)[1] and evaluate bone cell responses to this material by RT-PCR. The effect of SCPC coating on fibronectin adsorption is reported. Moreover, the secondary structure of adsorbed proteins was analyzed and co-related to cell function.

Methods: SCPC was coated on Ti-6Al-4V samples by electrophoretic deposition. A voltage of 50 V was applied for 30 sec in a 10 wt% SCPC suspension in ethanol followed by thermal treatment at 800 °C/1 hr under argon.[2] Ti-6Al-4V discs with and without SCPC coating were immersed in 1 mL of FBS at 37 °C for 4 hr. The adsorbed protein was extracted and analyzed by Western blot and ELISA techniques. A mouse monoclonal antibody was employed for the detection of adsorbed fibronectin. In addition, total protein adsorption was quantified using a Micro BCA assay kit (Thermo Scientific, Rockford, IL). The conformation of the adsorbed protein was analyzed using FTIR in the diffuse reflectance mode. Secondary structures within the amide I functional group, in addition to the ratio of amide I/amide II envelope, were determined. MC3T3-E1 osteoblast-like cells were seeded on the substrates and the expression of osteoblast-associated products was analyzed by measuring levels of mRNA encoding collagen-I, osteonectin, osteopontin, and osteocalcin by RT-PCR. Moreover, the inflammatory response to the substrates was determined by measuring the expression of inflammatory cytokines IL-6, IL-12 and RANK-L. In addition, the ionic composition of the tissue culture medium incubated with the different substrates in presence and absence of cells was also evaluated.

Results: Total protein analysis showed that SCPC-coated substrates adsorbed significantly higher amounts of serum protein than uncoated Ti-alloy (p<0.05). Moreover, Western blot and ELISA analyses showed preferential adsorption of fibronectin on SCPC-coated samples (Fig. 1a). FTIR studies of the adsorbed protein showed that the ratio of amide I/amide II functional groups was significantly higher (p<0.05) on SCPC-coated than that on the uncoated samples (Fig. 1b). RT-PCR results showed that the cells attached to SCPC-coated substrates expressed higher levels of osteocalcin mRNA compared to that expressed by cells attached to uncoated Ti-alloy. In addition, the release of the inflammatory cytokines IL-6

and RANK-L was significantly lower (p<0.05) on SCPC-coated compared to uncoated Ti-alloy implants.

Fig. 1: (a) Western blot showing preferential fibronectin adsorption to the SCPC-coated substrate; (b) FTIR analyses showed that proteins bound to SCPC-coated samples demonstrated significantly higher ratio of amide I/amide II functional groups than the uncoated samples.
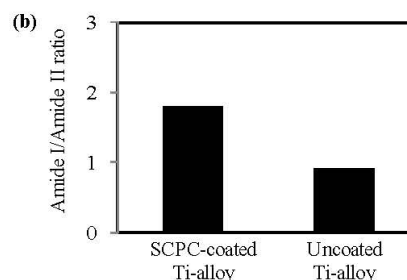
Conclusions: The results of the present study show that SCPC-coated substrate selectively adsorbs a significant amount of fibronectin, an attachment protein known to stimulate bone cell adhesion and function. Moreover, SCPC coating induces a favorable protein conformation with high ratio of amide I to amide II. Published studies have shown that higher amide I expression enhances cell adhesion and cellular proliferation leading to enhanced tissue integration.[3] The superior protein adsorption and the bioactive characteristics of the implant coating material synergistically stimulates the rapid expression of osteoblast products associated with de novo bone deposition in the absence of a significant inflammatory response. The minimal production of pro-inflammatory cytokines would be anticipated to limit leukocyte recruitment to the implant site and restrict osteoclast maturation and activation.[4] As such, the use of SCPC-coated Ti-alloy implants has the potential to improve bone-tissue integration and enhance implant longevity.

References:
[1] El-Ghannam A. JBMR-Part A. 2004; 69: 490-501
[2] Aniket. JBMR-Part B (under publication)
[3] Buchanan LA. JBMR-Part A. 2010; 93: 537-546
[4] McInnes IB. Nat Rev-Immunology. 2007; 7: 429-442

Osteoblast Gene Expression on a Novel Bioactive Ceramic Coating for Orthopedic Implants

Aniket; Young, A B; Marriott, I; + El-Ghannam, A

The University of North Carolina at Charlotte, NC

ABSTRACT INTRODUCTION:

Enhanced tissue integration between bone and orthopedic implant devices is essential for implant fixation and longevity. An immunological response leads to fibrous encapsulation of metallic implants. Bioactive ceramics have the ability to make a direct bond with bone. Coating orthopedic implants with bioactive ceramics is an attractive mean of improving the in vivo performance of load bearing implants. Silica-calcium phosphate nano composite (SCPC) is a novel bioactive resorbable ceramic that has the ability to bond to bone and expedite bone formation[1]. In our previous work, we have demonstrated the coating of bioactive SCPC on medical grade Ti-6Al-4V implants using electrophoretic deposition (EPD)[2]. The objective of the present study is to evaluate bone cell responses to the SCPC-coated implant material. In particular, the effect of the SCPC coating on gene expression is evaluated. Moreover, the release of cytokines from bone cells as a result of cell/material interaction is described.

METHODS:

Ti-6Al-4V discs (n = 5) were coated with SCPC as described elsewhere[2]. Briefly, the discs were passivated in 34% HNO_3 and the EPD coating was carried out in 5% (w/v) SCPC suspension in ethanol for 30 sec at 50 V followed by thermal treatment at 800 °C under argon. MC3T3-E1 osteoblast-like cells were seeded on SCPC-coated and uncoated Ti-6Al-4V discs at a cell density of 6 x 10^5 cells/sample and covered with 6 mL tissue culture medium (TCM) containing 10% fetal bovine serum, 0.05% gentamycin and 0.1% amphotericin-B in DMEM. Cells seeded on tissue culture polystyrene (TCPS) served as control. The samples were incubated for 48 hrs at 37 °C with 5% humidified CO_2 following which the TCM was replaced and supplemented with 10^{-8} M dexamethasone and 50 µg/mL ascorbic acid. The samples were incubated for another 48 hrs and the total mRNA was extracted using the TRIZOL reagent. The purified mRNA from each sample type was pooled together and cDNA generated using random hexamer primers and reverse transcriptase. Polymerase chain reaction (PCR) was performed for the expression of mRNA encoding osteoblast phenotypic markers including collagen-I (Col-I), osteonectin (OSN), osteopontin (OPN) and octeocalcin (OCN) as well as the housekeeping gene glyceraldehyde 3-phosphate dehydrogenase (G3PDH) and the products were analyzed by agarose gel electrophoresis. Moreover, real-time PCR was performed to quantify gene expression levels. In addition, the morphology of the cells on SCPC-coated and uncoated Ti-6Al-4V samples was analyzed using SEM-EDX after 24 hrs and 96 hrs of incubation in TCM. In-situ release of interleukins IL-6 and IL-12 was measured to determine the cellular immune response as a result of cell/material interaction. The levels of IL-6 and IL-12 were measured in TCM using respective ELISA kits as per the manufacturer's instructions (R&D Systems, MN). Statistical analysis was performed using student's t-test with p < 0.05, indicating a statistically significant difference.

RESULTS:

PCR analyses confirmed the expression of the osteoblast phenotypic markers Col-I, OSN, OPN and OCN in all samples. Real-time PCR analyses indicated greater up-regulation of Col-I, OSN and OPN on uncoated Ti-6Al-4V and TCPS samples as compared to the SCPC-coated Ti-6Al-4V samples. However, OCN expression on SCPC-coated samples was increased by over 10 fold versus uncoated samples and this, in turn, was higher than that measured on TCPS (Fig. 1). SEM analyses of the MC3T3-E1 cells attached to SCPC-coated Ti-6Al-4V samples incubated in TCM for 24 hrs showed that the cells transformed to acquire polygonal shape and formed multiple cellular processes. EDX analyses of the cell layer showed rapid Ca^{2+} assimilation as indicated by the greater Ca/P ratio. After 96 hrs incubation, the cells attached to the uncoated Ti-6Al-4V sample acquired "fibroblast-like" morphology, as indicated by their shape (Fig. 2a) while those attached to the SCPC-coated Ti-6Al-4V sample formed a confluent cell layer (Fig. 2b). The formation of extra-cellular matrix was observed on both samples; however matrix mineralization was limited to the SCPC-coated samples. As a result of cell/material interaction, the MC3T3-E1 cells released interleukins IL-6 and IL-12 into the tissue culture media. Significantly lower IL-6 levels (p<0.05) were produced by cells attached to SCPC-coated samples as compared to uncoated or TCPS samples (Fig. 3). On the other hand, lower levels of IL-12 were present in the SCPC-coated sample than the uncoated Ti-6Al-4V sample, although this difference was not statistically significant (p > 0.05). Minimal IL-12 release was measured for the cells on TCPS.
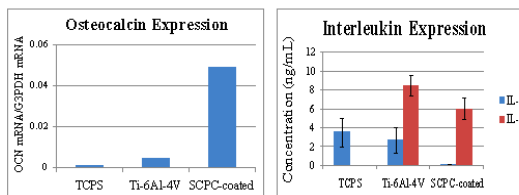

Fig. 1: Osteocalcin mRNA expression after 96-hr incubation.

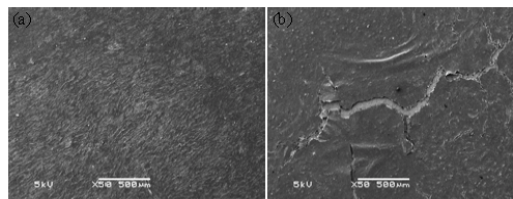Fig. 3: Evaluation of IL-6 and IL-12 production at 96 hrs.

Fig. 2: SEM images of the MC3T3-E1 cells on uncoated Ti-alloy disc and SCPC-coated Ti-alloy disc after incubation for 4 days. (a) The cells on the Ti-alloy surface acquired "fibroblast-like" morphology while (b) those on the SCPC-coated sample formed a dense confluent cell layer over the SCPC coating.

DISCUSSION:

The MC3T3-E1 osteoblast-like cells expressed osteoblast phenotypic markers Col-I, OSN, OPN, and OCN mRNA upon interaction with SCPC-coated Ti-6Al-4V samples. More importantly, the bioactive SCPC coating stimulated enhanced up-regulation of OCN and hence rapid mineralization of the extracellular matrix. On the other hand, cells on the uncoated Ti-6Al-4V samples showed a delayed response towards synthesizing mineralized matrix as indicated by the lower OCN levels. The up-regulation of OCN, in conjunction with the down-regulation of OPN, co-related well with the marked decrease in the expression of Col-I on the SCPC-coated samples. These results reflect a temporal variation in the gene expression pattern of osteoblasts wherein the levels of Col-I and OPN are lowered during OCN expression. It should be noted that osteocalcin is expressed only postproliferatively during the bone mineralization stage by the differentiating osteoblasts. Hence, an early expression of OCN is indicative of the strong stimulatory effect of SCPC on bone cell differentiation. Osteolytic reactions around orthopedic implants are promoted by the production of inflammatory and osteogenic mediators such as IL-6 and IL-12 by osteoblasts. In the present study, we showed that SCPC-coated Ti-6Al-4V samples stimulated significantly lower release of IL-6 as compared to the uncoated samples. The lower release of both IL-6 and IL-12 may enhance orthopedic implant fixation by limiting leukocyte recruitment and reducing the formation and activity of bone-resorbing osteoclasts that can lead to aseptic loosening. Experiments are currently ongoing to evaluate the role of other selected cytokines in the osteoblast immune response. Moreover, protein expression analyses are underway to co-relate osteoblast gene expression with protein synthesis.

REFERENCES:

[1] El-Ghannam A, J Biomed Mater Res 69A: 490–501, 2004

[2] El-Ghannam A and Aniket, Proc Mat Res Soc-Fall 2009

Enhancement of Bone-Implant Integration Using a Novel Bioactive Ceramic Coating

Aniket, Amy Young, Ian Marriott and Ahmed El-Ghannam
The University of North Carolina at Charlotte, NC, USA

Tissue integration between bone and orthopedic implant is essential for implant fixation and longevity. Host tissue response against metallic implants results in the formation of a non-adherent fibrous capsule that can lead to micro-motion resulting in implant failure. Bioactive ceramics have the ability to directly bond to bone and expedite bone formation; however they have inappropriate mechanical properties for load bearing applications. Silica-calcium phosphate nanocomposite (SCPC) is a novel ceramic that has demonstrated superior bioactivity, mechanical properties and resorbability than traditional ceramics, such as hydroxyapatite or bioactive glass. The objective of this study is to coat medical grade Ti-6Al-4V implant with SCPC and evaluate the effect of ceramic composition and coating parameters on the adhesion strength between the bioactive ceramic and the metal substrate. Moreover, protein adsorption onto the coated substrate has been correlated to osteogenic gene expression of bone cells.

SCPC was prepared using powder metallurgy technique and ground into nano-particles (50 – 200 nm) using a planetary ball mill. The structure of SCPC was analyzed using XRD, FTIR, SEM and EDX techniques. Ti-6Al-4V was coated with SCPC nano-particles using electrophoretic deposition. Efficient and stable coating was achieved by optimizing SCPC concentration, coating duration, voltage and thermal treatment process. Adhesion strength at the interface of SCPC and Ti-6Al-4V was measured according to ASTM standard protocol (F1147-05) and the fractured surface was analyzed using SEM-EDX. Moreover, the protein binding capability of SCPC-coating was assessed using western blot analysis. In-vitro bioactivity of bone cells on SCPC-coated Ti-6Al-4V was analyzed by measuring gene expression and protein synthesis using RT-PCR and spectrophotometric techniques respectively. In addition, the immunological response of bone cells on SCPC-coated Ti-6Al-4V was evaluated using ELISA.

XRD, FTIR and EDX analyses showed that SCPC coating was composed of β-rhenanite and α- cristobalite nano-crystals. Mechanical tests showed that the adhesion strength between the SCPC coating and Ti-6Al-4V increased with increasing thermal treatment temperature and reached a maximum strength of 47 ± 4 MPa after treatment at 800 ºC; a strength value that exceeded the ASTM requirement of 30 MPa. Moreover, the interface between the ceramic and metal was intact even after the fracture which speaks volumes for the strong adhesion between the SCPC and Ti-6Al-4V. Western blot analysis showed selective adsorption of fibronectin by SCPC coating which would enhance cell attachment and proliferation. Importantly, it was found that the bone cells attached to SCPC-coated Ti-6Al-4V implant up-regulated the synthesis of vital genes responsible for de novo bone formation. Moreover, a favorable minimal immunological response of the cells towards SCPC coating was observed which would further enhance the fixation of the implant inside the bone.

In conclusion, a successful coating of a uniform and stable layer of bioactive SCPC on Ti-6Al-4V implant was achieved using electrophoretic deposition. In-vitro analyses showed that SCPC coating promoted bone formation through up-regulation of osteoblastic gene expression and protein adsorption. Hence, SCPC coating has the potential to expedite bone bonding to the implant and improve longevity.

A Novel Bioactive Ceramic Coating for Improved Fixation of Orthopedic Implant

Aniket and Ahmed El-Ghannam
The University of North Carolina at Charlotte, Charlotte, NC 28223

Coating orthopedic implants with bioactive ceramics facilitates bone tissue integration, implant fixation and hence longevity. Various bioactive ceramics have been used for coating with limited success due to instability of the ceramic/metal interface. Silica calcium phosphate nano-composite (SCPC) is a novel bioactive resorbable ceramic that has the ability to bond to bone and expedite bone formation. In the present study, we coat medical grade Ti-6Al-4V implants with SCPC using electrophoretic deposition (EPD) and demonstrate the stability, uniformity and bioactivity of the ceramic coating.

Flat Ti alloy discs were passivated in 34% HNO_3. EPD was carried out in 2-7.5% (w/v) SCPC suspension in ethanol for 60-600 sec at 30-120V. The coated discs were treated at 600-800 ºC under argon. Adhesion strength was measured and the fractured surface was analyzed using SEM-EDX. The coated discs were immersed in phosphate buffer for 7 days and the adhesion strength was evaluated thereafter. Foam Ti alloy discs were coated with SCPC using optimized EPD parameters, cold-mounted in epoxy and sectioned using diamond wheel. The thickness of the SCPC coating on the surface of the inner and outer pores was measured.

A uniform 30 - 40 μm SCPC layer was detected on passivated Ti alloy surface after 3 min EPD coating in 5% (w/v) SCPC suspension using 50 V. Tensile tests showed that the adhesion strength between SCPC and passivated Ti alloy after thermal treatment at 800ºC was 47 ± 4 MPa. Although the adhesion strength was higher for samples treated at 800ºC than those treated at 700ºC or 600ºC, the difference was not statistically significant. Fracture surface analyses revealed that the failure was largely at the ceramic/polymer interface or within the ceramic layer, suggesting a strong ceramic/metal interface. SEM analyses of the cross section of Ti alloy foam showed that after 30 sec coating, the entire thickness of the porous structure was coated with a uniform 4 μm thick SCPC layer. The interface between the ceramic and metal appeared to be very intact. After 7 days immersion in physiological solution, SCPC enhanced the deposition of a biological hydroxyapatite layer on its surface. Mechanical testing showed that the fracture occurred at the interface between the precipitated hydroxyapatite and the SCPC layer at 6.4 ± 1.8 MPa.

In conclusion, successful coating of a thin and uniform layer of bioactive SCPC on the surface of Ti alloy implant material was achieved using EPD. The SCPC layer was strongly adhered to the metal surface even after immersion in physiological solution. Moreover, the SCPC coating enhanced the bioactivity properties of the implant as indicated by the formation of a biological hydroxyapatite layer on the material surface. Therefore, SCPC coating has the potential to expedite bone bonding to the metallic implant, improve fixation and longevity. Currently we are evaluating the interaction between bone cells and the SCPC coated Ti alloy implant.

SBC2008-192883

ZETA POTENTIAL OF SILICA CALCIUM PHOSPHATE NANOCOMPOSITE: EFFECT OF MATERIAL COMPOSITION AND MEDIUM pH

Aniket, Ahmed. R. El-Ghannam

Department of Mechanical Engineering and Engineering Science
The University of North Carolina at Charlotte
Charlotte, North Carolina

INTRODUCTION

Biodegradable ceramics have lately found exciting applications in orthopedic and maxillofacial surgeries as agents for bone repair, drug delivery vehicles and filling materials. A novel bioactive resorbable ceramic that demonstrated a superior mechanical properties, bioactivity and resorbability compared to traditional calcium phosphate ceramics or bioactive glass is bioactive silica-calcium phosphate nanocomposite (SCPC) [1, 2]. Previous studies have demonstrated that the enhanced bioactivity of SCPC is attributed to its nano structure as well as other physicochemical properties of the material [2]. Surface charge is one of the most important factors that control tissue and cell response to the implant material. Additionally, surface charge enhances the adsorption of biological molecules onto the material surface. The objective of the present work is to investigate the effect of SCPC composition and medium pH on the zeta potential and conductance of the material.

MATERIALS AND METHODS

Ceramic Preparation

Three different chemical compositions of SCPC – SCPC25, SCPC50 and SCPC75 containing calcium phosphate/silica components in the ratio of 75/25, 50/50 and 25/75 respectively were prepared following the method reported in the literature [1]. The ceramic was sintered at 850°C for 2 hours, ground and sifted to particles of sizes less than 1.5μm.

Particle size measurements

The particles were suspended in 50% ethanol, ultrasonicated in a water bath and the particle size was measured (using zeta potentiometer; Brookhaven's ZetaPALS) at every 15 minutes interval till the smallest size measured was consistent.

Zeta Potential Measurements

Zeta potential and conductance measurements were performed for all three SCPC compositions under similar conditions of suspension medium. 1.5 mg of ceramic particles was suspended in 15 ml 50 % (vol/vol) ethanol in water. The pH of the medium was varied from 2-9. Prior to measurements, the samples were subjected to ultra-sonic agitation for 45-50 minutes to assure homogenous particle distribution. Similar experiments were performed in 100% ethanol and pure water as suspension medium to determine the contribution of suspension medium to the zeta potential and conductance. Disposable polystyrene cuvettes were used for all measurements. The zeta potential, conductance and particle size were measured.

RESULTS

Optimization of Sonication time

Ultra-sonic agitation had a proclaimed effect on reducing the clump formation and achieving homogeneous distribution of separated particles. Fig. 1 shows that after 45-50 minutes the particle size was 1.5 μm. Ultrasonication for longer periods did not change the particle size.

Effect of pH

Fig. 2 shows the variation of Zeta Potential with pH in 50% ethanol for different SCPC compositions. The iso-electric point for the three SCPC compositions was identical and occurred between pH 2-3. The maximum absolute value of zeta potential for all the three compositions was observed at pH 6-8. SCPC25 and SCPC50 had

highest zeta potential at pH 6 and 7 respectively whereas SCPC75 had comparable values at pH 6 and 8. The highest zeta potential for all the three ceramics was around -43 mV.
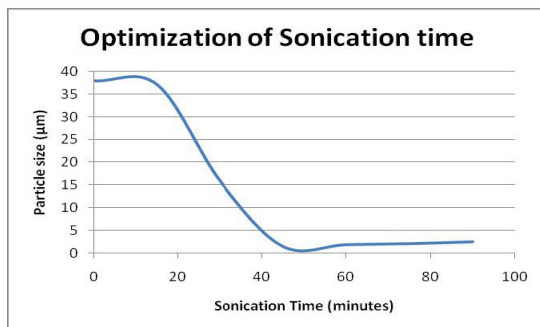

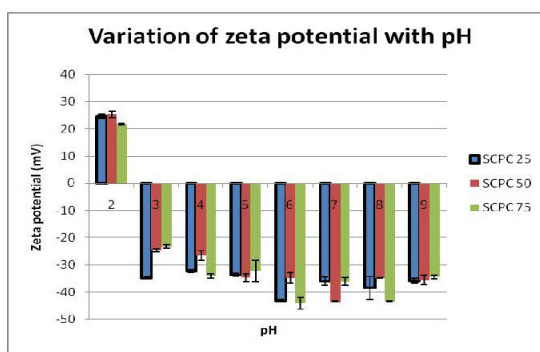Figure 1: Effect of ultra-sonic agitation on particle size

Figure 2: Comparison of zeta potential for SCPC 25, 50 and 75

Effect of SCPC composition on zeta potential

Fig. 3 shows the zeta potential of SCPC of various compositions measured in pure water, 50% and 100% ethanol at pH 7. The values of the zeta potential for SCPC75 in all solutions were lower than that of SCPC25 and SCPC50, however, the difference was not statistically significant. Moreover, comparable values of zeta potential were measured in the three media for all compositions. The highest zeta potential was found to be -43 mV for SCPC50 suspended in 100% ethanol.

Effect of SCPC composition on conductance

Fig. 4 shows the conductance of various SCPC compositions measured in pure water, 50% and 100% ethanol at pH 7. The conductance of SCPC in water is considerably higher than in alcohol and decreases as the alcohol concentration is increased. It is observed that the conductance of SCPC increases in the three medium as the concentration of the silica components in SCPC is increased. Over the pH range 2-9, the conductance is very high at pH 2 and drops sharply as the pH is increased. At pH 6-8, the conductance is the minimum for all compositions, with SCPC25 having the lowest value.
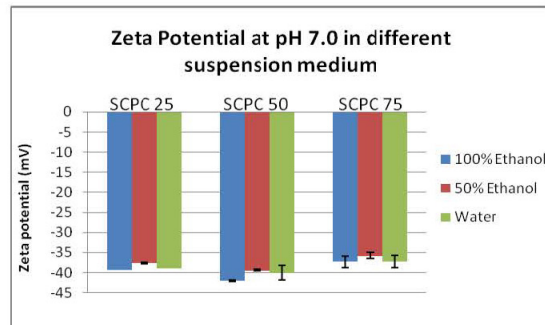

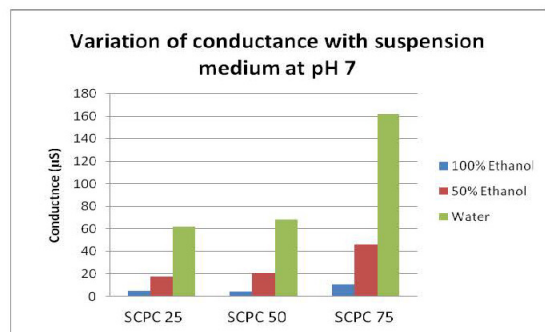Figure 3: Effect of suspending medium on zeta potential

Figure 4: Variation of Conductance in suspending medium

CONCLUSIONS

Comparable values of zeta potential in the three suspending medium indicate that there is no significant contribution from the medium that alters the particle's surface charge. Hence, the particle's surface charge will completely dominate over any charge contained solely within ethanol. It also suggests that there is no differential modification of the particle's surface. The iso-electric point of the three SCPC compositions is between pH 2-3 and the transition is quite rapid. The region of pH 6-8 will be of special interest when considering applications that involve particle mobility under applied electric field, as they offer higher potentials and lower conductance values and is also around the physiological pH. Zeta potential of -30 mV or more exists over a large pH range which suggests good colloidal stability. The alcohol content of the medium has a significant contribution on the conductance, indicating that the SCPC particles are more ionic in water than in alcohol. The ionic content is also dependent on the silica content so that SCPC75 exhibits highest conductance and SCPC25 exhibits the lowest. In summary, SCPC's of various compositions exhibit closely related surface properties although they may be different in their bulk properties.

REFERENCES

1. Gautam Gupta, Sreenatha Kirakodu, Ahmed El-Ghannam, 2007, "Dissolution kinetics of a Si-rich nanocomposite and its effect on osteoblast gene expression", Journal of Biomedical Materials Research Part A; Volume 80A, Issue 2, 486-496
2. El-Ghannam A, Ning CQ, Mehta J, 2004, "Cyclosilicate nanocomposite: a novel resorbable bioactive tissue engineering scaffold for BMP and bone-marrow cell delivery" Journal of Biomedical Materials Research Part A; Volume 71A, Issue 3, 377-390

VITA

Date of Birth: March 2nd, 1984

Place of Birth: Patna, India

Education:

> Viswesvaraya Technological University, India
>
> Degree awarded: Bachelor of Engineering (in Biotechnology)

Employments:

- Software Engineer, Cerner Corporation, Bangalore, India (2006 – 2007)

- Intern, Biocon Ltd., Bangalore, India (2005 – 2006)

Honors and Awards:

- Awarded Graduate Assistant Support Plan scholarship (2007 – 2012)

- Awarded Graduate Life Fellowship (2008 – 2009)

- Winner of graduate student poster competition at the Charlotte Biotechnology Conference, 2010.

- Ranked nationally among top 60 high school students at National Science Talent Search Examination, India, 1999

Community Leadership:

- Student Officer, Helping International Students (HIS) (2008 – 2010)

- Committee Member, Graduate & Professional Student Government, UNC Charlotte, (2007 – 2008)

Journal Publications:

- <u>Aniket</u> and A El-Ghannam, Electrophoretic Deposition of Bioactive Silica-Calcium Phosphate Nanocomposite on Ti-6Al-4V Orthopedic Implant, J Biomed Mat Res Part B: Appl Biomater, 2011, 99B: 369 – 379

- <u>Aniket</u>, A Young, I Marriott and A El-Ghannam, Promotion of Pro-Osteogenic Responses by a Bioactive Ceramic Coating, J Biomed Mat Res Part A, 2012 (in press)

- A Sparnell, <u>Aniket</u> and A El-Ghannam, Machining of a Bioactive Nanocomposite Orthopedic Fixation Device, J Biomed Mat Res Part B: Appl Biomater, 2012 (in press)

Conference Proceedings:

- <u>Aniket</u>, I Marriott and A El-Ghannam, Effect of Bioactive Surface Coating on Protein Adsorption, Bone Cell Differentiation and Immune Response, Proceedings of the 2011 Annual Meeting of the Society for Biomaterials, 2011

- <u>Aniket</u>, A Young, I Marriott and A El-Ghannam, Osteoblast Gene Expression on a Novel Bioactive Ceramic Coating for Orthopedic Implants, Proceedings of the 57th Annual Meeting of the Orthopedic Research Society, 2011

- <u>Aniket</u>, M Mansourian, K Vedantham and A El-Ghannam, Engineering Surface of Orthopedic Implants for Bactericidal Effect and Bone Bonding Enhancement, Proceedings of the 57th Annual Meeting of the Orthopedic Research Society, 2011

- K Vedantham, <u>Aniket</u>, A Young, I Marriott and A El-Ghannam, Bone Tissue Engineering Scaffold for Infection Treatment and Tissue Regeneration, Proceedings of the 57th Annual Meeting of the Orthopedic Research Society, 2011

- <u>Aniket</u>, A Young, I Marriott and A El-Ghannam, Enhancement of Bone-Implant Integration Using a Novel Bioactive Ceramic Coating, Proceedings of the 3rd International Workshop on Advanced Materials, Ras Al-Khaimah, UAE, 2011

- <u>Aniket</u> and A El-Ghannam, A Novel Bioactive Ceramic Coating for Improved Fixation of Orthopedic Implant, Proceedings of the 2009 Fall Meeting of the Material Research Society, 2009

- <u>Aniket</u> and A El-Ghannam, Zeta Potential of Silica-Calcium Phosphate Nano composite: Effect of Material Composition and Medium pH, Proceedings of the American Society of Mechanical Engineering Summer Bioengineering Conference, 2008